AFFDL-TR-74-19

LEESIDE FLOW FIELD DESCRIPTION
OVER CONES AT LARGE INCIDENCE

Victor Zakkay, Constantino Economos
and Edgar Alzner

Advanced Technology Laboratories, Inc.

FOREWORD

This report was prepared by Advanced Technology Laboratories, Inc., Merrick and Stewart Avenues, Westbury, New York 11590, under contract F33615-73-C-3010 and is identified by the contractor as ATL TR 191. The Air Force program monitors were E. D. McElderry and V. Dahlem (AFFDL/FXG), whose cooperation and assistance in carrying out this effort the authors are pleased to acknowledge. The research was performed during the period 1 November 1972 to 28 October 1973, and this report was submitted on 25 January 1974. The computer program and user's manual prepared in conjunction with the analyses described herein have been delivered to the AFFDL/FXG to whom requests for copies by qualified users should be directed.

This report has been reviewed and is approved.

PHILIP P. ANTONATOS
Chief, Flight Mechanics Divison
Air Force Flight Dynamics Laboratory

ABSTRACT

A semi-empirical analytic model for leeside flow field behavior over
sharp circular cones at large incidence is described. The methodology in-
volves replacement of the actual body by an inviscid equivalent body over
which the flow field is developed. The equivalent body is selected by a
combination of turbulent boundary layer analysis up to the primary separa-
tion point and correlation of available experimental results within the
separated regions. The inviscid flow field over the equivalent body is
developed by means of a numerical finite difference marching technique
(Kutler program).

Computer programs for implementing the analysis were developed and
delivered to the AFFDL/FXG together with user's manuals. The performance
of these programs is demonstrated by several numerical examples and com-
parisons with experiment.

TABLE OF CONTENTS

Page

LIST OF ILLUSTRATIONS

LIST OF ILLUSTRATIONS (Continued)

LIST OF ILLUSTRATIONS (Continued)

LIST OF SYMBOLS

C_∞ — temperature-viscosity law constant of proportionality

F_4 — correlation parameter for leeward pressure-see Equation (25)

h_2 — streamline spreading parameter

M_∞ — free stream Mach number

p — static pressure

P — p/p_∞

P_t — stagnation pressure

$\acute{P}_t$ — pitot pressure

q_w — wall heat transfer per unit area per unit time

r — cylindrical coordinate-see Figure (12)

r_n — nose radius

R — spherical coordinate (see Figure 12) or gas constant

$Re_{\infty,x}$ — Reynolds number based on free stream conditions and distance along cone generator

s — distance along streamline measured from stagnation point or cone apex

S — entropy

St — Stanton number based on boundary layer edge mass flux rate-$\rho_e u_e$

St_∞ — Stanton number based on free stream mass flux rate-$\rho_\infty u_\infty$

v_R — velocity component in R-direction

v_ϕ — velocity component in ϕ-direction

V_R — v_R/V_L

V_ϕ — v_ϕ/V_L

V — $(V_R^2 + V_\phi^2)^{\frac{1}{2}}$

V_∞ — free stream velocity normalized with respect to V_L

LIST OF SYMBOLS (Continued)

V_L — limiting velocity

x, z — Cartesian coordinates-see Figure (12)

α — angle of attack

γ — specific heat ratio

δ^* — displacement thickness-shear layer thickness

η — transformed independent variable defined by Equation (3) or relative angle of incidence α/θ_c

θ — momentum thickness

θ_c — cone half angle

κ — transformation parameter-see Equation (1)

ξ — transformed independent variable defined by Equation (2)

ϕ — spherical coordinate-see Figure (12)

X_c — viscous interaction parameter-see Equation (24)

ψ — angle between streamline and cone generator

Subscripts

b — body or effective body

c — geometric cone

s — shock

-x-

SECTION I

INTRODUCTION AND BACKGROUND

Up until the last decade very little interest existed for development of computational methods for describing flow field behavior on the leeside of conical bodies at very large incidence. This lack of interest was a consequence primarily of practical considerations since, until that time, sustained flight at angles of attack comparable to or greater than the vehicle thickness to length ratios was not required to fulfill any practical mission requirements.

With the advent of the space shuttle concept and the rapid improvement of ABM performance this situation has changed dramatically, as evidenced by the many studies of this problem undertaken during the past several years. As might be expected, many of these studies were of an experimental nature (References 1-6), with most analysis restricted to treatment of cones at yaw angles only up to about the cone half angle (References 7-13). The problem, of course, is an exceedingly difficult one since it involves the growth and separation of a three dimensional boundary layer which subsequently interacts with the outer inviscid flow. This phenomenon can effect vehicle performance aerodynamically (stability) as well as thermodynamically (heating rates). The location of the separation lines and the strength of the vortices which result from rollup of the shear layer evidently can influence the flight dynamics of a given vehicle configuration. Furthermore, with regard to the heating situation, it was found experimentally that heat transfer rates on the leeward surfaces could achieve levels comparable to those on the windward side and, under certain conditions, even exceed these values. The practical implication of these observations was apparent and provided the motivation for developing analytic techniques capable of describing the details of the phenomenon.

Prior to ATL's current study, such analyses as were available were restricted to relatively low angles of attack and laminar conditions. Reference (13) is a representative example of these studies but the flow field treated therein differs in a fundamental way from that investigated by ATL during the past year.

-1-

In order to clarify these differences it is instructive to examine and compare the information presented in Figures (1a), (1b) and (1c) with that in Figures (2a), (2b) and (2c). It is evident from this comparison that there are two distinct flow patterns associated with the small and large angles of attack. The first type consists of one separation point and a single recirculating region. The other consists of two separation points and two recirculation regions. It has been concluded from our research effort during the past year that the single separation exists for the following conditions:

1. Low angles of attack ($\alpha/\theta_c < 1.2$) for both laminar and turbulent conditions, high and low Mach numbers.

2. High angles of attack, $M_\infty > 5$, and low Reynolds number.

The double separation type of flow field which has been investigated at ATL exists for the following conditions:

(a) High Reynolds number (turbulent) for all ranges of Mach number and for $\alpha/\theta_c > 1.2$.

(b) Low Mach number, laminar flow conditions and $\alpha/\theta_c > 1.2$.

A direct comparison of these two patterns is depicted schematically in Figure (3). The associated pressure distributions are shown in Figure (4). While conditions for laminar flow could be analytically treated and has been treated recently for the single type of separation, the double separation flow field for turbulent conditions is complex and requires a semi-empirical type of analysis.

From a practical point of view, the motivation for developing an analytic capability for describing the second type of flow phenomenon ultimately derives from a need to compute heat transfer characteristics on the leeward surfaces when these double recirculation zones or vortices are present. Note that considerable evidence exists which indicates that the observed high heating rates

-2-
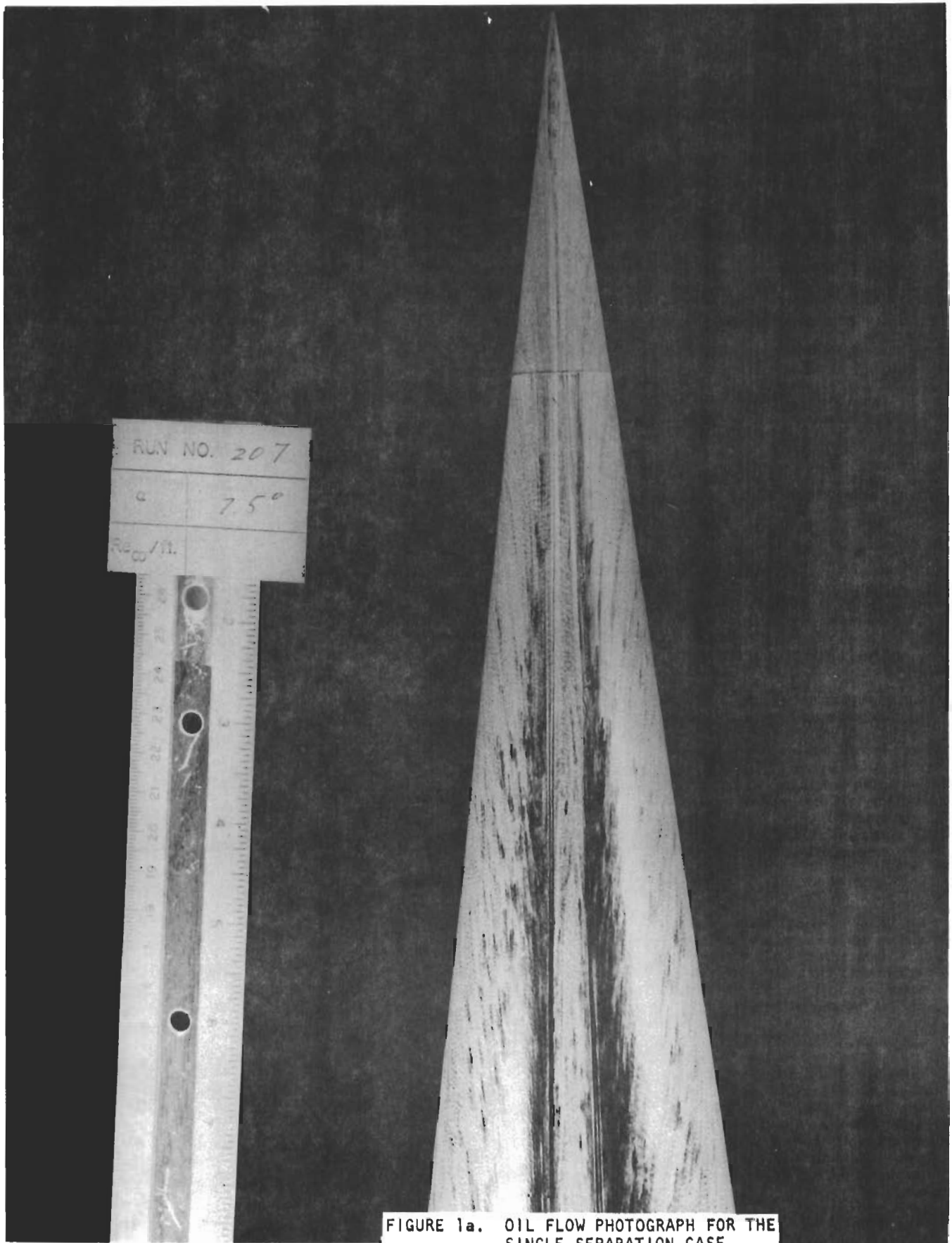
FIGURE 1a. OIL FLOW PHOTOGRAPH FOR THE
SINGLE SEPARATION CASE

-3-
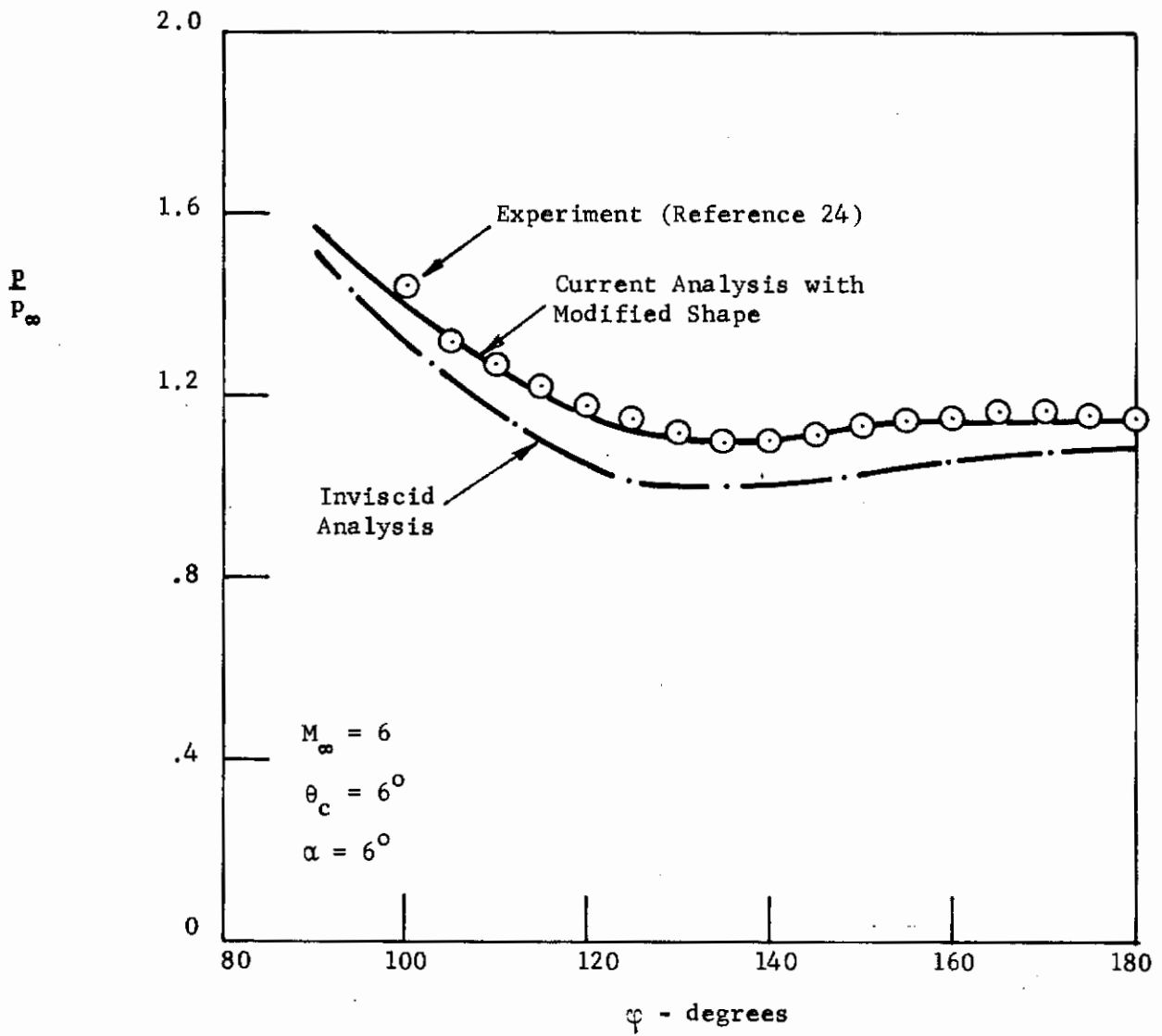
FIGURE 1B TYPICAL PRESSURE DISTRIBUTION FOR THE SINGLE
SEPARATION CASE-COMPARISON OF THEORY AND
EXPERIMENT

-4-

SEPARATION

ONCOMING
BOUNDARY
LAYER

$\varphi \simeq 150^{\circ} \sim 165^{\circ}$
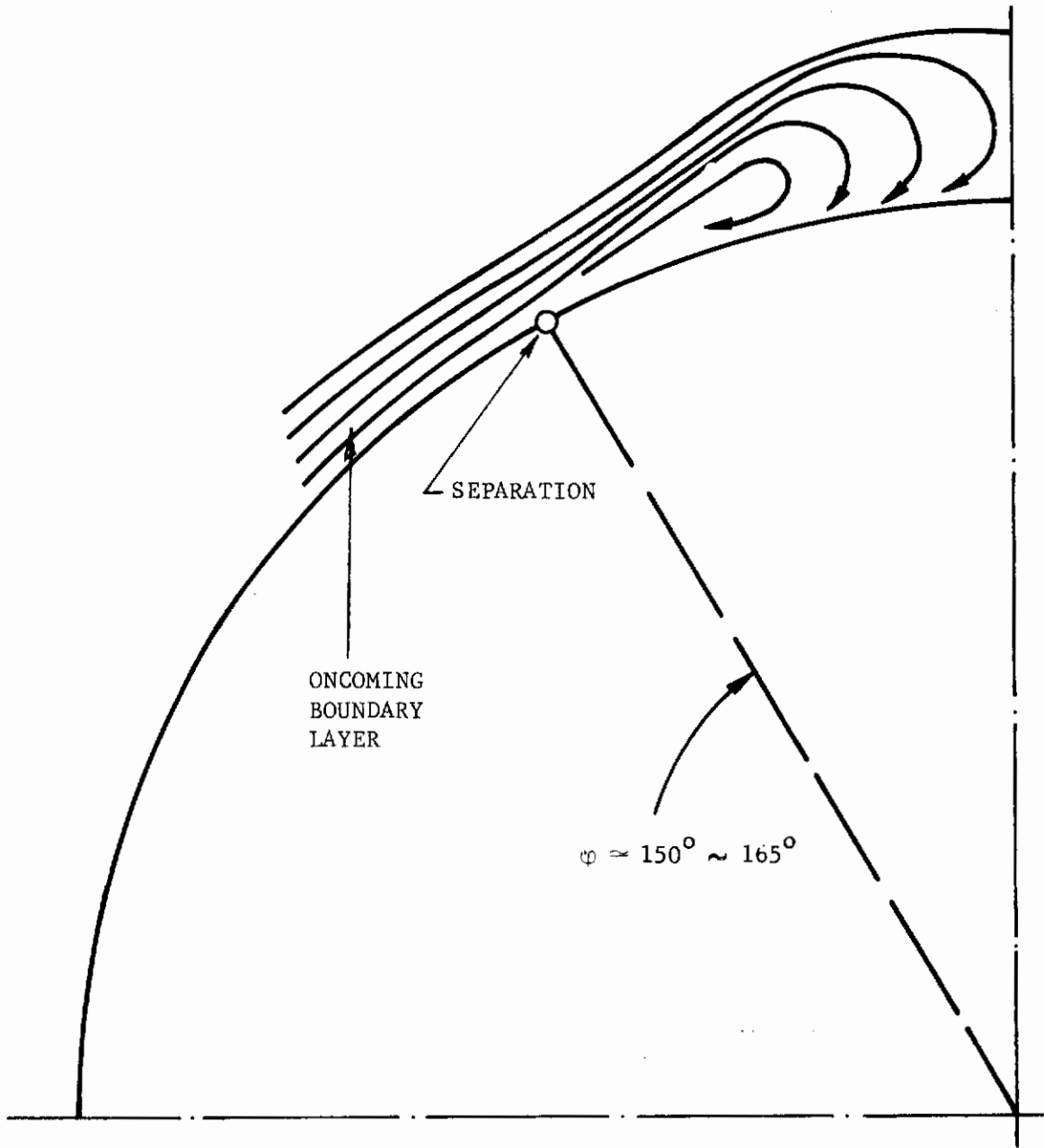
FIGURE 1c   CONCEPTUAL REPRESENTATION OF FLOW FIELD FOR THE SINGLE
SEPARATION CASE

RUN NO. 208
α   15°
Re₀/ft
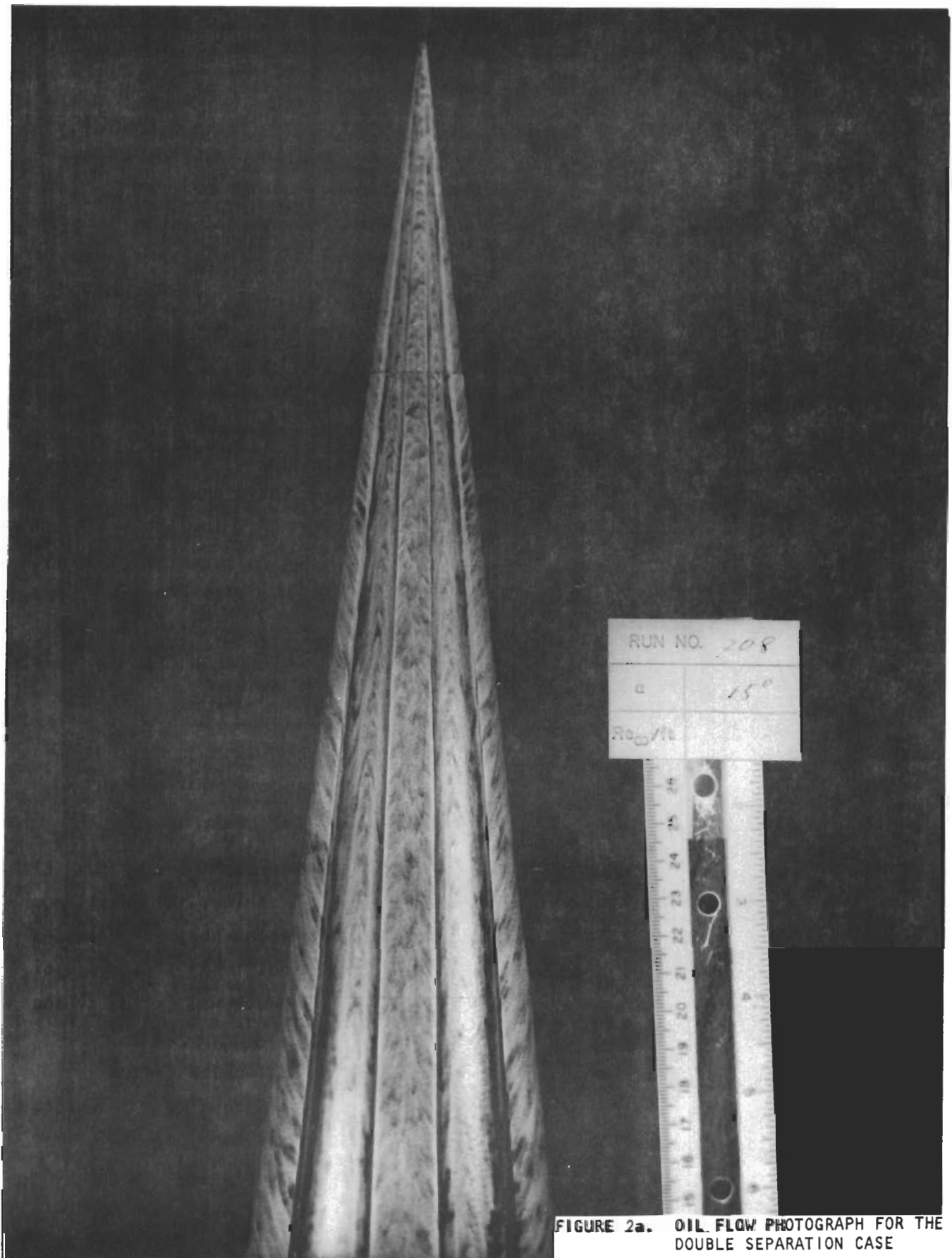
FIGURE 2a.   OIL FLOW PHOTOGRAPH FOR THE DOUBLE SEPARATION CASE

-6-
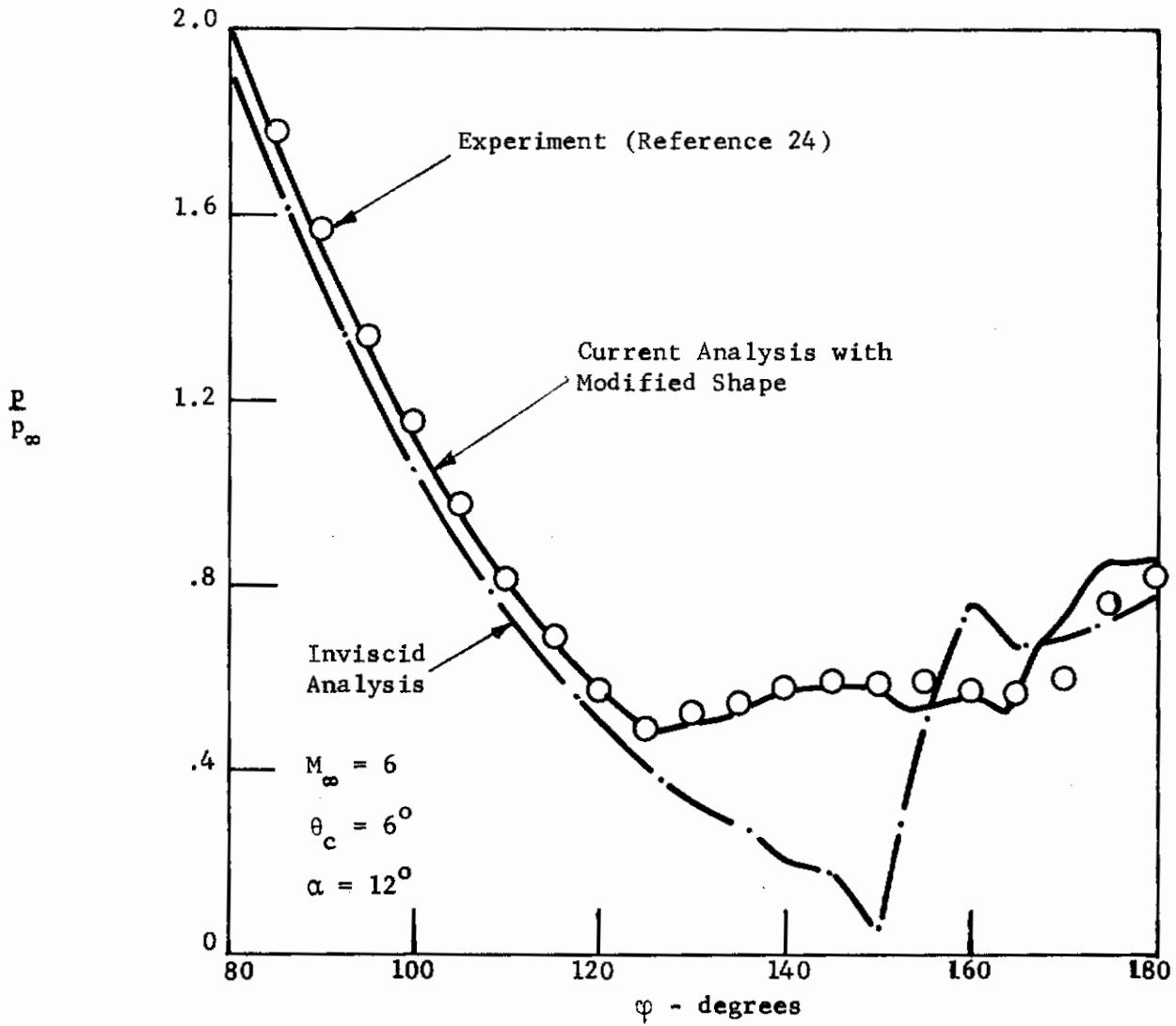
FIGURE 2b TYPICAL PRESSURE DISTRIBUTION FOR THE DOUBLE
SEPARATION CASE-COMPARISON OF THEORY AND
EXPERIMENT
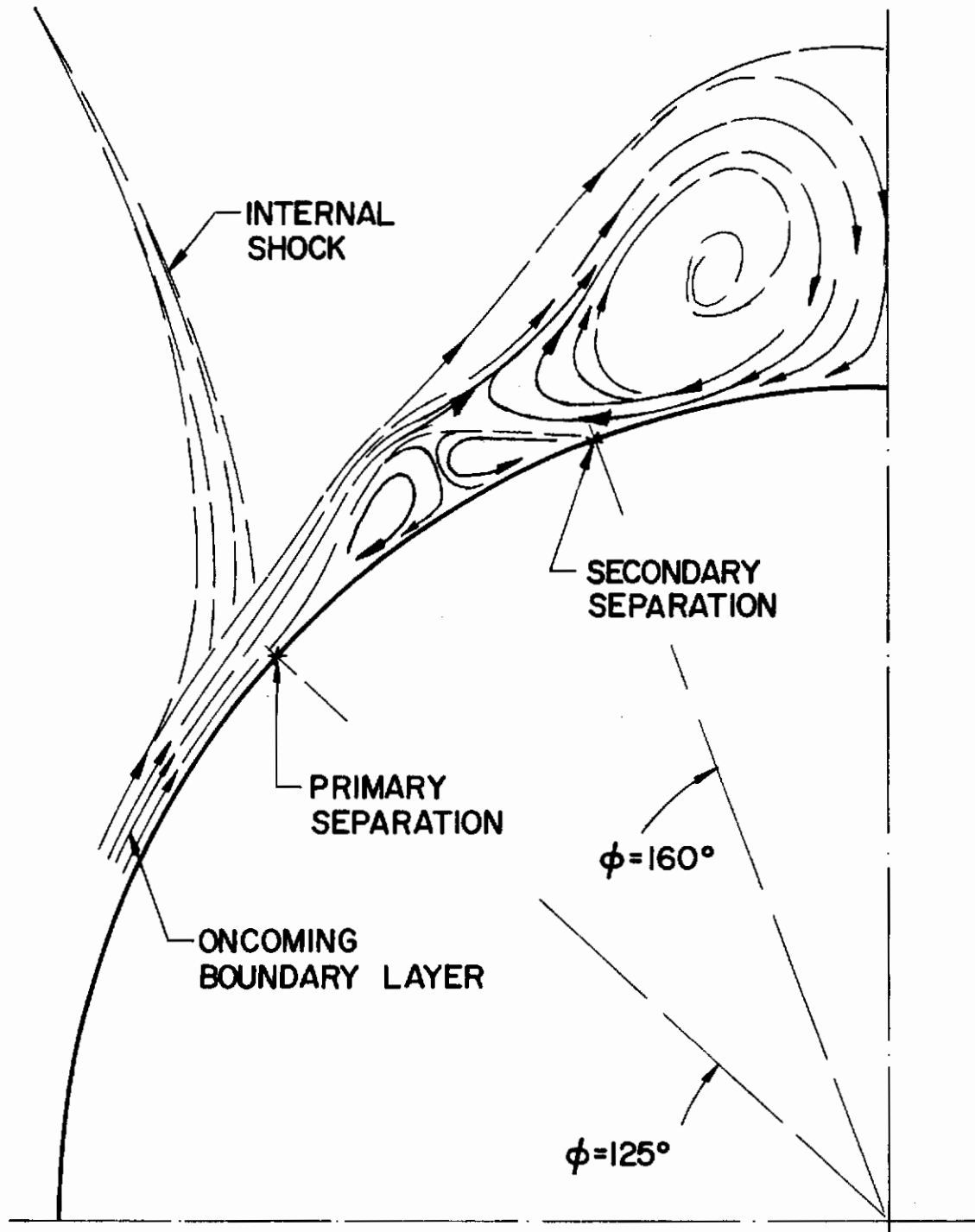
FIGURE 2C CONCEPTUAL REPRESENTATION OF FLOW FIELD FOR THE DOUBLE
SEPARATION CASE
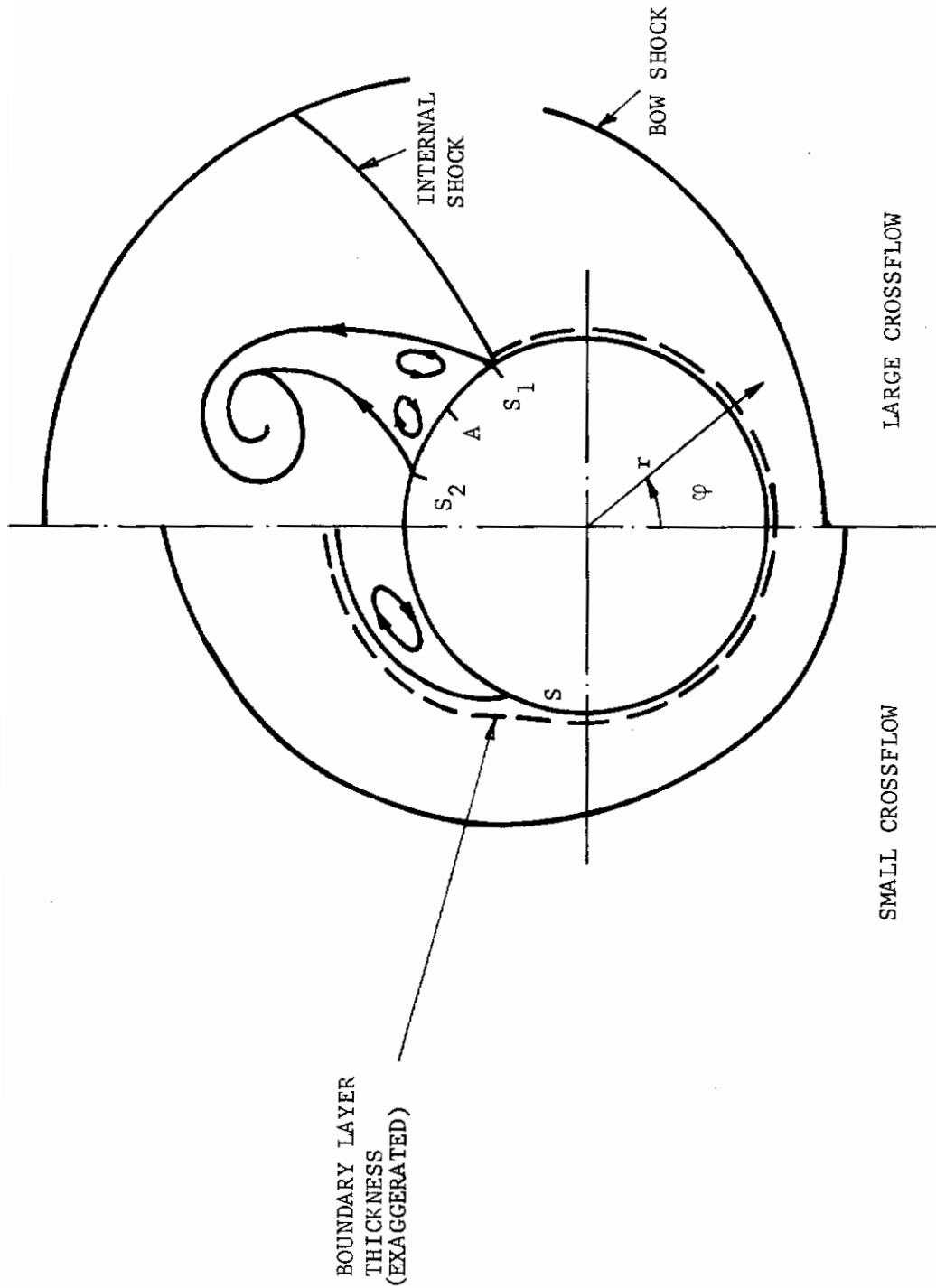
FIGURE 3   SCHEMATIC OF FLOW FIELD PATTERNS IN THE CROSS-FLOW PLANE OF A CONE AT INCIDENCE

I. Subsonic Cross Flow Regime

II. Intermediate Regime

III. Supersonic Cross Flow with Vortex
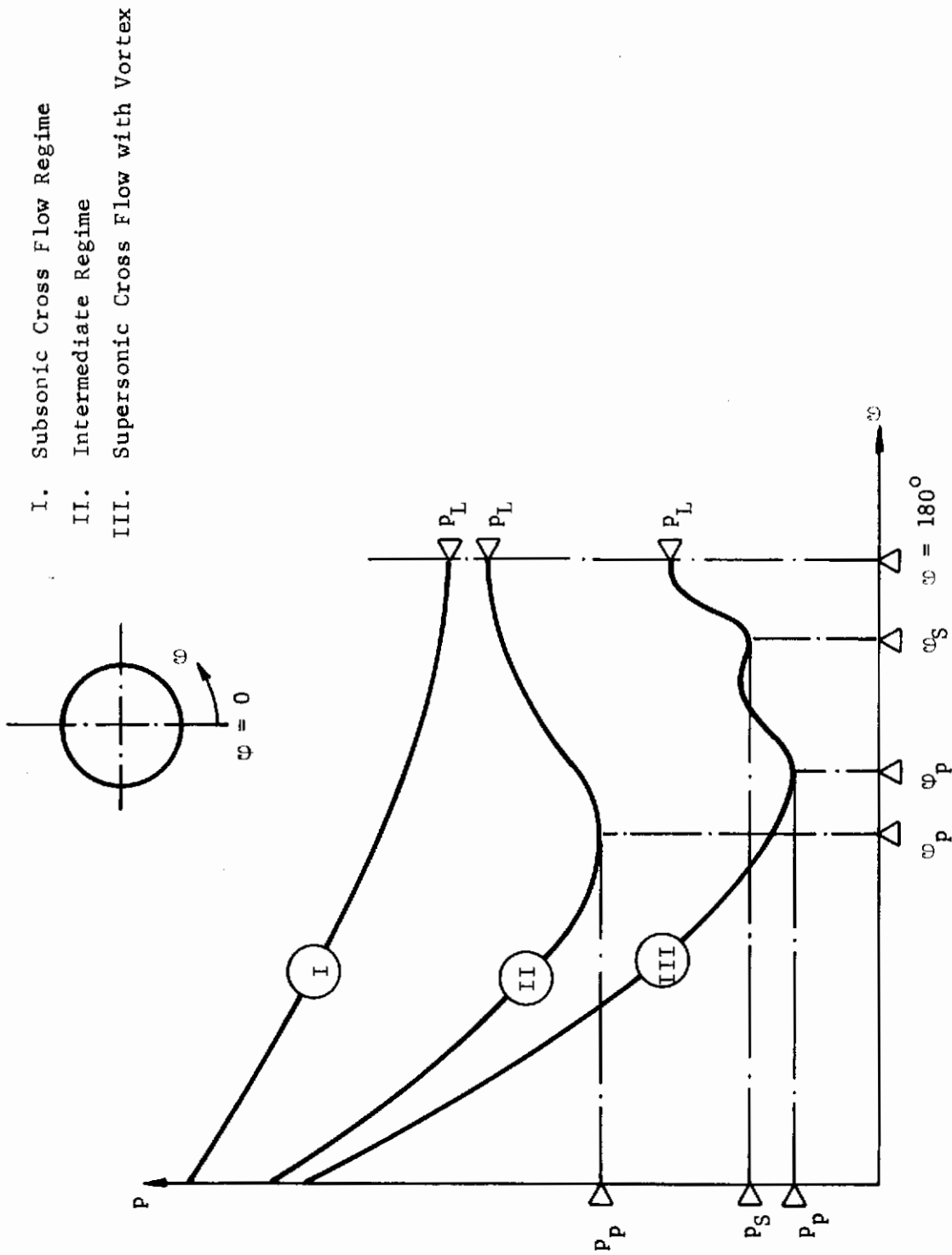
FIGURE 4 PRESSURE DISTRIBUTIONS ON YAWED CIRCULAR CONES

-10-

mentioned earlier are directly attributable to the formation of such vortices.

Under certain conditions associated with practical flight trajectories of blunted cones, regions of laminar and turbulent conditions can occur simultaneously. It is conceivable that this transition can trigger the vortices which would not occur under purely laminar conditions. Evidently, the availability of a reliable flow field predictive technique is a prerequisite for determination of when and if these mechanisms occur.

In some recent experiments conducted at the New York University Aerospace Laboratory (Reference 14), some peculiarities with regard to heat transfer measurements have been observed. These could be explained in the light of the phenomena described above. A summary of these results is presented in Figure (5). In this case, heat transfer rates on the leeward plane are not only higher than those on the windward plane under laminar conditions but under turbulent conditions as well. The area on the cone associated with these regions of high heating may be seen in the oil film picture (Figure 6) where the feather type markings are located.

Similar behavior has been observed on space shuttle type vehicles by Whitehead at Langley Field (Reference 15). Figure (7) shows the dependence of these heating rates on Reynolds number while Figure (8) shows the variation with Reynolds number, Mach number and angle of attack. It is evident from these results that vortex heating is significant and needs to be accounted for to insure proper design of high performance reentry configurations.

The method of approach and analysis utilized by ATL to treat this problem during the past year is described in the next two sections. Results and comparisons with experiment are presented in the subsequent section.
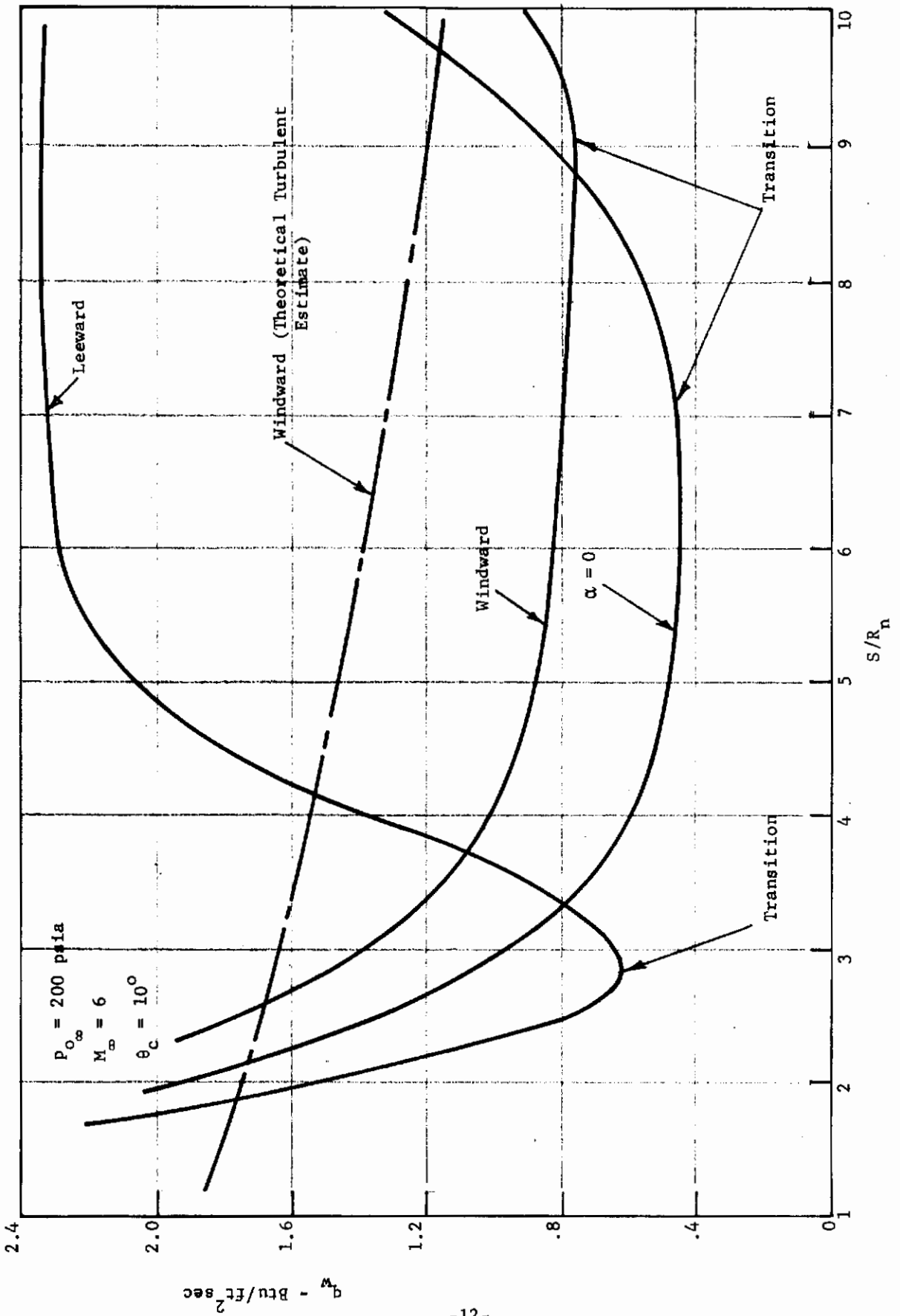
FIGURE 5   MEASURED HEAT TRANSFER RATES ON THE SURFACE OF BLUNTED CONES AT INCIDENCE-DATA FROM REFERENCE 2

-12-
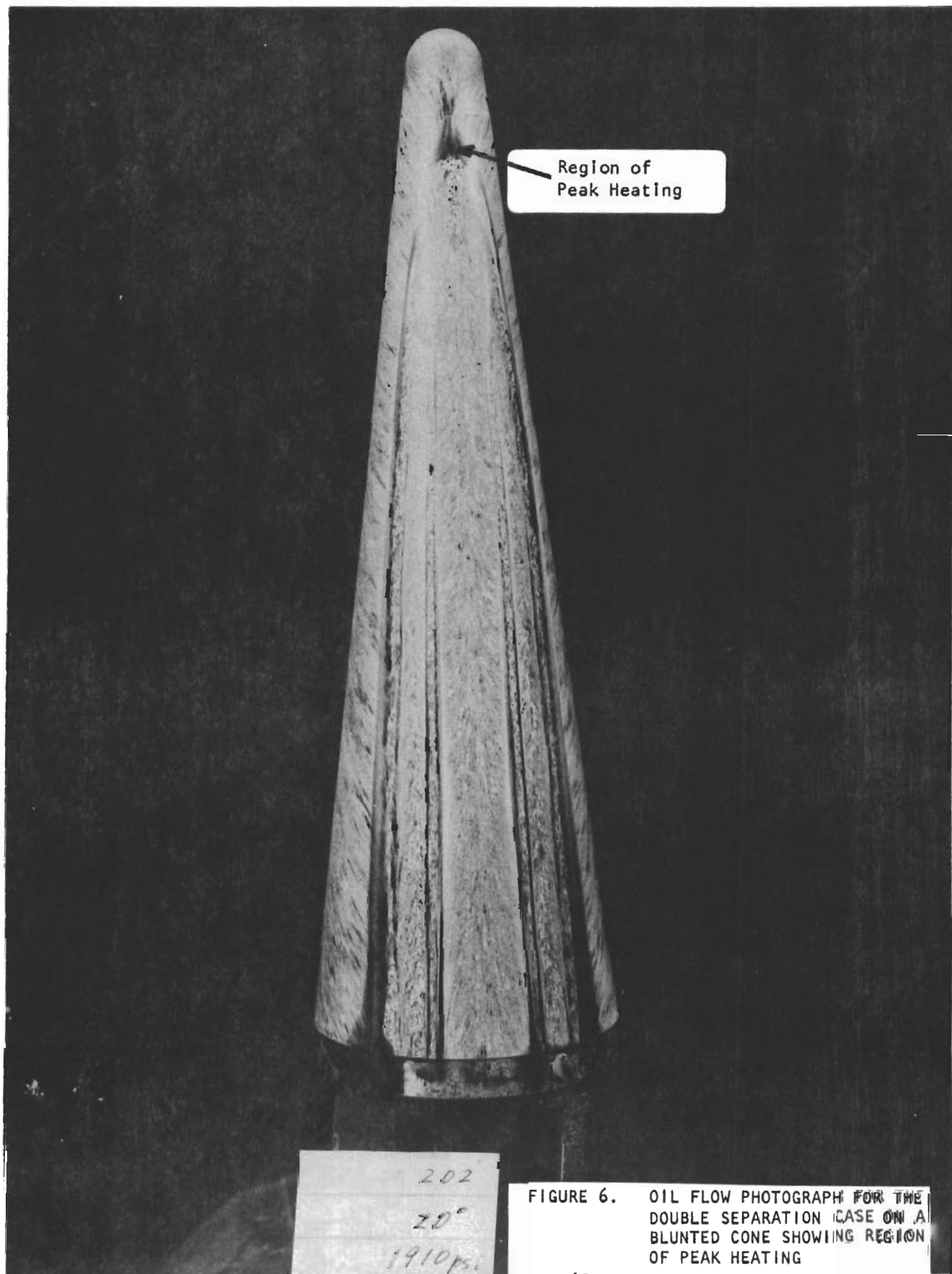
Region of
Peak Heating

.202

20°

1910 psi

FIGURE 6.   OIL FLOW PHOTOGRAPH FOR THE
DOUBLE SEPARATION CASE ON A
BLUNTED CONE SHOWING REGION
OF PEAK HEATING

-13-
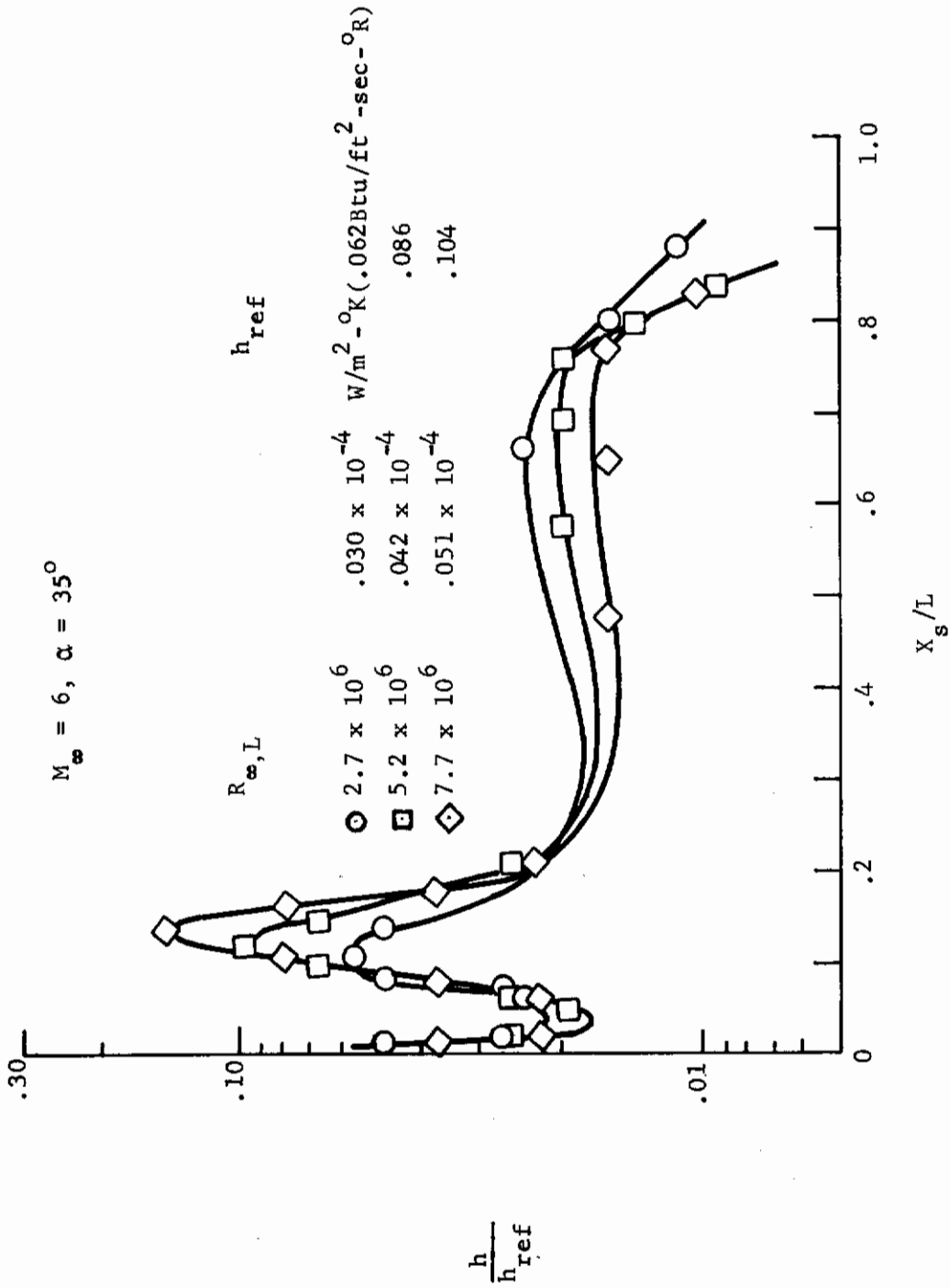
FIGURE 7   EFFECT OF REYNOLDS NUMBER ON CENTERLINE LEE-SURFACE HEATING
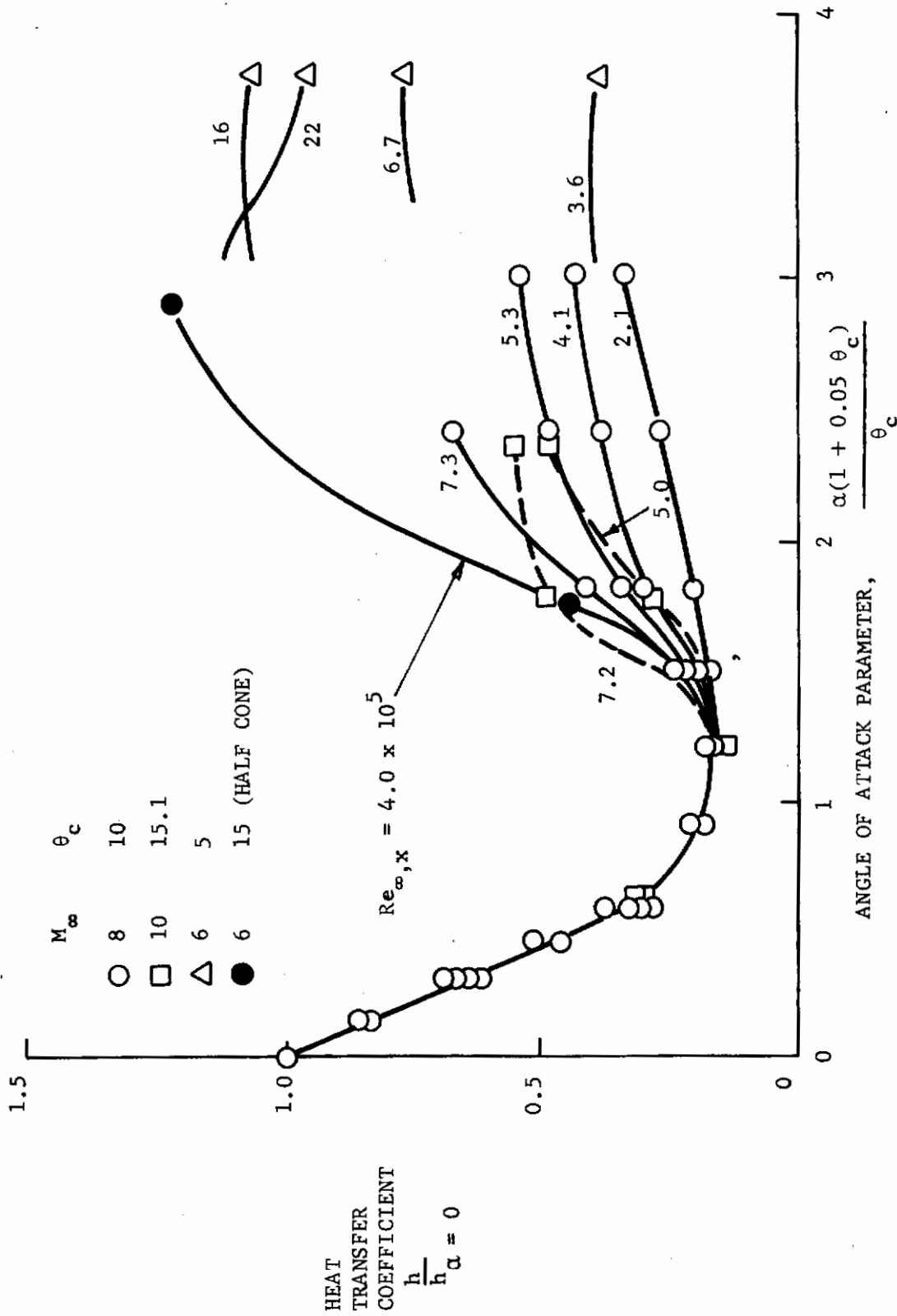
FIGURE 8 HEAT TRANSFER COEFFICIENT ON LEE SIDE OF CIRCULAR CONES

SECTION II
METHOD OF APPROACH AND ANALYSIS

The overall objective of the current effort was to develop a numerical computation scheme which would provide a description of the flow field characteristics and surface conditions on the leeside of cones at large incidence and at conditions corresponding to a turbulent boundary layer state. The method of approach utilized to achieve this objective is a semi-empirical one which utilizes an inviscid equivalent body in order to develop the flow field. The equivalent body is derived from a combination of viscous turbulent boundary layer program up to the primary separation point and a correlation of flow field data within the separated region. The method involved the following ingredients:

A. <u>Physical Model</u> - The physical model which was employed incorporates the concept of an "effective" body to represent the region of high shear adjacent to the geometric body. That is, the shear layer, including both the boundary layer proper and the vortices, was considered to be enclosed by a streamline or stream surface which divided the region of high shear from the outer inviscid shock layer. The pressure across this shear layer is assumed constant and the inviscid flow field develops as if in the presence of a body whose cross sectional geometry is defined by the aforementioned dividing stream surface.

B. <u>Flow Field Computation Scheme</u> - Once the effective body shape has been determined a computation scheme capable of determining a three dimensional, supersonic flow field is required. Actually, as will be discussed below, this scheme is also utilized to aid in the determination of the effective body shape. The flow field computation scheme (FFCS) selected for this purpose is that due to Kutler, Reference (16) which was specifically designed to analyze the flow field over three dimensional configurations at high angles of attack at NASA-Ames.

The analysis involves numerical integration of the finite difference analogue of the conservation equations for three dimensional inviscid iso-

energetic flow. The working independent variables in this numerical scheme
are related to the cylindrical coordinates z, r, and ϕ according to

$$z = z \tag{1}$$

$$\xi(z,r,\phi) = (r-r_b)/(r_s-r_b) \tag{2}$$

$$\eta(\phi) = \arctan(\kappa \tan \phi) \tag{3}$$

where z is aligned with the body axis. Here $r_b=r_b(z,\phi)$ and $r_s=r_s(z,\phi)$ represent
the vehicle body geometry and shock location respectively. The parameter κ is
a free parameter which serves the purpose of distorting the mesh in the physical
plane; i.e.: equal increments of η results in a clustering of ϕ-increments in
the vicinity of $\phi=90^{\circ}$ when $0 < \kappa < 1$ while for $\kappa > 1$ the clustering occurs in
the vicinity $\phi=0$, 180°. For $\kappa \to 1$ of course the spacing approaches uniformity.

The integration scheme involves a straight marching procedure in the
hyperbolic coordinate z. Accordingly, the scheme can be applied only to a
supersonic domain and further requires specification of valid initial data
along some starting line. For the general case this must be supplied by other
means (e.g.: a subsonic blunt body scheme). For the present application, how-
ever, where body geometries are restricted to the conical case (dr_b/dz = constant)
initial data can be arbitrary since, for sufficiently large z, the desired
conical solution will be obtained independent of the correctness of the initial
data.

Details of the analysis and the numerical methods associated with the com-
putation scheme are not included here since they are well documented in Refer-
ence (16). In particular, it is noted that ATL's involvement in the develop-
ment of the FFCS consisted solely of developing a specialized geometry package
suitable for the present purpose. This geometry package has been substituted
for the version incorporated by the original computer code as received from
NASA-Ames.

The necessity for revising the geometric representation is exemplified by the comparison shown in Figure (9). As can be seen, the general character-istics of the geometry needed to represent the shear layers on cones at high incidence differ in a very profound way from the shuttle-like configuration for which the original computer code was intended.

The geometry used to represent the shuttle configuration in Reference (16) is indicated in Figure (10) and is labelled Kutler's geometry where it is compared with our initial proposed modifications. The proposed changes consisted of the addition of two sets of four segments between straight line segment 5-6 and the original ellipse 6-7. Each set of segments consisted of ellipse, line, cubic and line. The additional geometrical segments were as follows: ellipse - segment 6-7 (defined using point i), line - segment 7-8, cubic - segment 8-9, line - segment 9-10, ellipse - segment 10-11 (defined using point j), line - segment 11-12, cubic - segment 12-13 and line - segment 13-14. The original ellipse 6-7 was replaced by the equivalent ellipse 14-15. Specification of these 8 additional segments required 16 input parameters namely X_u, Y_u, Y_7, Y_8, X_9, Y_9, θ_9, Y_{10}, X_h, Y_h, Y_{11}, Y_{12}, X_{13}, Y_{13}, θ_{13} and Y_{14} with Y_{15} replacing Y_7 of the original input. Figure (11) is a chart indicating the changes which were required to the input of the program.

These modifications were implemented and a series of calculations were attempted with this version of the computer code. It was found, however, that even this augmented version of 14 segments was unsatisfactory in terms of providing the flexibility to reproduce the desired pressure variations. Ac-cordingly, a further modification was implemented involving a straightforward tabular input of effective body radius at each of the peripheral grid points. This scheme proved to be successful and determination of effective body shapes was achieved without further difficulty.

Once this had been accomplished these body shapes were generalized in terms of their dependence on displacement thickness at the primary separation point and angle of attack as is discussed in Section IIIE. The logic of the

-18-

EDGE OF VISCOUS LAYER
(FOLLOWING REF. 2)

BASIC CONE

r_b

x

ω

TYPICAL SHUTTLE
CONFIGURATION
(FOLLOWING REF. 6)
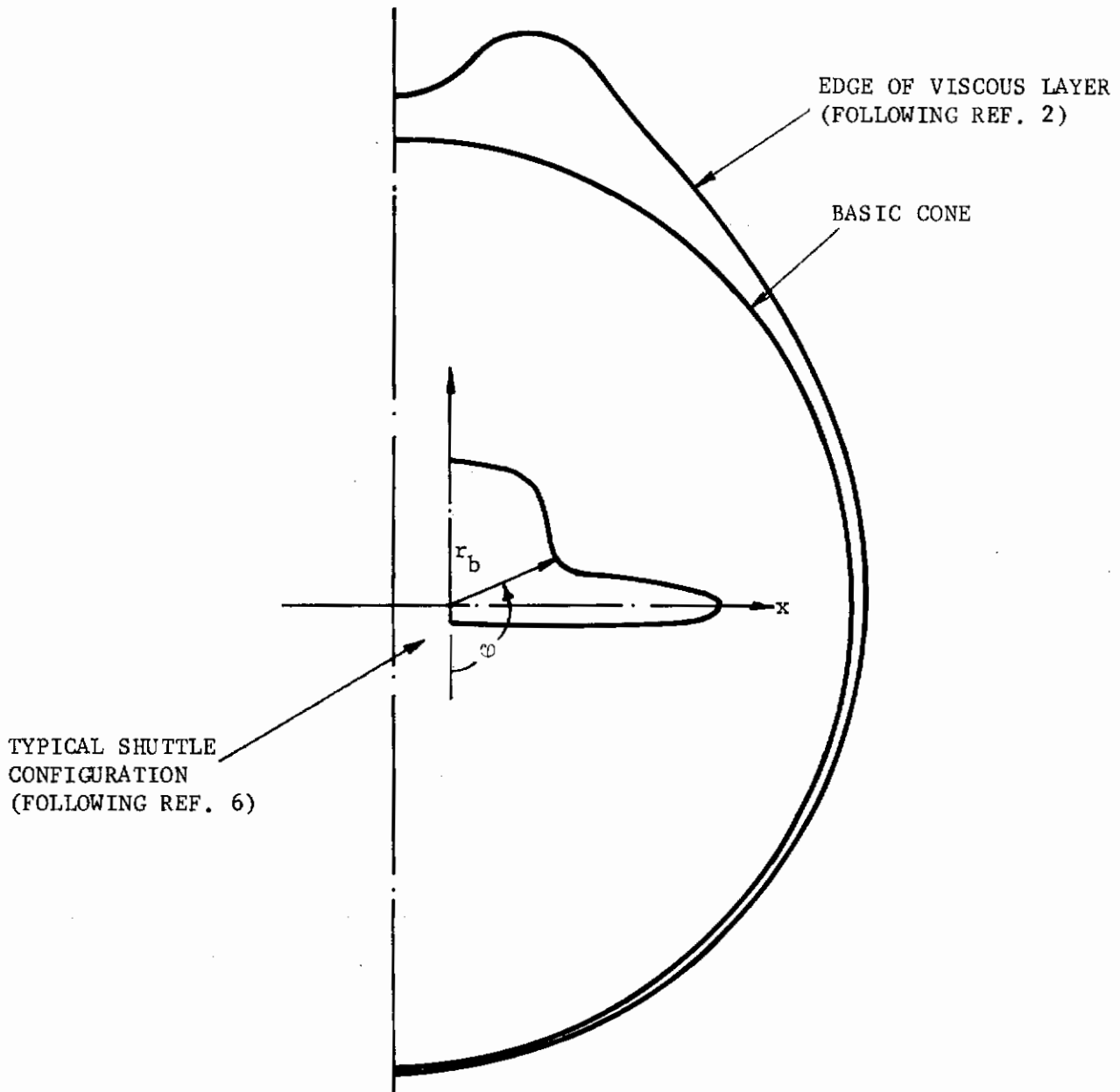
FIGURE 9   COMPARISON OF GEOMETRIES ASSOCIATED WITH SPACE SHUTTLE AND EFFECTIVE
BODY FOR CIRCULAR CONES AT INCIDENCE

SEGMENT	CURVE
1 - 2	LINE
2 - 3	ELLIPSE(x,y)
3 - 4	LINE
4 - 5	CUBIC
5 - 6	LINE
6 - 7	ELLIPSE(y_7)

KUTLER'S GEOMETRY

SEGMENT	CURVE
1 - 2	LINE
2 - 3	ELLIPSE(x,y)
3 - 4	LINE
4 - 5	CUBIC
5 - 6	LINE
6 - 7	ELLIPSE(x_i,y_i)
7 - 8	LINE
8 - 9	CUBIC
9 - 10	LINE
10 - 11	ELLIPSE (x_j,y_j)
11 - 12	LINE
12 - 13	CUBIC
13 - 14	LINE
14 - 15	ELLIPSE(y_{15})
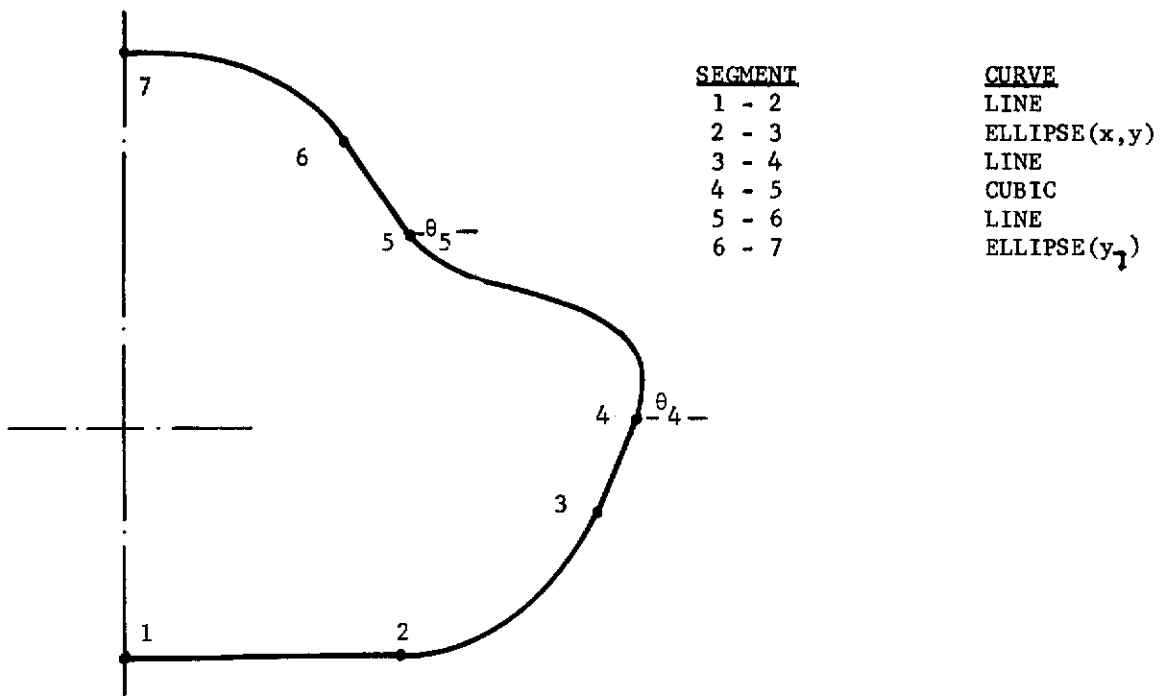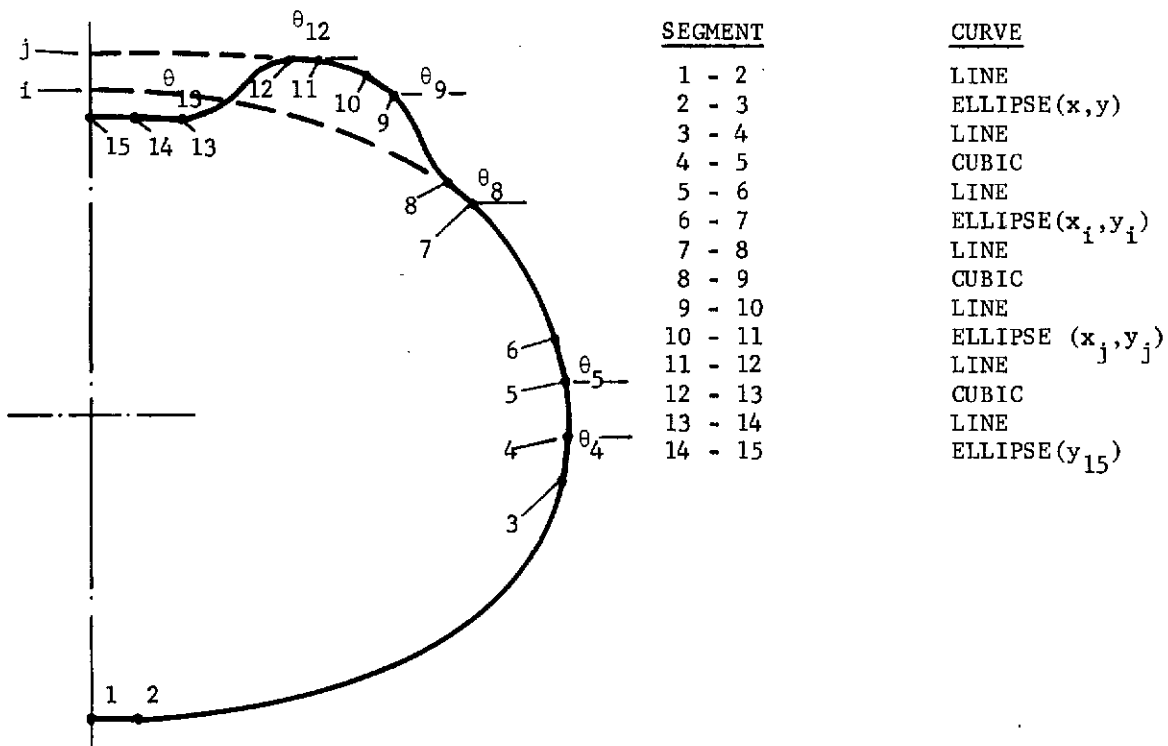
PROPOSED GEOMETRY

FIGURE 10   SCHEMATIC OF KUTLER AND PROPOSED GEOMETRY FOR BODIES AT ANGLE
OF ATTACK

-20-

Kutler	Curve	Proposed
Y_1	$>$ Line $<$	Y_1
Y_2	$>$ Ellipse $<$	Y_2
Y_3	$>$ Line $<$	Y_3
X_4, Y_4, θ_4	$>$ Cubic $<$	X_4, Y_4, θ_4
X_5, Y_5, θ_5	$>$ Line $<$	X_5, Y_5, θ_5
Y_6	$>$ Ellipse $<$	Y_6
Y_7		X_γ, Y_γ
		$Y_7 \rightarrow \theta_7$, X_7
11 Parameters	Line $<$	
		$Y_8 \rightarrow X_8$, $\theta_8 = \theta_7$
	Cubic $<$	X_9, Y_9, θ_9
	Line $<$	Y_{10}
	Ellipse $<$	X_j, Y_j
		$Y_{11} \rightarrow \theta_{11}$, X_{11}
	Line $<$	$Y_{12} \rightarrow X_{12}$, $\theta_{12} = \theta_{11}$
	Cubic $<$	X_{13}, Y_{13}, θ_{13}
	Line $<$	Y_{14}
	Ellipse $<$	Y_{15}
		27 Parameters

Figure 11, INPUT FOR GEOMETRY DESCRIPTION

-21-

geometry subroutine was subsequently modified so that the requisite tabular inputs are generated internally consistent with this generalization. This aspect is discussed in detail in Section IIIE, as well as in the user's manual for the FFCS which has been delivered to the AFFDL/FXG.

C. <u>Boundary Layer Computation Scheme</u> - A boundary layer computation scheme (BLCS) is needed for two reasons. First, in order to characterize the effective body shape in the separated region the boundary layer state up to the primary separation point needs to be defined. Furthermore, once the effective body shape has been determined, boundary layer calculations within this region are needed to define the surface conditions.

The boundary layer scheme selected for this purpose utilizes the streamline tracing concept with a small cross-flow assumption proposed by Vaglio-Laurin References (17) and (18). Details of the analysis may be found in References (19) and (20). These also describe the numerical procedures and computer code developed to implement this scheme. A user's manual for the BLCS is also available from the AFFDL/FXG. The selected method provides the three dimensional capability which is an essential feature of the viscous flow phenomena involved in the present study.

It should be noted that implementation of this computation scheme requires a priori knowledge of the inviscid pressure* variation along streamlines as well as the distribution of h_2, the parameter which characterizes the streamline spreading. Determination of these properties requires a streamline tracing capability. During the current contractual effort a special scheme valid for sharp nosed circular cones was developed which permitted boundary layer calculations to be performed up to the primary separation point only. A description of this analysis is given in the next section.

---

*For blunted cones the variation of edge entropy is also needed. This application has not been considered during the present study.

-22-

D. <u>Streamline Tracing Analysis</u> - The assumptions on which this analysis is based include that the flow is conical, the bow shock is straight and attached and the flow downstream of the shock is isentropic. Under these circumstances the components of velocity on the cone surface in the peripheral direction v_ϕ is related to that along cone generators v_R by the differential equation

$$\frac{d\,V_R}{d\phi} = V_\phi \sin\theta_c \tag{4}$$

where $V_\phi \equiv v_\phi/V_L$ and $V_R \equiv v_R/V_L$ are the velocity components normalized with respect to the limiting velocity and θ_c is the cone half angle. The coordinate notation is defined in Figure (12). Equation (1) follows from Equation (14-4) of Reference (21) when applied to the surface of the cone .

The velocity components can also be related to the local pressure via the equation

$$\frac{p}{p_\infty} = \left(\frac{1 - V^2}{1 - V_\infty^2}\right)^{\frac{\gamma}{\gamma-1}} \exp(-\Delta S/R) \tag{5}$$

where
$$V^2 \equiv V_\phi^2 + V_R^2 \tag{6}$$

V_∞ is the free stream velocity normalized with respect to V_L and $\Delta S/R$ represents the entropy jump across the oblique shock on the windward side in the plane of symmetry; i.e.:

$$\exp(-\Delta S/R) = p_{t_2}/p_{t_\infty} \tag{7}$$

The quantity $\Delta S/R$ is a constant under the assumed conditions and can be evaluated once and for all when the shock inclincation θ_s is known.

-23-
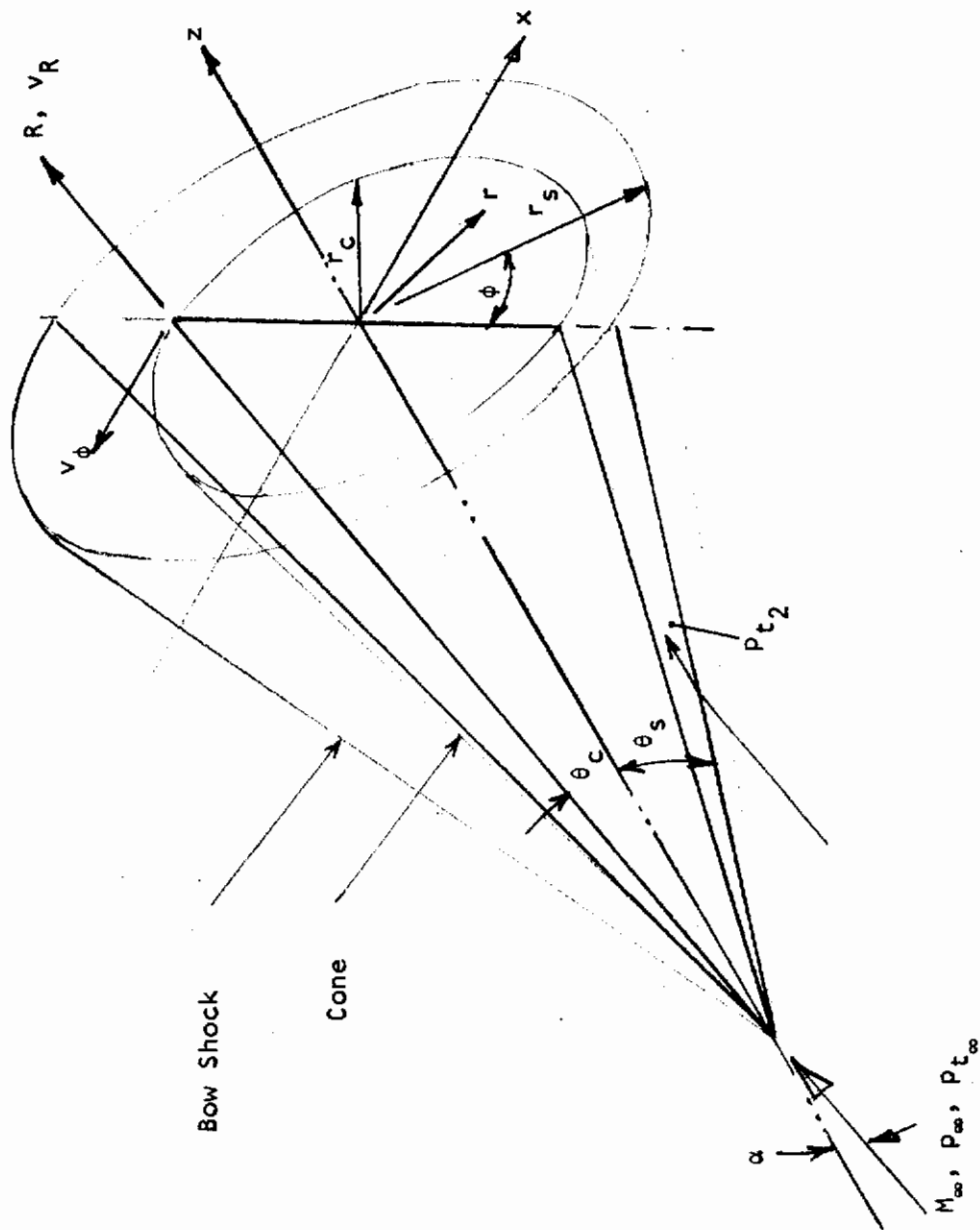
FIGURE 12. COORDINATE SYSTEM AND NOTATION

If the pressure distribution is prescribed as a function of ϕ Equations (4), (5) and (6) represent three equations for the determination of the two velocity components V_ϕ and V_R and the resultant V. This is the approach adopted here. Specifically, the pressure variation is considered to be given either as a tabular input, or, alternately is represented by curve fitting three points in accordance with the trigonometric relation

$$P(\phi) = A \cos \phi + B \cos 2\phi + C \tag{8}$$

where

$$P \equiv p/P_\infty$$

The coefficients appearing in Equation (8) are evaluated by specifying the pressures P_1, P_2 and P_3 at values of the peripheral angles ϕ_1, ϕ_2 and ϕ_3 respectively. Then

$$A = [P_1(B_2-B_3) + P_2(B_3-B_1) + P_3(B_1-B_2)] \, D^{-1} \tag{9a}$$

$$B = [P_1(A_3-A_2) + P_2(A_1-A_3) + P_3(A_2-A_1)] \, D^{-1} \tag{9b}$$

$$C = [P_1(A_2B_3-A_3B_2) + P_2(A_3B_1-A_1B_3) + P_3(A_1B_2-A_2B_1)] \, D^{-1} \tag{9c}$$

where

$$D = A_2B_3 + A_3B_1 + A_1B_2 - A_2B_1 - A_1B_3 - A_3B_2 \tag{9d}$$

and

$$A_i \equiv \cos \phi_i$$
$$B_i \equiv \cos 2\phi_i$$

Equation (8) has been found to provide a good representation of pressure variation around sharp circular cones at incidence (Reference 22) at least for angles $0 < \phi < 120^\circ$.

With $P(\phi)$ specified the variation of the resultant velocity $V(\phi)$ can be obtained in an elementary manner from Equation (5). Determination of $V_\phi(\phi)$ and $V_R(\phi)$ requires numerical integration of Equation (4). The procedure utilized here is as follows. In terms of the finite difference mesh defined in Figure (13) we can write the central difference form of Equation (4) as

$$V_R(i) = V_R(i-2) + 2 V_\phi(i-1) \Delta\phi \sin \theta_c \tag{10}$$

Equation (10) permits calculation of V_R at a generic point i within an error of order $(\Delta\phi)^2$ in terms of data evaluated at the two preceding mesh points. The corresponding value of V_ϕ is given by virtue of Equation (6) as

$$V_\phi(i) = [V^2(i) - V_R^2(i)]^{\frac{1}{2}}$$

where we recall that $V(i)$ is known at all $\phi(i)$. To initiate this procedure we apply the boundary condition

$$V_\phi(1) = 0$$

$$V_R(1) = V(1)$$

which follows from symmetry considerations since $\phi(1) = 0$. We also make use of the one sided difference form of Equation (4); viz.

$$V_R(2) = V_R(1) + \frac{V_\phi(2)}{2} \Delta\phi \sin \theta_c \tag{11a}$$

also
$$V_R^2(2) + V_\phi^2(2) = V^2(2) \tag{11b}$$

Elimination of $V_R(2)$ between these two equations yields the quadratic relation

$$a V_\phi^2(2) + b V_\phi(2) + c = 0 \tag{12}$$
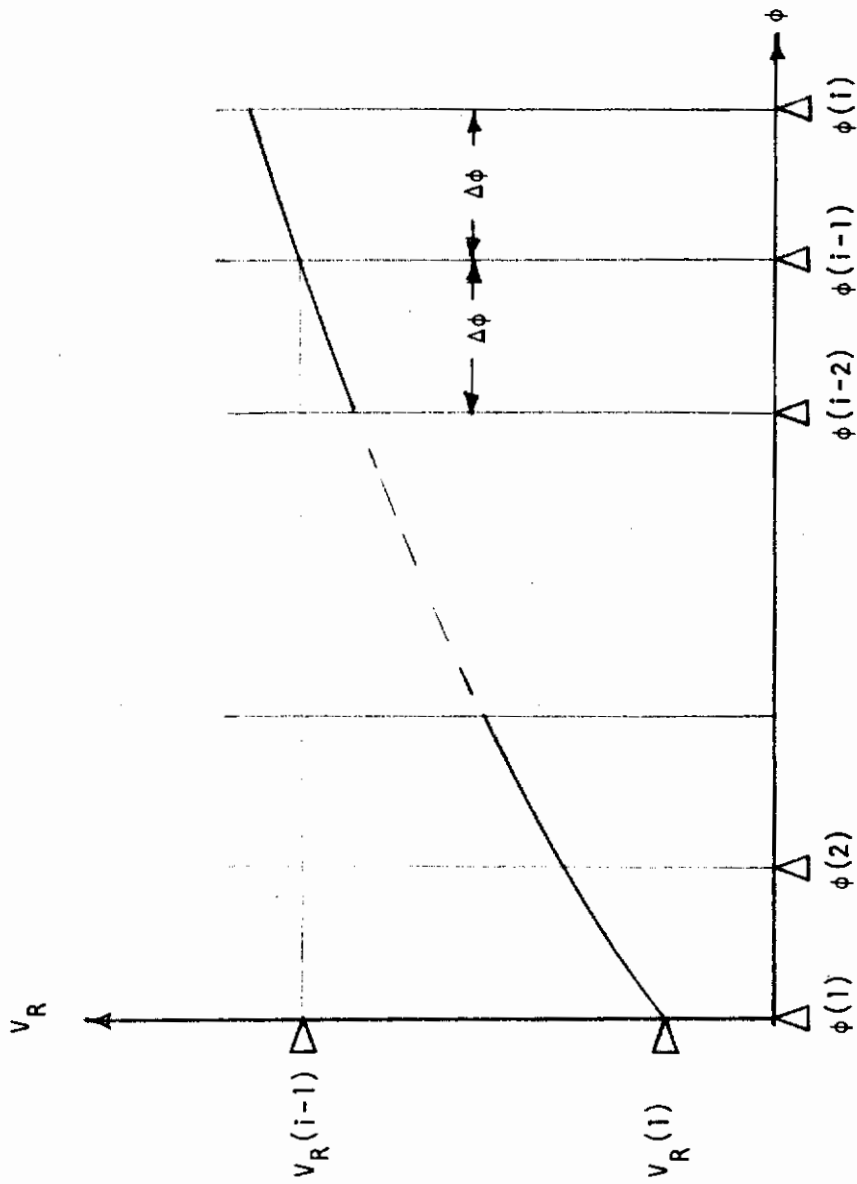
FIGURE 13. FINITE DIFFERENCE MESH FOR INTEGRATION OF CONICAL FLOW VARIABLES

where

$$a = 1 + \left(\frac{\Delta\phi \sin \theta_c}{2}\right)^2$$

$$b = V_R(1) \cdot \Delta\phi \sin \theta_c$$

$$c = V_R^2(1) - V^2(2)$$

Equation (11b) and (12) permit evaluation of $V_\phi(2)$ and $V_R(2)$, in this case, within an error of order $\Delta\phi$. Accordingly V_ϕ, V_R and V can be determined for all ϕ by a step by step integration procedure using Equation (10). Certain auxiliary relations which are of interest can then also be computed. In particular, the flow inclination relative to cone generators ψ is determined from the relation

$$\psi = \text{arc tan } (V_\phi/V_R) \tag{13}$$

The derivative $\partial V_\phi/\partial\phi$ is also needed. Following Reference (22) this is given by

$$\frac{1}{V} \frac{\partial V_\phi}{\partial\phi} = \left[\frac{\sin^2\theta_c}{4} - \frac{1}{\gamma M_e^2} \left(\frac{1}{P} \frac{\partial^2 P}{\partial\phi^2}\right)\right]^{\frac{1}{2}} - \frac{\sin \theta_c}{2} \tag{14}$$

where

$$M_e^2 = \frac{2V^2}{(\gamma-1)(1-V^2)} \tag{15}$$

For the case when the pressure distribution is curve fit, the second derivative of pressure follows immediately from Equation (8); viz:

$$\frac{\partial^2 P}{\partial\phi^2} = -(A \cos \phi + 4 B \cos 2\phi) \tag{16}$$

For the case where the pressure distribution is represented by a tabular input of P vs. ϕ Equation (14) is replaced by

$$\left(\frac{1}{V} \frac{\partial V_\phi}{\partial\phi}\right)_i = \frac{V_\phi(i+1) - V_\phi(i)}{V(i) \Delta\phi} \tag{17}$$

With the conical flow field thus established tracing of streamlines on the surface of the cone requires determination of the streamwise increment ds associated with an arbitrary increment dR along a conical ray starting at any generic point[*] $Q(R_j, \phi_j)$. This is given by

$$ds^2 = dR^2 + r_c^2 \, d\phi^2 \tag{18}$$

where r_c is the local radius of the cone which is a known function of R; i.e.: $r_c = R \sin \theta_c$. In Equation (18) $d\phi^2$ is obtained from

$$d\phi = \frac{\tan \psi_j \, dR}{R_j + dR} \tag{19}$$

which follows by definition from Equation (13). In Equation (19) the streamline inclination ψ is to be evaluated at $\phi = \phi_j$ as indicated by the subscript. On the other hand, the cone radius r_c is evaluated at $R = R_j + dR$. A step by step application of Equations (18) and (19) yields the streamline trace in terms of its coordinates R and ϕ. The pressure, velocities, etc., along the streamline can then be determined by interpolation with respect to ϕ within the conical solution previously obtained.

The final ingredient needed for the boundary layer analysis is the metric for the coordinate normal to the streamlines, h_2, which is a measure of the local streamline spreading. This can be determined from the differential equation[**]

$$\frac{d \ln h_2}{ds} = \frac{d \ln r_c}{ds} + \frac{1}{r_c V} \cdot \frac{\partial V_\phi}{\partial \phi} \tag{20}$$

---

[*]We use subscript j here to distinguish mesh points along streamline traces from the discrete intervals at which the conical solutions are obtained.

[**]Equation (20) is actually an approximate version of Equation (B-11) of Reference (17). The approximation resides in the fact that the cone radius r_c appearing on the right hand side should actually be the radius of the equivalent body of revolution as defined in Appendix B of Reference (17). For the relatively shallow cone half angles and angles of attack for which this analysis has been developed this approximation should be reasonable. Note that the percent difference between r_c and the actual curvature can be estimated to be on the order of $100 \, (1 - \cos \psi \, \cos \theta_c)$.

Again, a finite difference scheme is employed to integrate Equation (20).
The form taken is

$$(h_2)_{j+1} = \exp(F_1 + F_2) \tag{21a}$$

$$F_1 = \ln\left[(r_c)_{j+1} (h_2)_j (r_c)_j^{-1}\right] \tag{21b}$$

$$F_2 = \frac{ds}{2}\left[\left(\frac{1}{r_c V}\frac{\partial V_\phi}{\partial \phi}\right)_{j+1} + \left(\frac{1}{r_c V}\frac{\partial V_\phi}{\partial \phi}\right)_j\right] \tag{21c}$$

Initial conditions for Equation (20) are applied at $R = dR$ in accordance with

$$h_2 = \sin\theta_c (dR)^{1 + \frac{3}{2}k} \tag{22}$$

where

$$k = \frac{2}{3}\frac{\partial V/\partial \phi}{V \sin\theta_c} \tag{23}$$

Equation (22) gives the correct limiting behavior for zero angle of attack
(i.e. $h_2 \rightarrow r_c$) and is consistent with the known solution for $\phi = 0$ as developed by Roshotko (Reference 23).

The procedure utilized to integrate Equations (18) and (21) is as
follows:

1. Starting at a generic point j the variable R is incremented by an
   amount dR from which $(r_c)_{j+1} = (R_j + dR)\sin\theta_c$ is computed.

2. Since ψ_j is known, the increment $d\phi$ can be computed from Equation (19).

3. The increment ds then follows directly from Equation (18).

4. With $\phi = \phi_j + d\phi$ interpolation within the stored conical solution yields the value of $(1/V \, \partial V_\phi/\partial \phi)_{j+1}$ needed in Equation (21).

5. The right hand side of Equation (21a) can now be evaluated yielding the desired value of $(h_2)_{j+1}$.

In carrying out this procedure a test is made on the relative change of $1/V \, \partial V_\phi/\partial \phi$ corresponding to a choice of dR. If the change is greater than a certain tolerance the step size is halved and the integration step is repeated. Thus, the step size for integration is controlled internally by the computer logic based on the specified tolerance. Numerical experiments made using the computer code based on this analysis have shown that a relative change of 5% or less provides sufficient accuracy.

The computer code based on this analysis is called STRMLN and is described in detail in the user's manual which is available from the AFFDL/FXG Numerical results obtained using this code and an assessment of its accuracy are presented in Section IIIA below.

E. <u>Determination of Effective Body Shape</u> - The approach utilized to determine the effective body shape involved use of the FFCS described in Section IIB above in conjunction with data supplied by the Air Force, Reference (24). The latter consisted of surface pressure and heat transfer measurements around the periphery of a 6° half angle cone approximately 36 inches long and pitot and total temperature distributions throughout the shock layer. These measurements were obtained at a free stream Mach number $M_\infty = 6$ and unit Reynolds number of 4.25×10^5 per inch with the cone at angles of attack $\alpha = 3, 6, 9$ and 12 degrees. These tests were conducted with both a sharp cone and blunted cone (nose radius = 0.4 inches).

The effective body shapes for each of these cases was established by an iterative procedure wherein different body shapes were prescribed as input to the computer code until a satisfactory match of the calculated surface pressure

-31-

variation with the measurements was obtained. This procedure was entirely successful as will be demonstrated by the results presented in the next section. Further confirmation of the adequacy of the resulting flow field calculations was provided by comparison of the calculated and measured pitot pressure distributions. Again, excellent agreement was obtained. Results of these comparisons are also shown in the next section.

Once this step had been completed it was possible to characterize the effective body shape dependence on angle of attack by relating the peripheral distribution of shear layer thickness to the displacement thickness at the primary separation point. The latter, of course, was estimated by means of the BLCS described in Section IIC.

At this point in the development it was necessary to generalize the nominal body shapes thus established to account for the effects of Mach number and cone half angle[*] as well as for angles of attack greater than those studied above (i.e., $\alpha/\theta_c > 2$). This generalization, or extrapolation would be established by utilization of other data which is available (cf: Table I) as well as the pressure correlations which were developed under the current ATL effort. These pressure correlations are an essential ingredient of our method of approach and are discussed in the next section.

F. <u>Leeward Side Pressure Correlations</u> - Since the number of geometric and flight parameters which define the flow configuration are numerous (α, θ_c, M_∞, Re_∞) and their range of interest quite extensive it was recognized, at the outset of this study, that detailed analysis of data for all conditions and ranges of conditions would not be feasible. Accordingly, the approach adopted here was to establish the basic form of our analytic model from detailed examination of a limited set of experimental results and then utilize the remaining data to "calibrate" the model to properly account for variations in M_∞, etc.

---

[*]Reynolds number effects are taken into account automatically via the displacement thickness calculation at the primary separation point.

TABLE I

SOURCE OF EXPERIMENTAL DATA EXAMINED

Investigator and Reference	M_∞	$Re_\infty x$ (millions)	α(degrees)	θ_c(degrees)	(s/r_n)
Anderson (25)	10.8	.003 - .04	1-15	10.0	sharp
Buck (26)	7.5, 11.0, 14.0	1.6 - 50.0	5-20	7.0	25-80
Feldhuhn (3)	5.07	.5 - 5.0	10-30	5.0	sharp
Fitch (27)	10.2	.86 - 8.5	14.0	7.1	sharp
Horstmann (28)	41.0*	.04 - .5	5, 10, 15	3.0	sharp
Rhudy (24)	6.0	3.5 - 15.0	3-12	6.0	sharp + 22-84
Rainbird (2)	1.8, 4.25	21.2, 43.4	15.6, 22.8	12.5	sharp
Stetson (4)	14.5	.056 - .80	2-18	5.6	sharp + 8-92.5 2.4-23.6
Tracy (1)	7.95	.05 - .4	2-24	10.0	sharp
Widhopf (6)	5.0	1.0 - 50.0	10-27.5	9.0	1.05-5.25
Yahalom (5)	2.72	.35 - .56	5-30	10, 15, 20	sharp
Zakkay (29)	6.0	4.0 - 40.0	7.5-22.5	7.5	sharp

*Helium Tunnel

-33-

The Air Force data of Reference (24) was selected as the primary source for the model development since it provided the most detailed set of measurements at conditions which were of most interest from a practical standpoint and permitted systematic examination of the effect of angle of attack. The latter, of course, is the essential parameter controlling the phenomenon.

The remaining data was utilized to establish a correlation which could allow estimates to be made of the pressure ratios p_L/p_∞, p_p/p_∞ and p_s/p_∞ as defined in Figure (4) for given values M_∞, α/θ_c and Re_∞, x, the latter being a Reynolds number based on free stream conditions and length along a conical ray. Although some of the data sources gave anomalous results, a satisfactory correlation was achieved and is presented in the next section. With this correlation available the means for calibrating the analytic model for any combination of the controlling parameters is available.

G. <u>Summary</u> - ATL's method of approach may be summarized as follows:

1. The separated regions of high shear on the leeward side are represented analytically by modifying the body cross sections in an appropriate manner.

2. The form of these modifications is determined by an iterative procedure involving the Kutler flow field program and selected pressure data - a match of calculated and measured surface pressure distributions defines the desired body shapes.

3. Generalization of these effective body shapes for practical ranges of interest of the controlling parameters is established by "calibration" of the model using the available experimental data in the form of pressure correlations.

4. A description of the flow field throughout the shock layer is obtained by means of the Kutler program applied to a body geometry which takes on the effective shapes as deduced above.

SECTION III

NUMERICAL RESULTS AND COMPARISON WITH EXPERIMENT

A. Streamline Tracing Scheme - Typical results obtained with the STRMLN code are shown in Figure (14). These results correspond to one of the experimental cases of Reference (24) so that the requisite pressure input could be obtained directly from measurements. In Figure (15) the pressure distribution determined by Equation (8) is compared with these measurements. As can be seen the agreement is excellent and demonstrates the applicability of the form selected for curve fitting of these pressure distributions.

A further check on the validity of this formulation is provided by the results shown in Figure (16). Here we have compared the flow inclination ψ as computed by the STRMLN code with that predicted by the FFCS. Further indirect evidence of the satisfactory performance of the STRMLN is provided by the boundary layer results presented in the next section.

B. Boundary Layer Computation Scheme - To verify the adequacy of the selected BLCS a series of calculations were carried out at conditions for which experimental data were available for comparison. Representative results are shown in Figures (17) through (21). In Figure (17) estimates of Stanton number variation along the several streamlines defined in Figure (10) are shown. These include the most windward streamline ($\phi_o = 0^o$) as well as those which issue (initially) in the $\phi_o = 22\frac{1}{2}^o$, $47\frac{1}{2}^o$ and 60° azimuthal direction; i.e.: at zero incidence these streamlines would be coincident with the cone generators defined by these values of ϕ.

The Stanton number estimates are compared with the experimental distributions deduced from the Air Force data (Reference 24) in Figure (17) and indicate excellent agreement in both the laminar and fully turbulent regions.[*]

---

*Note that the computer code described in Reference (20) has both a laminar and turbulent boundary layer capability which has been exercised here. This program also has a built-in transition criterion and an entropy swallowing option as well. For the present purpose, however, the program's transition option was bypassed and transition was forced to occur at the axial station implied by the data as indicated in these figures. These options have been included in the BLCS.
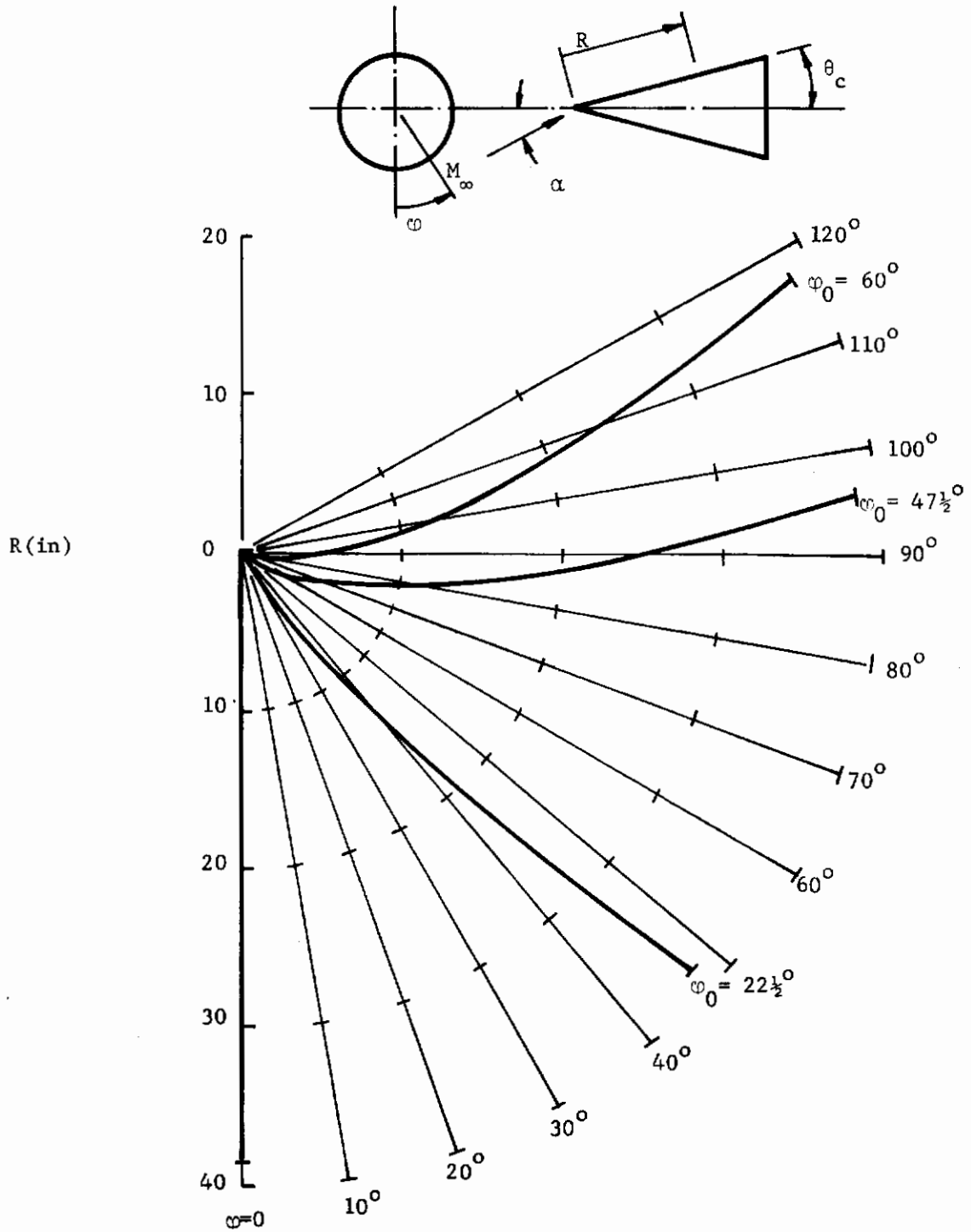
FIGURE 14   STREAMLINE TRACES ON SHARP CIRCULAR CONE AT INCIDENCE
$M_\infty = 6$, $\alpha = 12^o$, $\theta_c = 6^o$
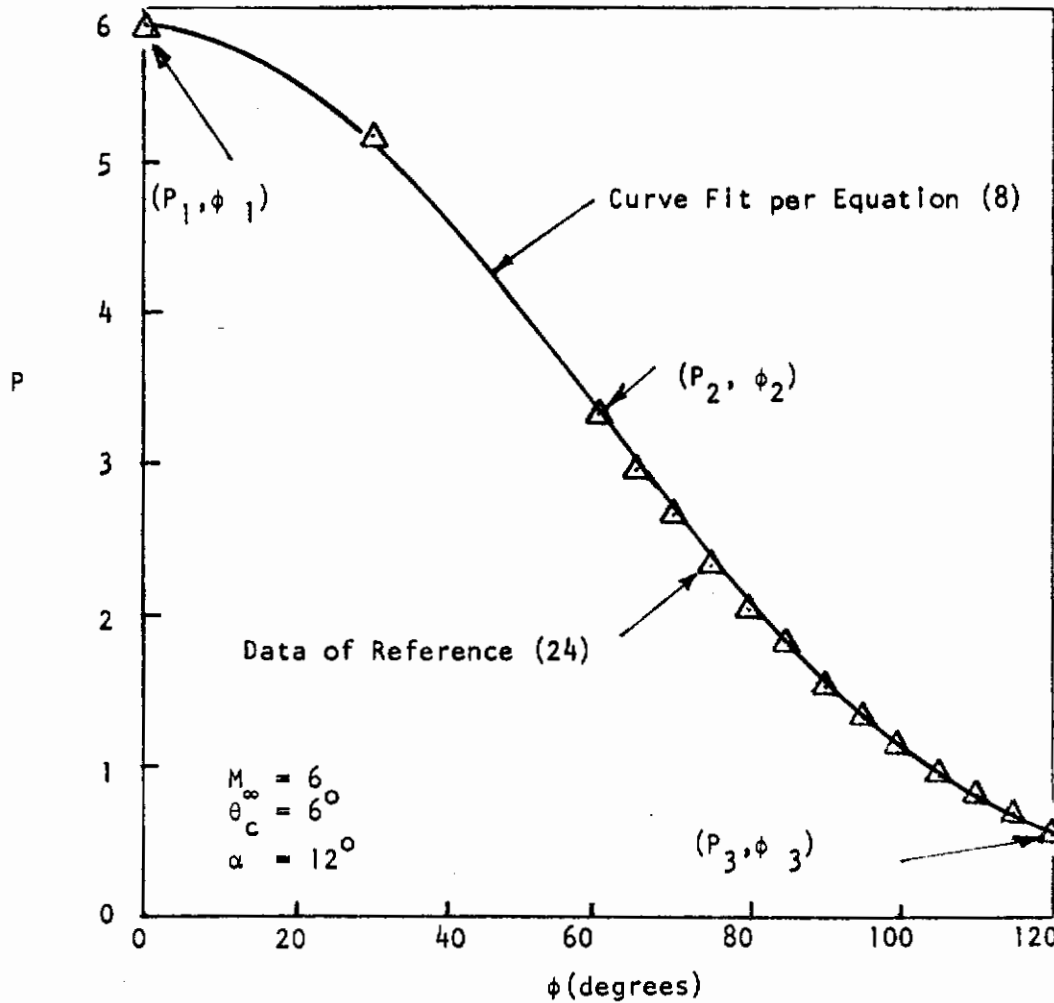
-36-

FIGURE 15.   COMPARISON OF MEASURED PRESSURE DISTRIBUTION WITH
             CURVE FIT REPRESENTATION FOR SHARP CONE AT
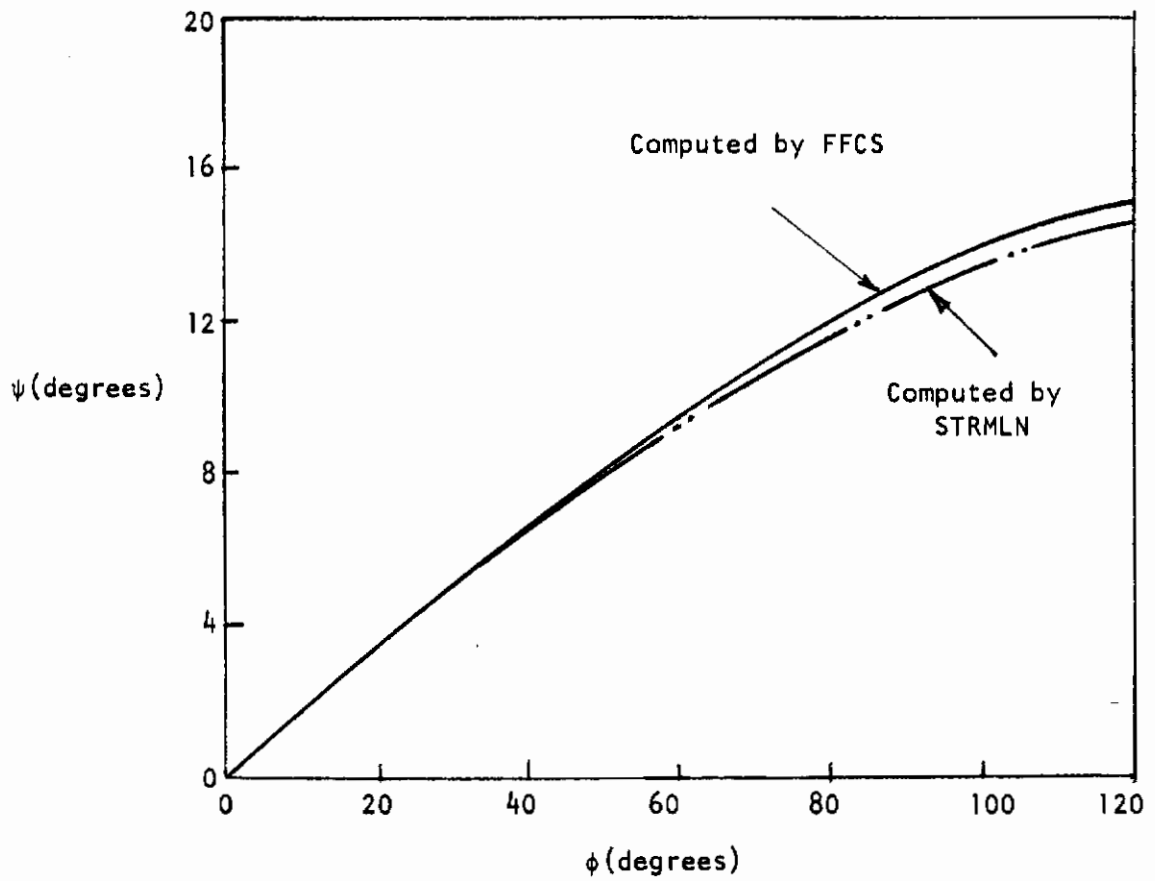   INCIDENCE

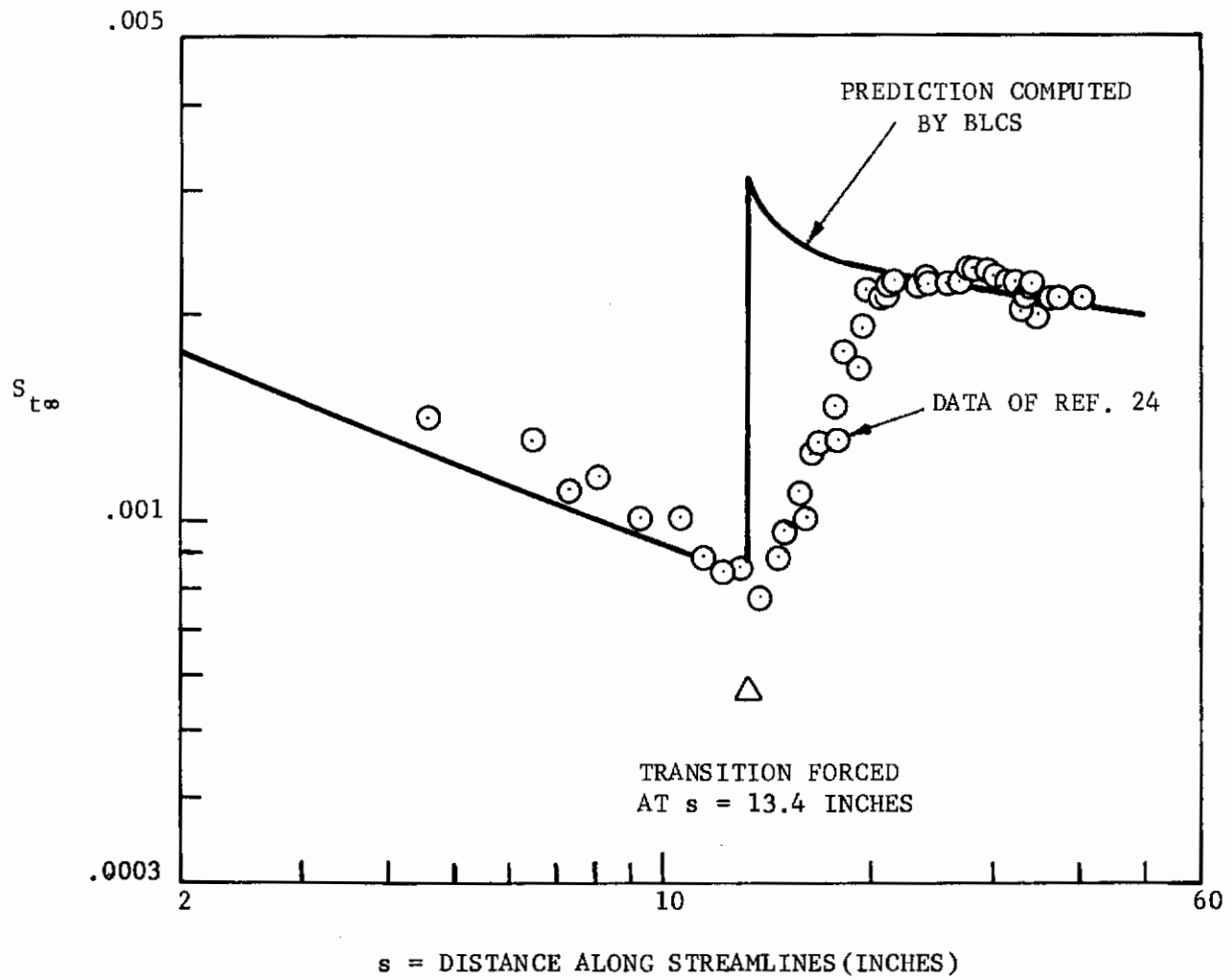FIGURE 16.   COMPARISON OF PREDICTIONS BY STRMLN AND FFCS
FOR FLOW INCLINATION

-38-

FIGURE 17   STANTON NUMBER VERSUS DISTANCE ALONG STREAMLINE FOR $\alpha = 12^{o}$
(a) WINDWARD PLANE ($\varphi_{o} = 0$)

-39-

FIGURE 17   (CONTINUED)
(b) $\omega_o = 22\frac{1}{2}^{\circ}$

-40-

FIGURE 17   (CONTINUED)
(c) $\psi_o = 47\frac{1}{2}^o$

-41-

$\triangle$ s = 8.4 INCHES
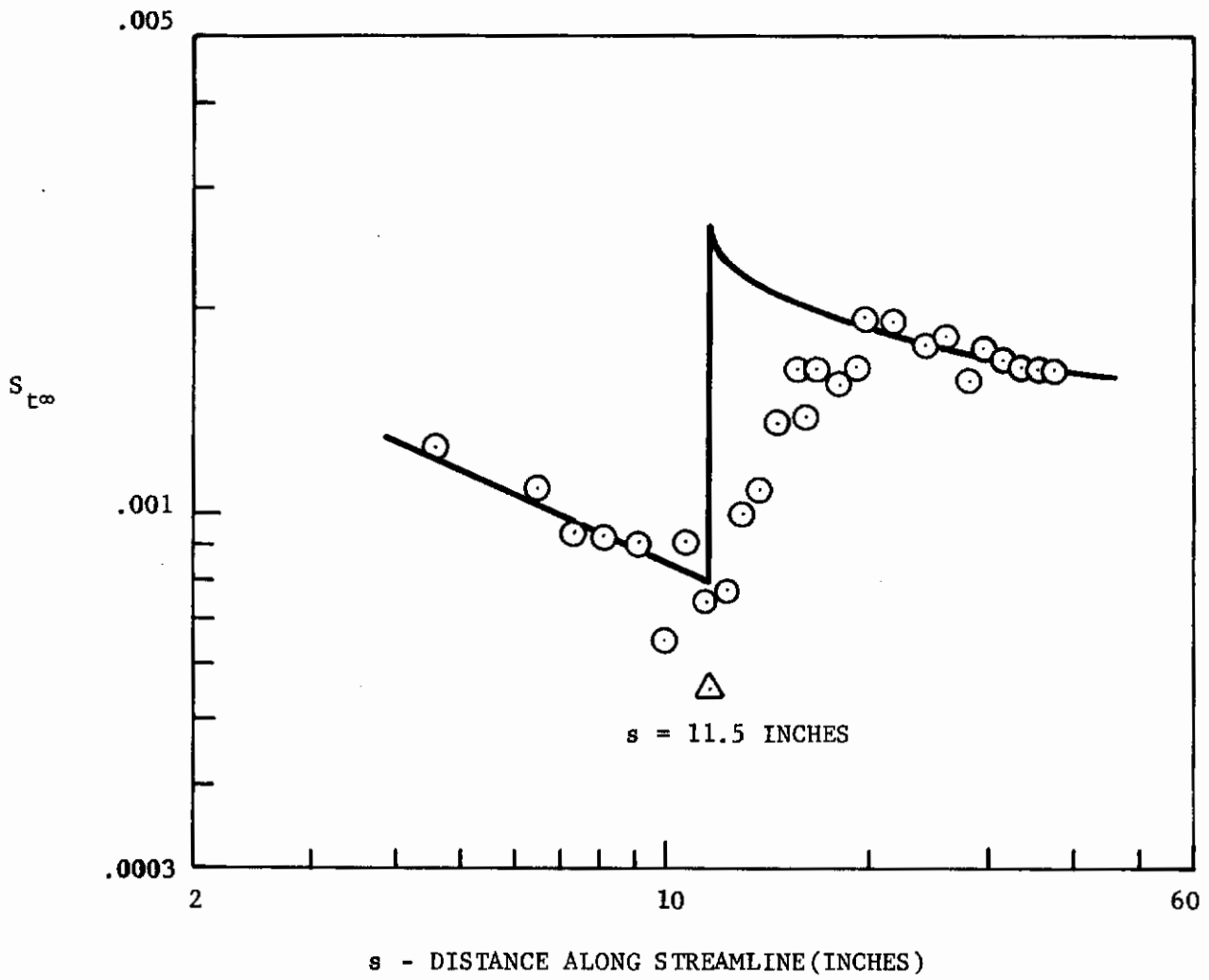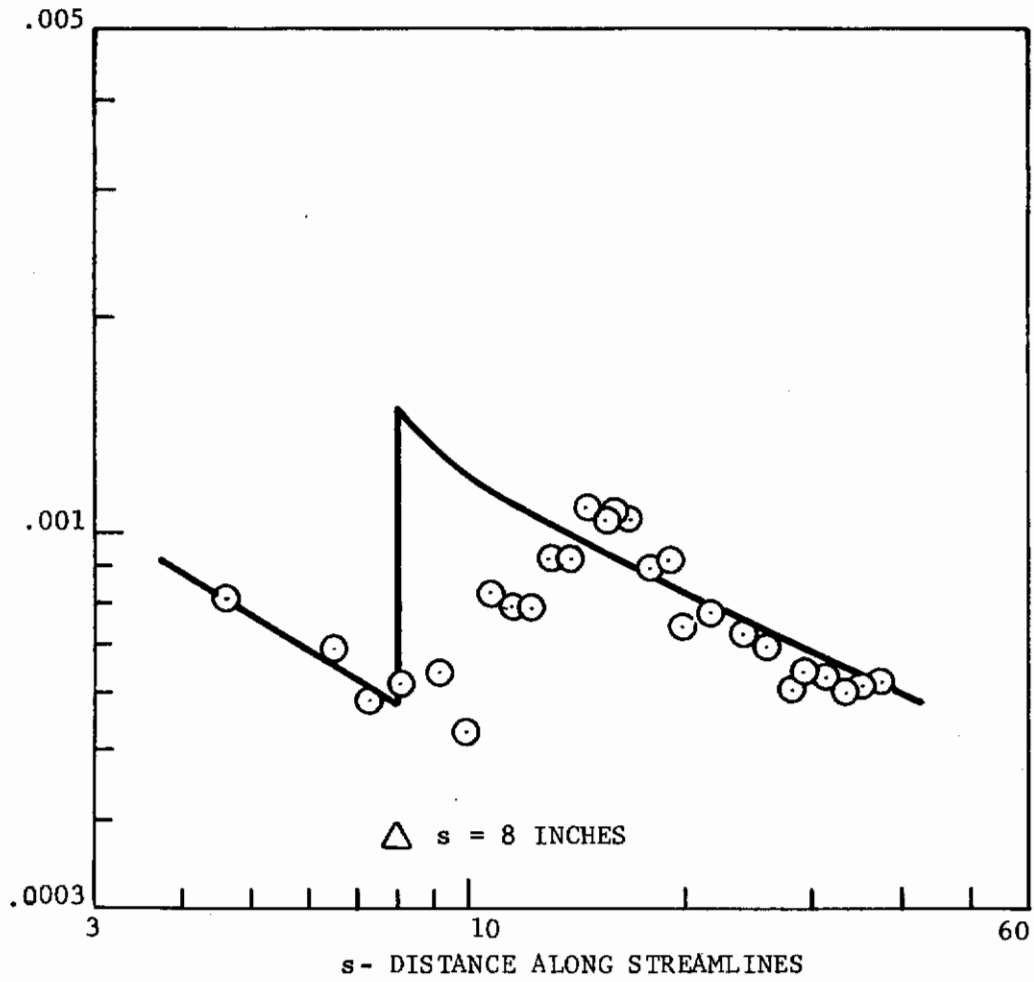
s - DISTANCE ALONG STREAMLINES (INCHES)
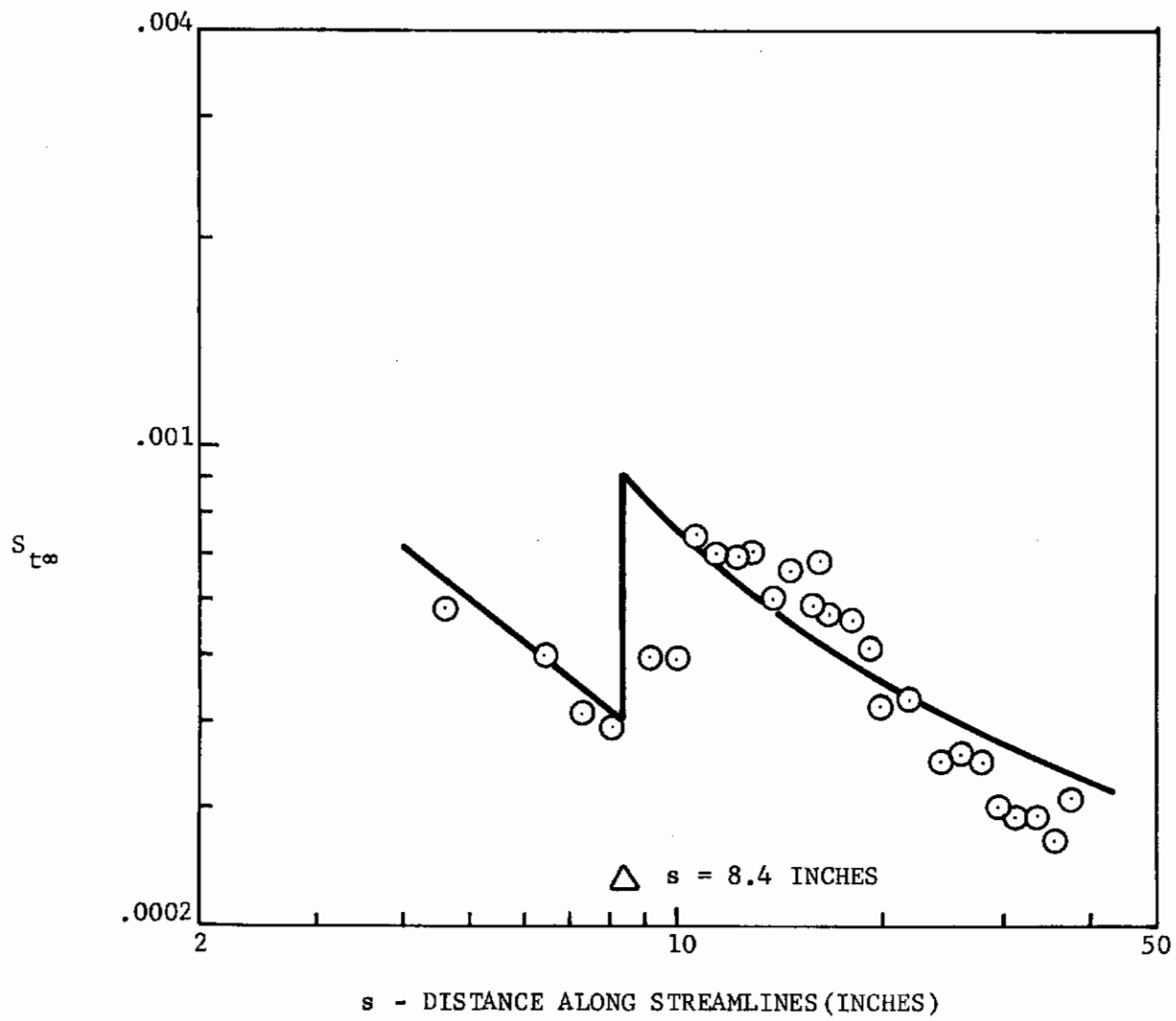
FIGURE 17 (CONTINUED)
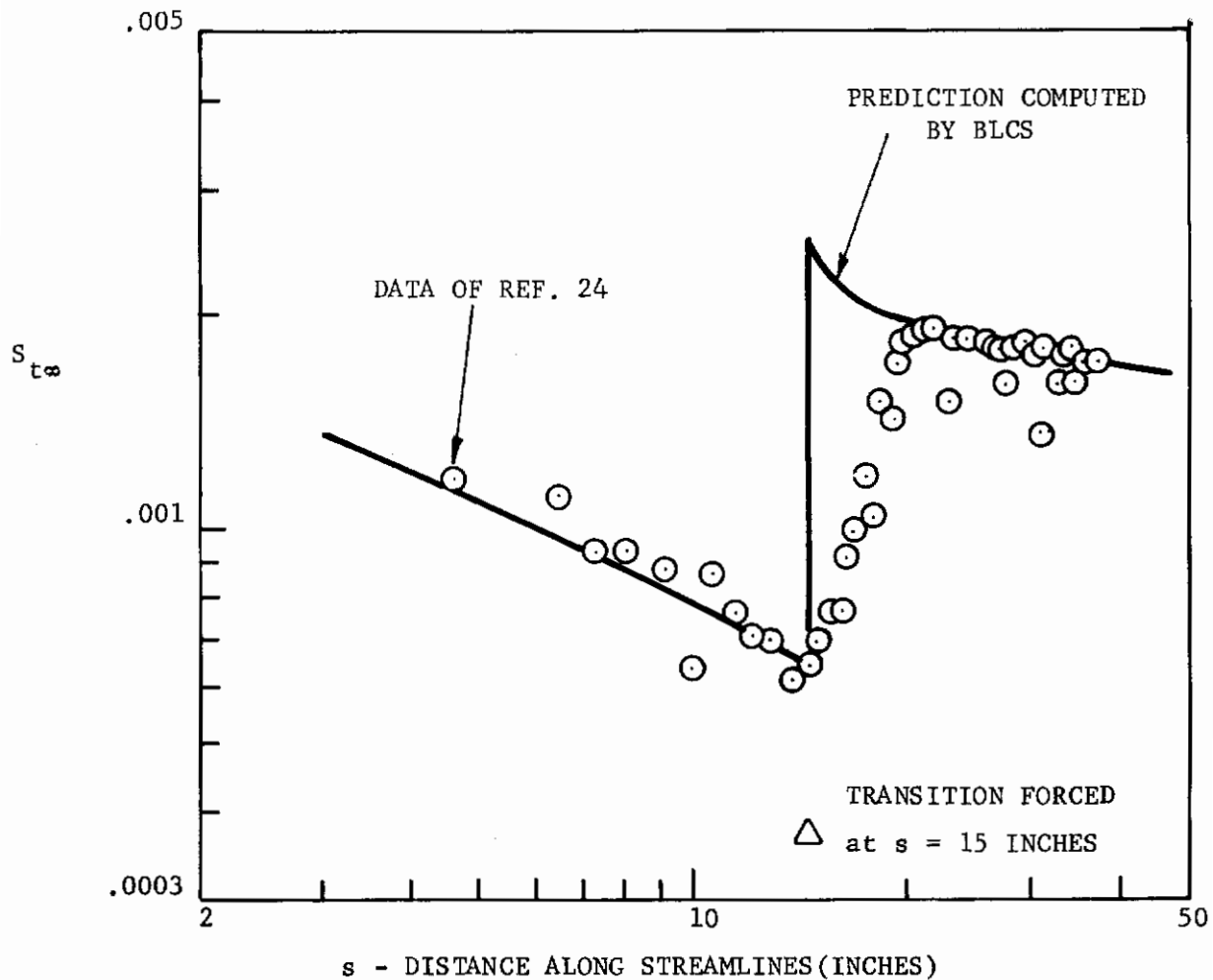(d) $\varphi_o = 60^o$

-42-

FIGURE 18   STANTON NUMBER VS. DISTANCE ALONG STREAMLINE ON
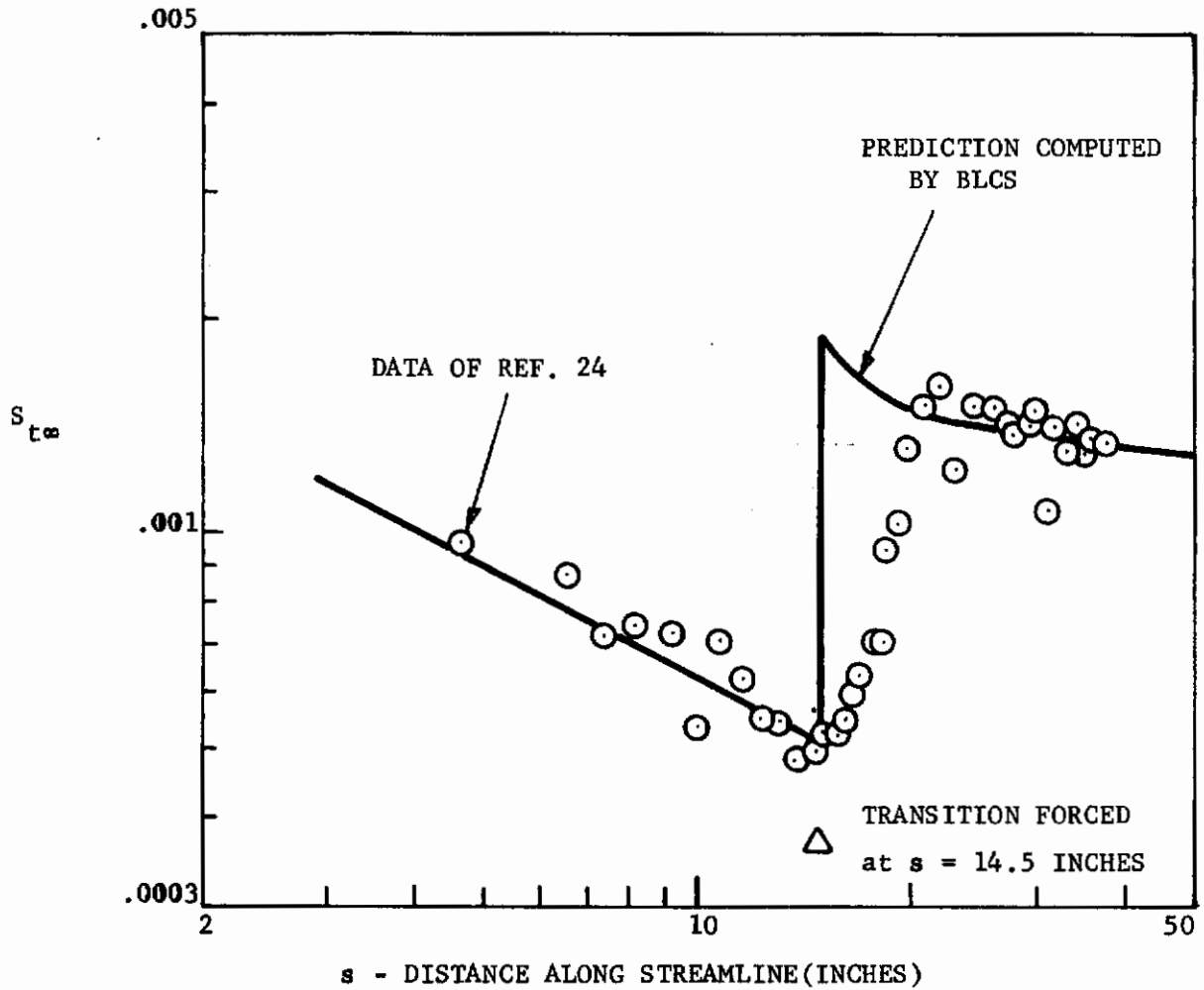WINDWARD PLANE FOR $\alpha = 6^{\circ}$

FIGURE 19   STATON NUMBER VS. DISTANCE ALONG STREAMLINE AT WINDWARD
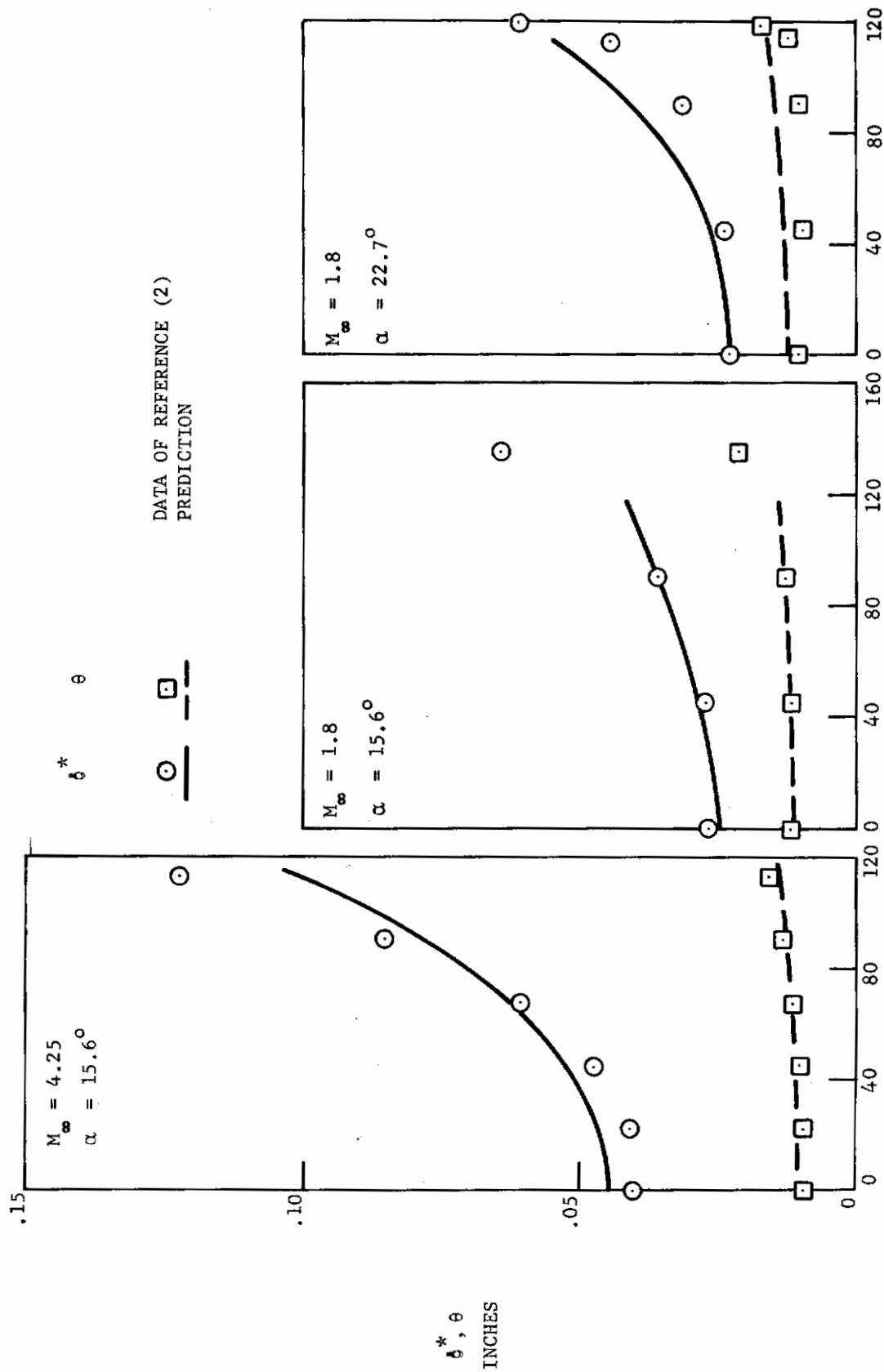PLANE FOR $\alpha = 9^\circ$

FIGURE 20 COMPARISON OF THEORY AND EXPERIMENT FOR INTEGRAL THICKNESS ON SHARP CIRCULAR CONE AT INCIDENCE ($\theta_c = 12\frac{1}{2}°$)

-45-

Additional comparisons for the windward streamline at angles of attack
$\alpha = 6^\circ$, 9° are presented in Figures (18) and (19) respectively. Evidently,
the agreement for these cases is as accurate as for the $\alpha = 12^\circ$ results
shown in Figure (17).

A demonstration of the adequacy of the BLCS in terms of its ability
to predict integral thickness variation around yawed cones is shown in
Figure (20). The comparison here is with the data of Rainbird (Reference
2). To obtain our theoretical estimates a number of streamlines were
traced at the appropriate values of angle of attack and Mach number up to
an axial station $x \stackrel{\sim}{=} 35$ inches corresponding to the point where Rainbird's
profile data and integral thicknesses were determined. With the pressure
distribution and spreading parameter h_2 thus determined, the BLCS was
exercised yielding the variation of δ^* and θ along the entire streamline.
The desired values needed for comparison with the experimental results were
then read off at the appropriate axial stations.

The results are shown in Figure (20) for all of the cases examined in
Reference (2). As can be seen, the agreement for both integral thicknesses
is satisfactory up to peripheral angles of $\phi \stackrel{\sim}{\sim} 120^\circ$.

Additional evidence of the excellent performance of the BLCS in terms
of displacement thickness predictive capability is demonstrated in Figure
(21). Here we have compared the pressure measurements of Reference (24)
with those computed by means of the FFCS with and without the displacement
thickness effect predicted by the BLCS. The latter distributions are shown
in Figure (22). It is interesting to note that despite the relatively high
Reynolds numbers which are involved here a small but discernible viscous
interaction effect is evident even on the windward portions of the cone.

Finally, in Figures (23) and (24), results are presented which demon-
strate, indirectly, the satisfactory performance of the STRMLN code in terms
of the computation of the streamline spreading parameter h_2. Thus, in Figure

-46-

DATA OF REFERENCE(22) ($M_\infty = 6$; $\theta_c = 6^\circ$; $X/L = .955$)

PREDICTION WITH DISPLACEMENT THICKNESS

PREDICTION FOR CIRCULAR CONE

$\alpha = 6^\circ$

$\alpha = 9^\circ$

$\alpha = 12^\circ$

φ - degrees

p/p_8
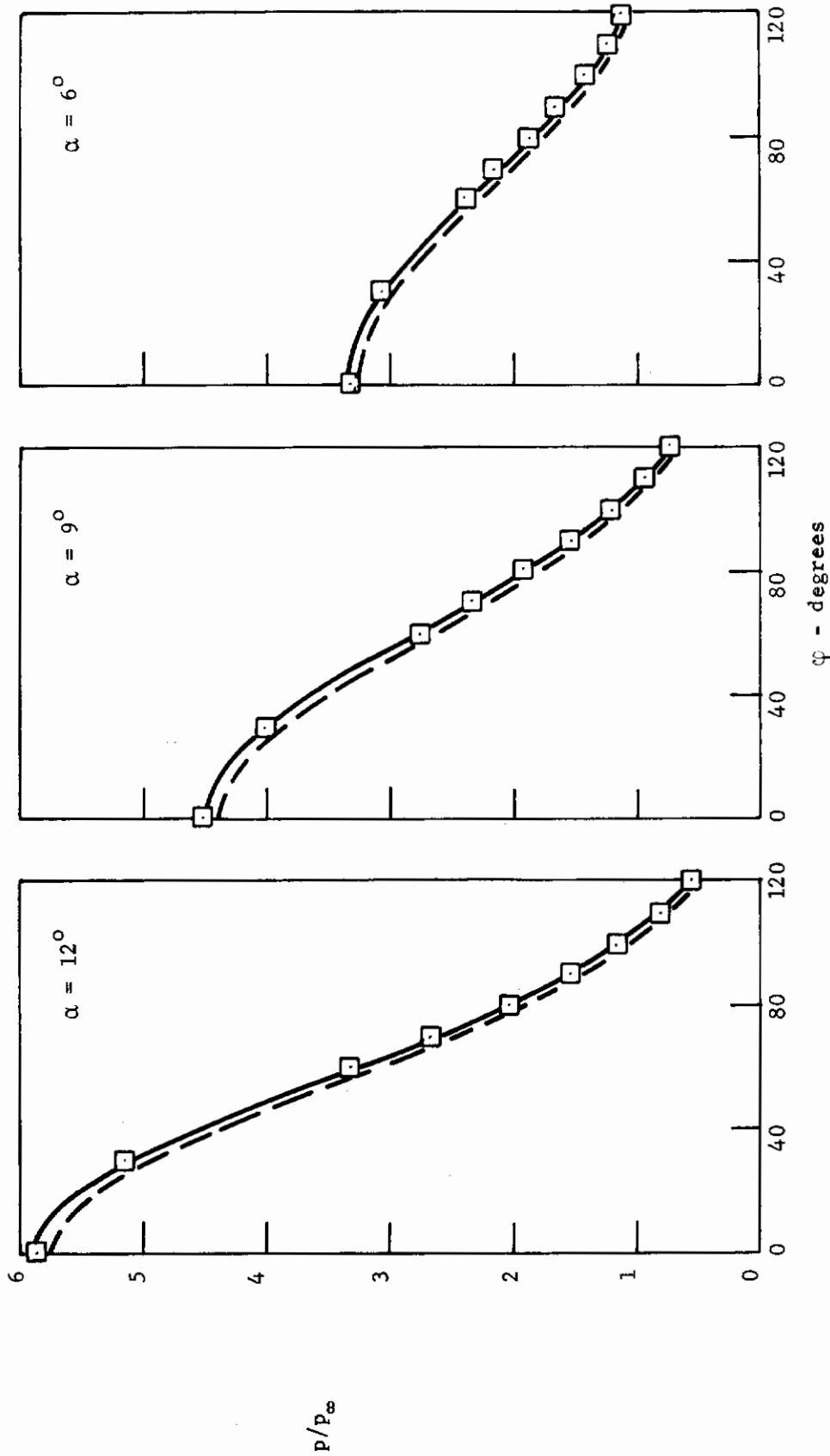
FIGURE 21   COMPARISON OF THEORY AND EXPERIMENT FOR PRESSURE DISTRIBUTION OVER SHARP CONES AT INCIDENCE

$M_\infty = 6$; $\theta_c = 6°$; $Re_\infty/ft = 5.1 \times 10^6$

R_c (CONE RADIUS) = 3.83 INCHES

$\alpha = 0$

$3°$

$6°$

$9°$

$12°$

φ - degrees

δ^*/R_c
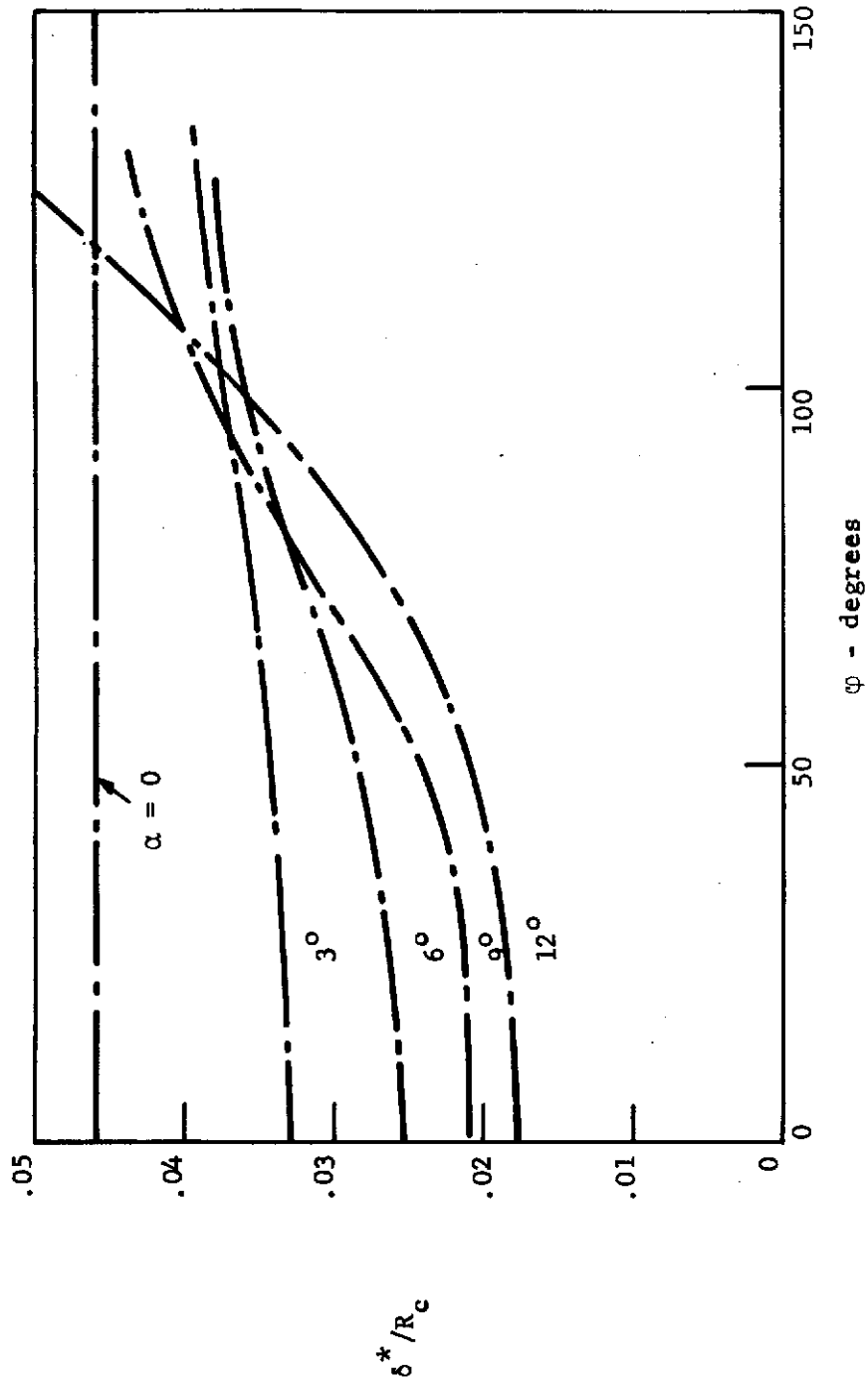
FIGURE 22 ESTIMATED DISPLACEMENT THICKNESS DISTRIBUTION OVER SHARP CONES AT INCIDENCE
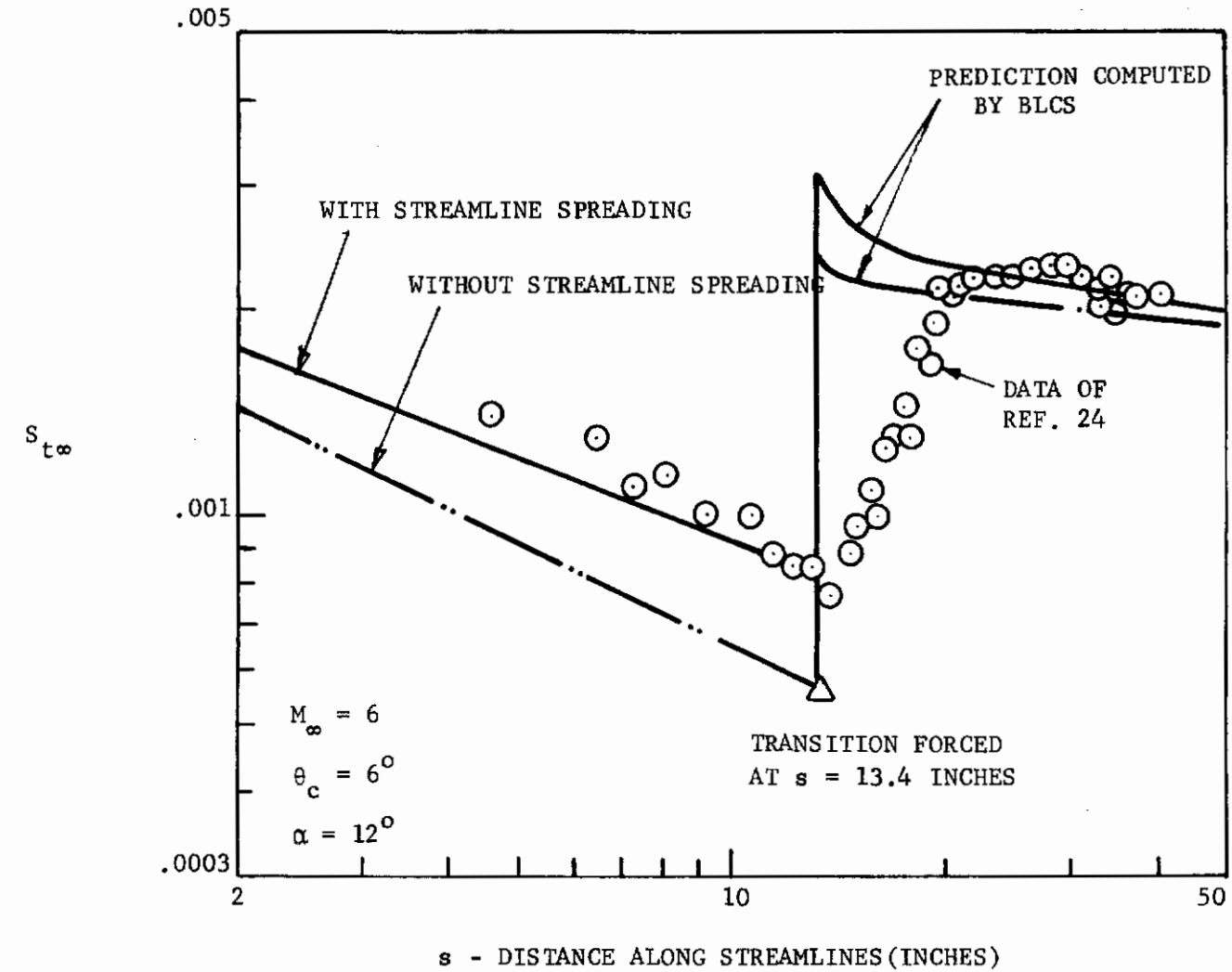
FIGURE 23 COMPARISON OF STANTON NUMBER VARIATION COMPUTED WITH AND
WITHOUT THE EFFECT OF STREAMLINE SPREADING

-49-

δ^*, INCHES

.06

.04

.02

0

DATA OF REFERENCE (2)

S_t

.002

WITH STREAMLINE SPREADING

WITHOUT STREAMLINE SPREADING

.001

0

0   10   20   30   40

s - INCHES

FIGURE 24   COMPARISON OF DISPLACEMENT THICKNESS AND STANTON NUMBER
VARIATION ALONG THE WINDWARD PLANE WITH AND WITHOUT THE
STREAMLINE SPREADING EFFECT.

$M_\infty = 4.25$; $\theta_c = 12\frac{1}{2}^\circ$; $\alpha = 15.6^\circ$

(23) we repeat the comparison shown earlier in Figure (17a) and include an additional computation due to the BLCS but without the effect of streamline spreading. That is, in one case the computation was carried out using the h_2 distribution determined by the STRMLN while in the second case the actual geometric body r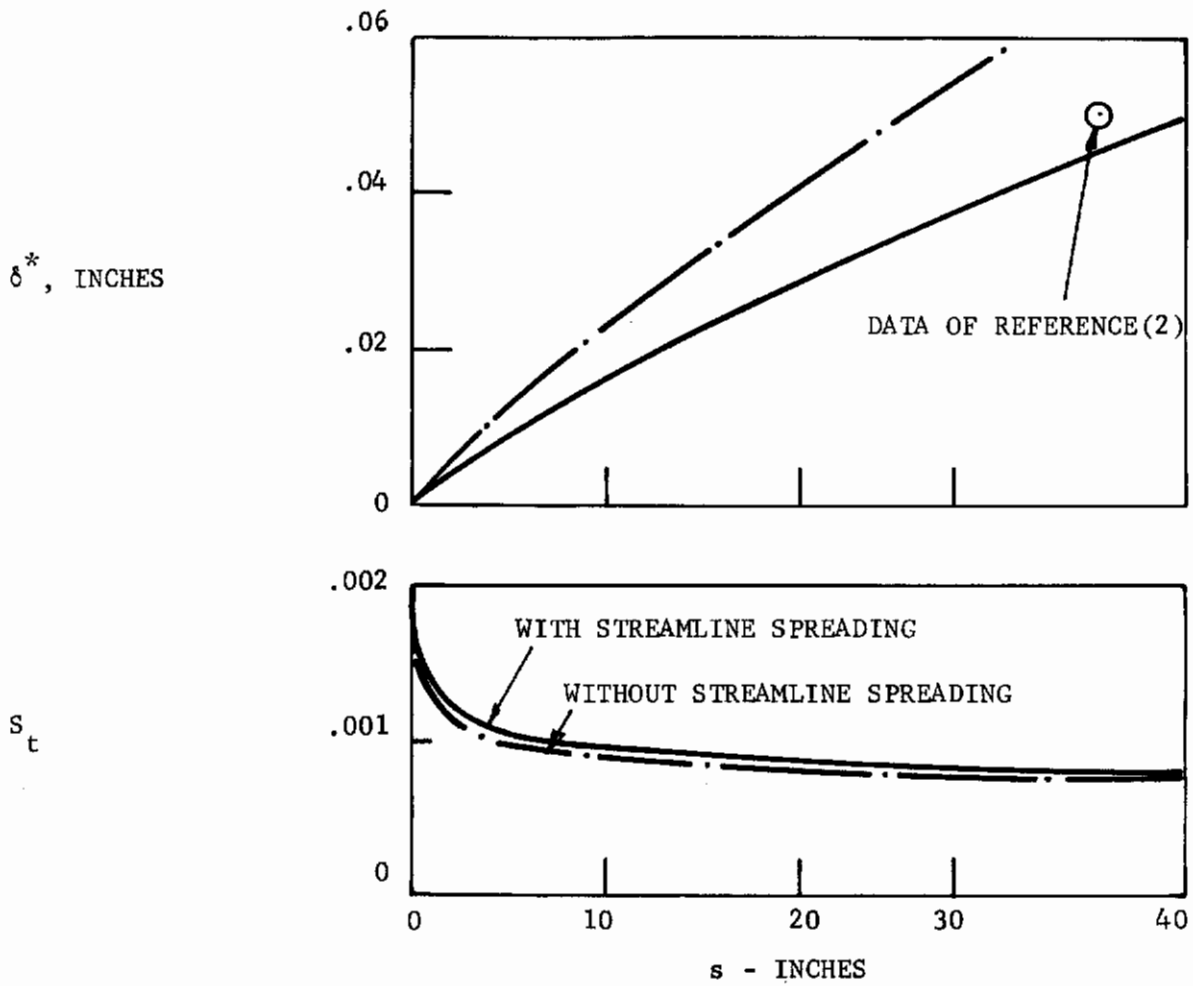adius was utilized to represent the h_2 distribution. As can be seen in Figure (23) the Stanton number predictions are in substantial disagreement with the measurements when the body radius is utilized, particularly for the laminar case, while the prediction based on the h_2 variation generated by the STRMLN provides excellent agreement with the data.

A similar result is shown in Figure (24). Here we have compared the variation of Stanton number and displacement thickness on the windward plane for one of Rainbird's cases ($M_\infty = 4.25$, $\alpha = 15.6^\circ$) as determined with and without the streamline "spreading" effect. It is apparent that the effect of streamline spreading on the Stanton number level is not too significant as has previously been pointed out by Widhopf (Reference 30). Note, for example, that at $x \overset{\sim}{=} 35$ the percent difference between the two values of S_t is only 5%. However, the corresponding influence on displacement thickness is far from negligible. Indeed, the displacement thickness at this station would be over predicted by about 60% if streamline spreading were neglected. In contrast, with the spreading effect included the prediction is within approximately 10% of the measured value. In the present application, of course, an accurate representation of integral thicknesses is crucial. Thus, these results demonstrate the importance of utilizing computational tools which properly reflect the three dimensional character of both the inviscid and viscous flow phenomena which is of interest.

C. <u>Determination of Effective Body Shape</u> - The results of our efforts to deduce appropriate body shapes to represent the viscous layers on the cones studied in Reference (24) are summarized in Figures (25) through (30). Figure (25) shows the final selections of shear layer thickness distributions. The pressure variation computed by the FFCS for these effective bodies is compared with the experimental data in Figure (26). Comparison of pitot pro-
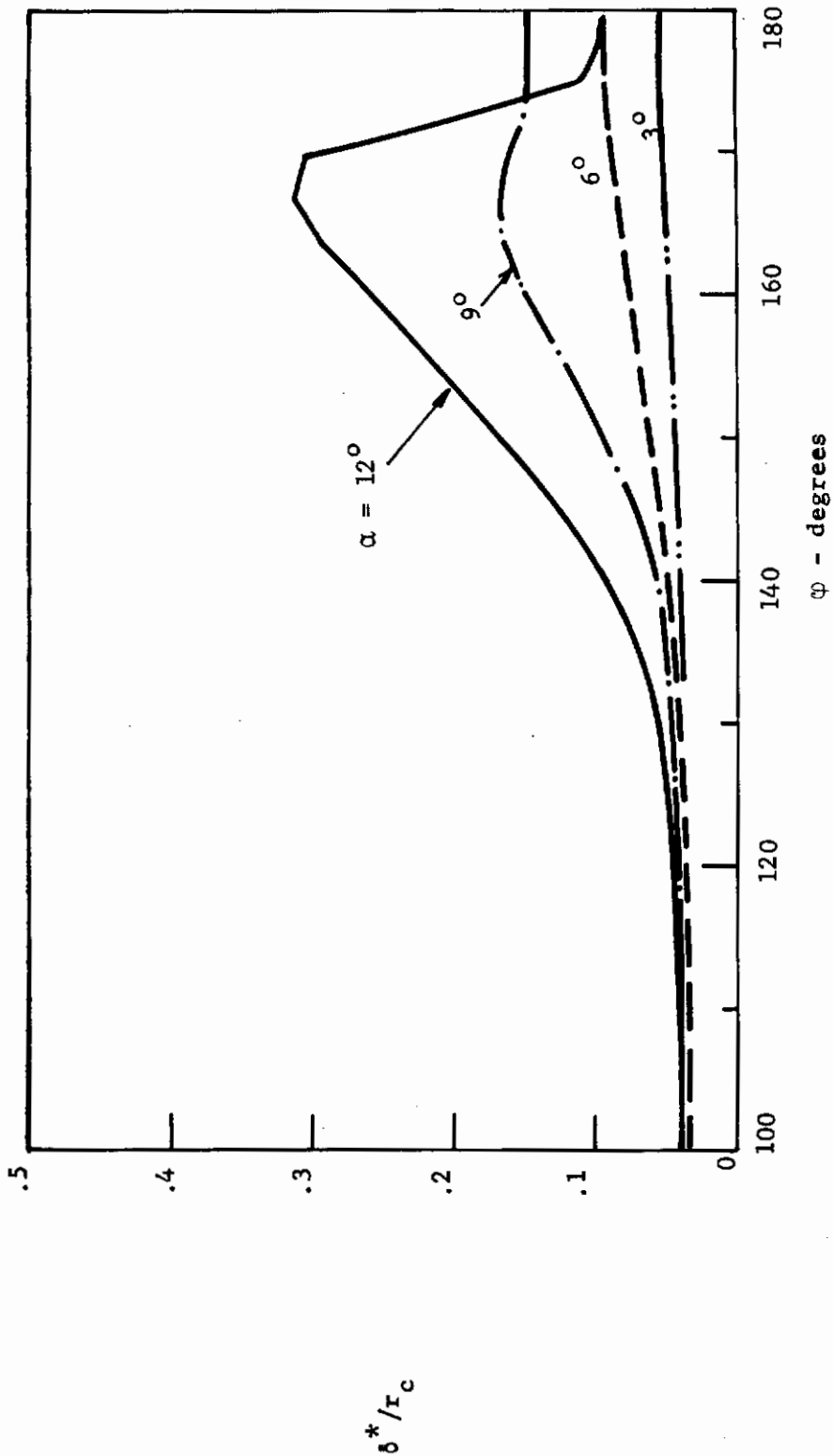
FIGURE 25   EFFECTIVE BODY SHAPES UTILIZED TO COMPUTE PRESSURE DISTRIBUTIONS
SHOWN IN FIGURE (26)
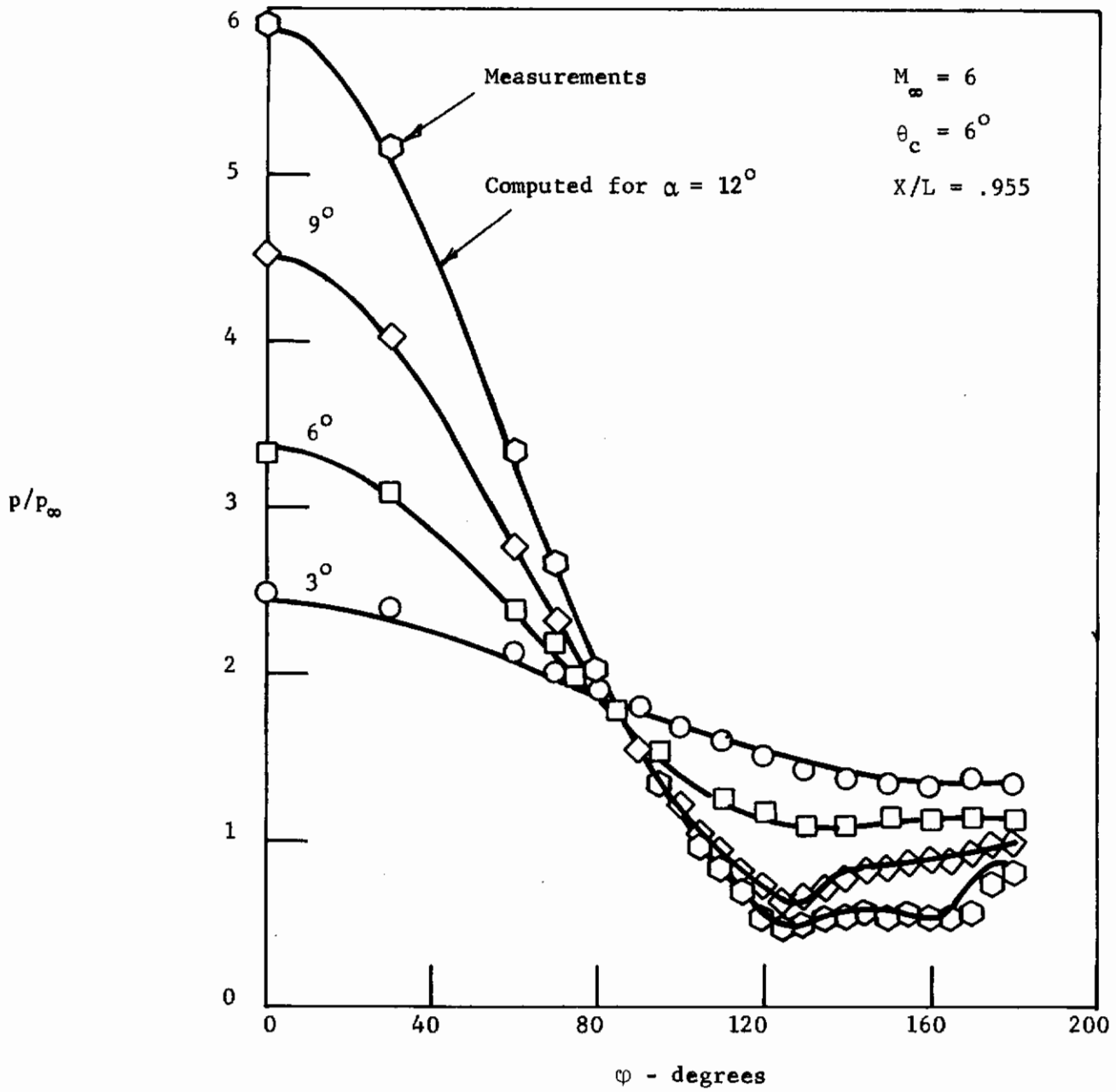
FIGURE 26   COMPARISON OF COMPUTED SURFACE PRESSURE DISTRIBU-
TIONS WITH MEASUREMENTS OF REFERENCE (24)

-53-
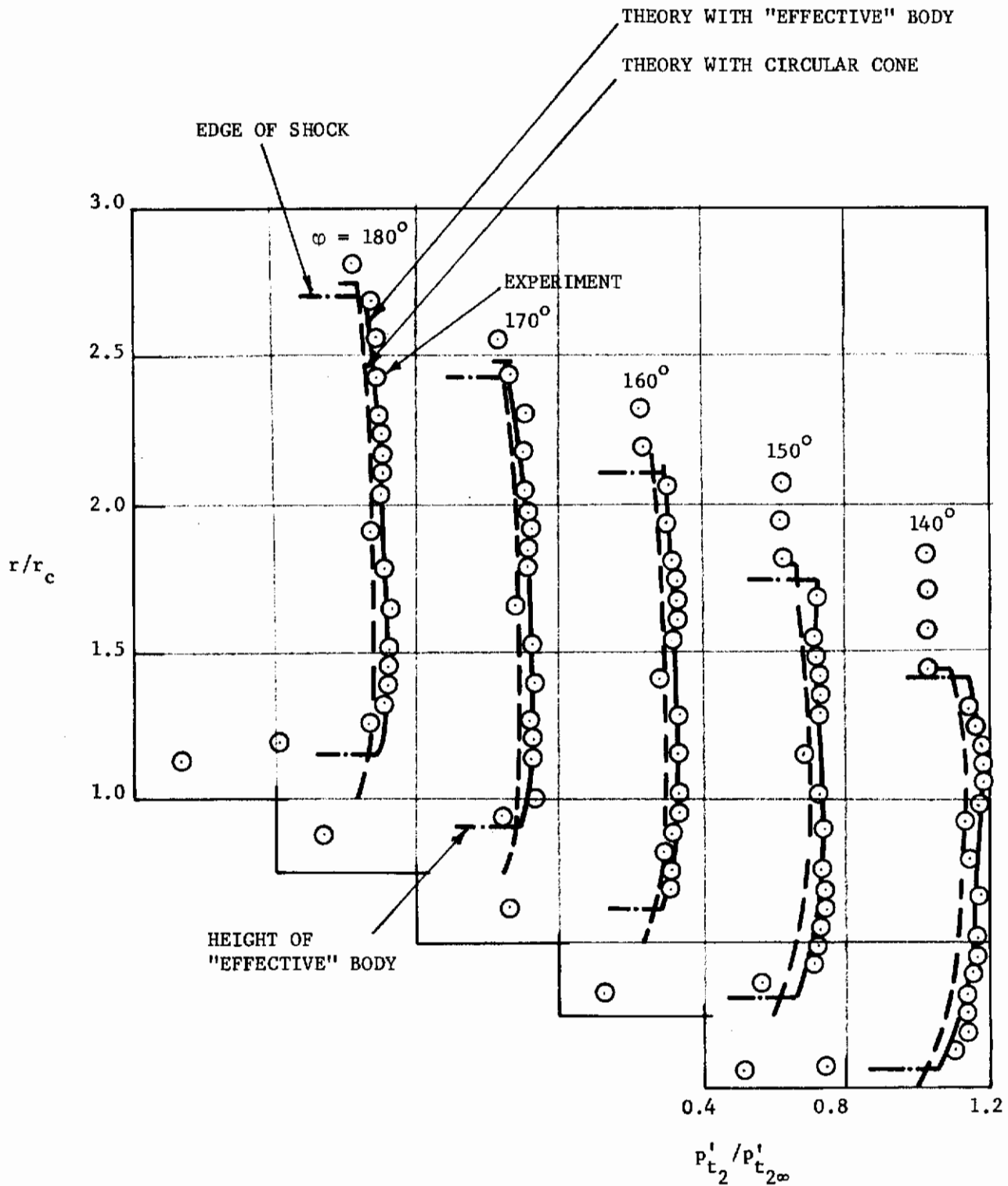
FIGURE 27   COMPARISON OF THEORY AND EXPERIMENT FOR RADIAL PITOT DISTRIBUTION
DATA OF REFERENCE (24) $\alpha = 6^{\circ}$
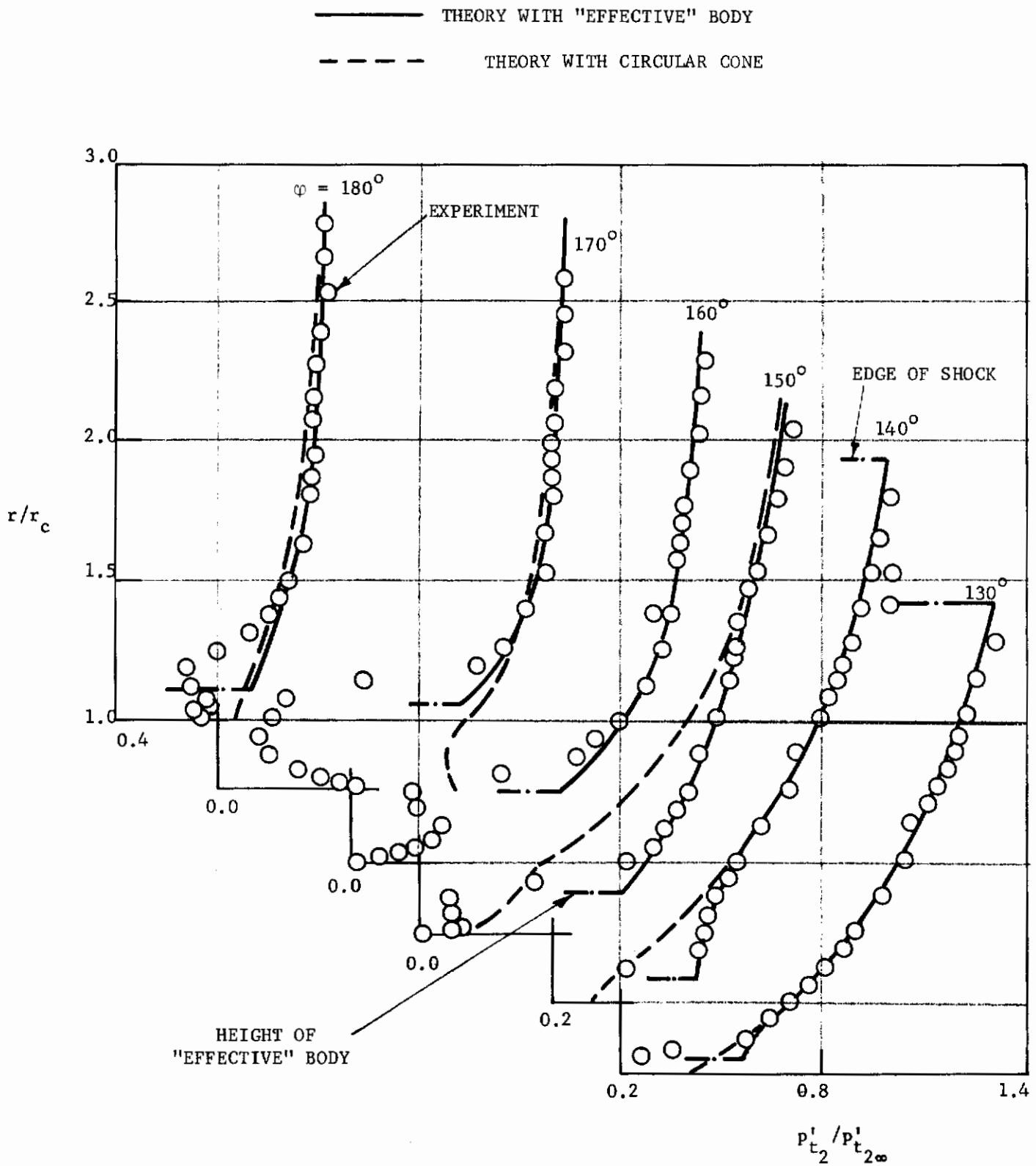
FIGURE 28   COMPARISON OF THEORY AND EXPERIMENT FOR RADIAL PITOT DISTRIBUTION
DATA OF REFERENCE (24) $\alpha = 12^{\circ}$

-55-
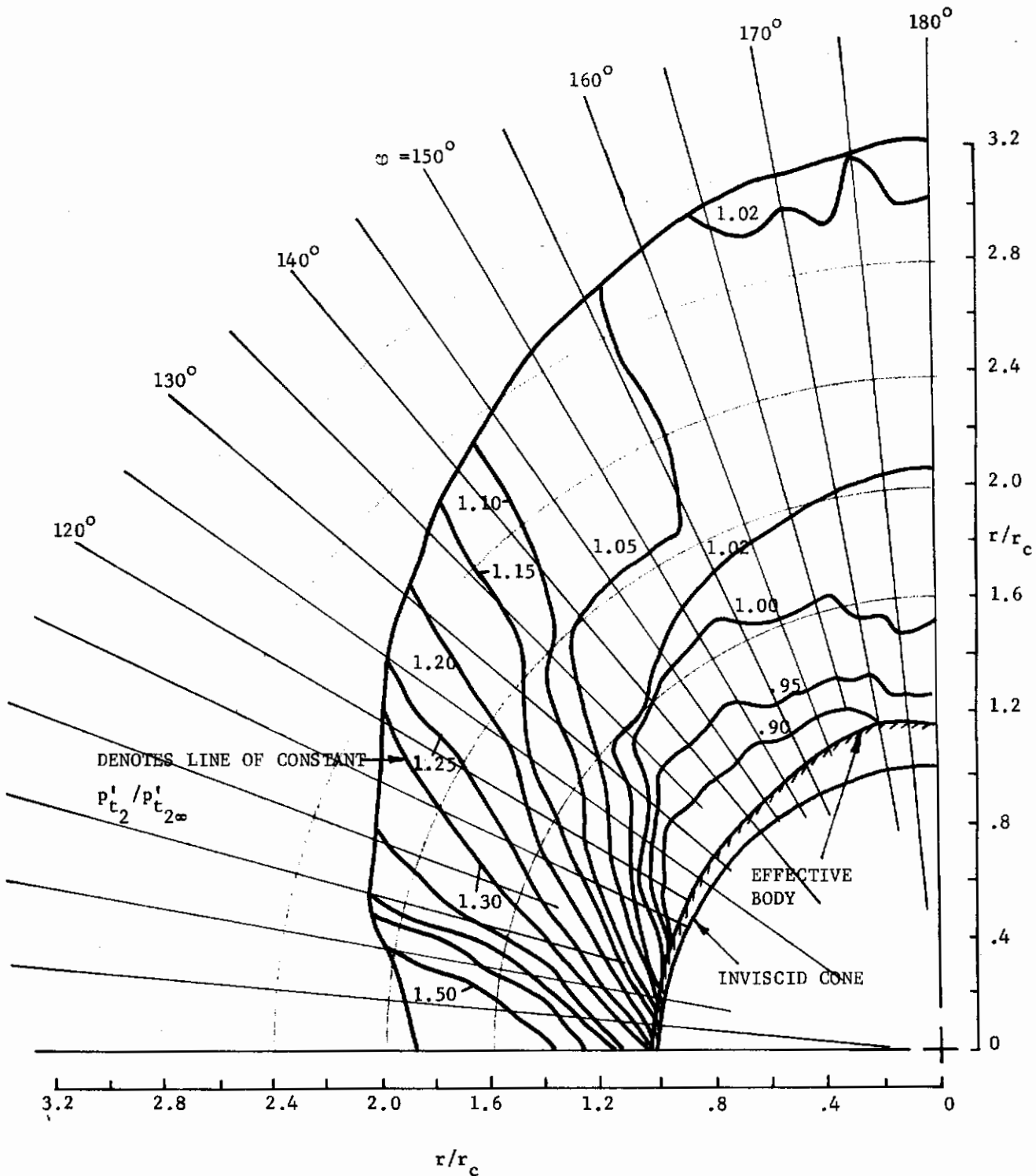
FIGURE 29a   THEORETICAL PITOT PRESSURE MAP WITHIN SHOCK LAYER ON SHARP CONE AT
INCIDENCE;

$M_\infty = 6$, $\theta_c = 6^o$, $\alpha = 9^o$
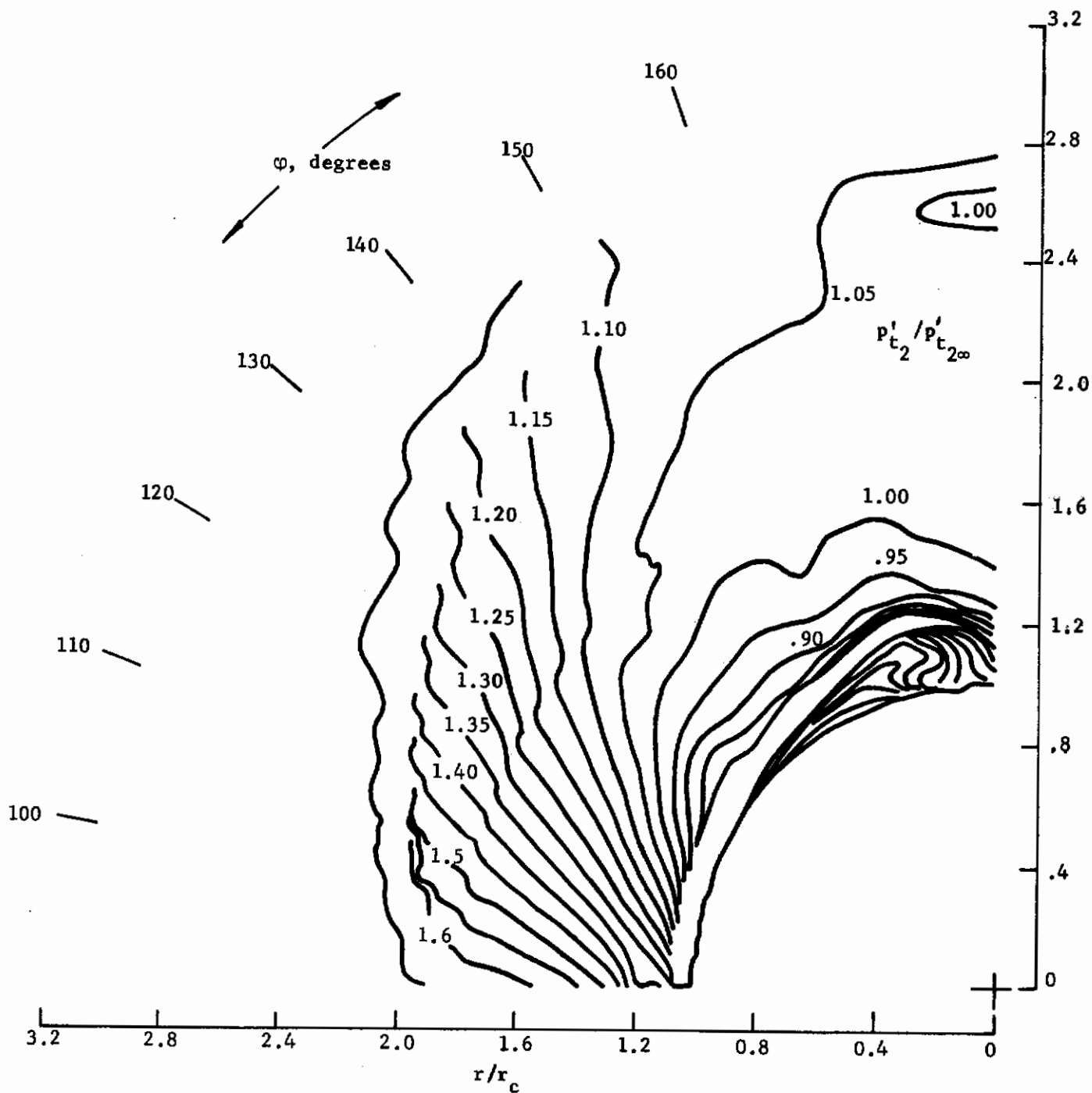
FIGURE 29b EXPERIMENTALLY DETERMINED PITOT PRESSURE MAP WITHIN SHOCK LAYER ON SHARP
CONE AT INCIDENCE: $\alpha = 9°$ DATA FROM REFERENCE (24)

FIGURE 30   COMPARISON OF DEDUCED EFFECTIVE BODY WITH PITOT MAPS FROM
REFERENCE (24)

-58-

files for the $\alpha = 6^{\circ}$ and 12° cases is shown in Figures (27) and (28).

For the $\alpha = 12^{\circ}$ case a pitot pressure map was also prepared and is shown in Figure (29a). This may be compared with the corresponding experimental map shown in Figure (29b) as provided in Reference (24).

Finally in Figure (30) there is presented an expanded view of the pitot maps for all three angles of attack to permit a detailed comparison o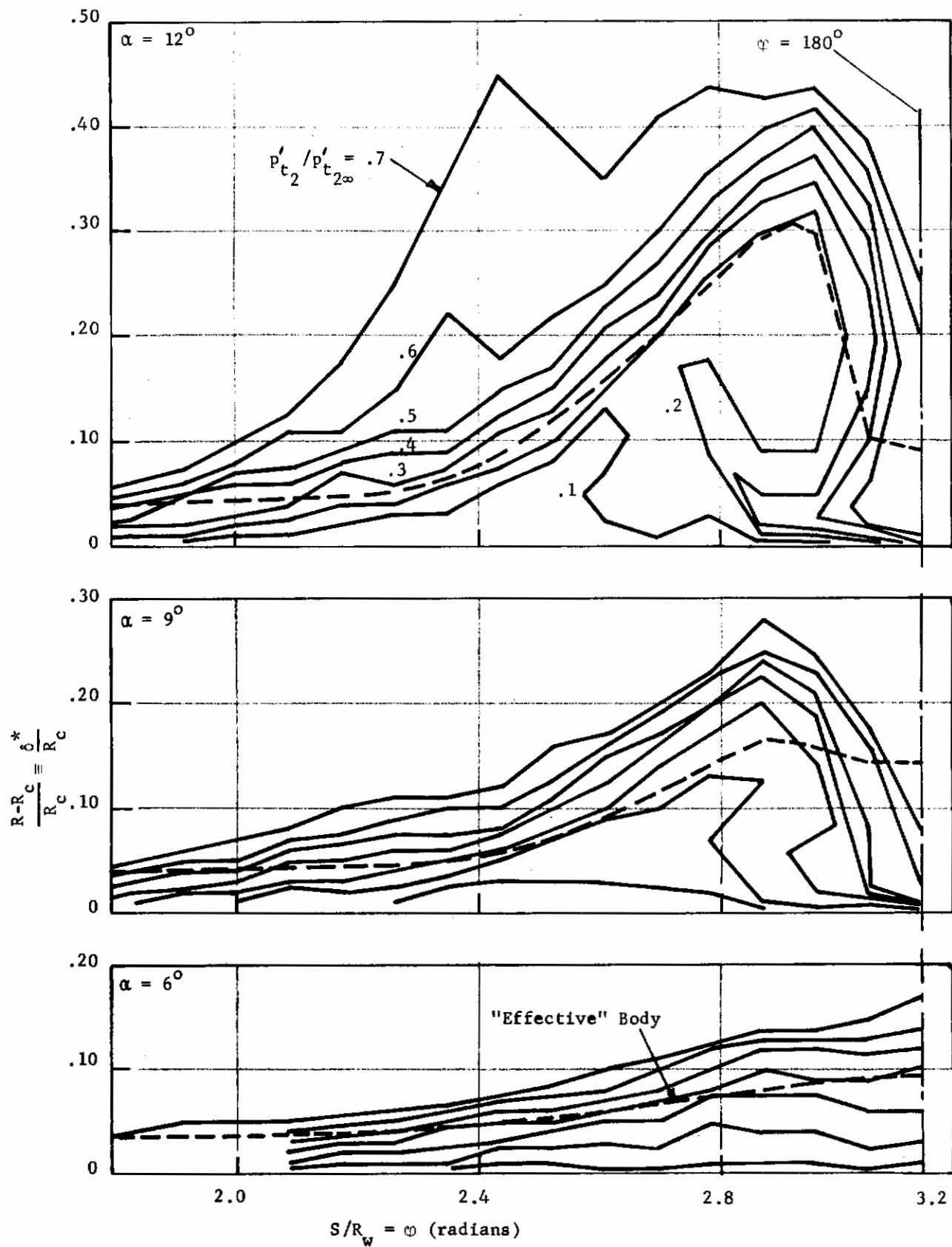f the region of high shear $(p'_{t_2}/p'_{t_{2\infty}} \overset{\sim}{<} 0.7)$ and the effective body thicknesses. Recall that the latter were determined by matching the peripheral static pressure distributions. This comparison as well as all the other results shown in Figures (25) through (29) demonstrate that our choices of effective body shape adequately represent the viscous phenomenon occurring on the cone surface.

D. <u>Pressure Correlations</u> - The source of the data examined for this correlation has been enumerated in Table I. Figure (31) summarizes all of the results obtained from these sources for the leeward pressure ratio p_L/p_∞ in terms of the Reynolds number $Re_{\infty,x}$. No effort at a correlation is intended here but the data is presented in this manner to provide a convenient reference and to indicate the degree of scatter which exists.

ATL's effort to correlate all of these disparate data involved an examination of a variety of parameters with the initial attempt being the use of the correlation suggested by Feldhuhn (Reference 3). These and other intermediate results will not be reported here but can be found detailed in the several progress reports issued under the current contractual effort.

The final choice of correlation schemes involves the use of a modified form of the viscous interaction parameter for a cone

$$\chi_c \equiv M_\infty \ (C_\infty/Re_{\infty,x})^{\frac{1}{2}}/\sin^2\theta_c \qquad\qquad (24)$$

The modification involves a combination of χ_c with the relative angle of in-
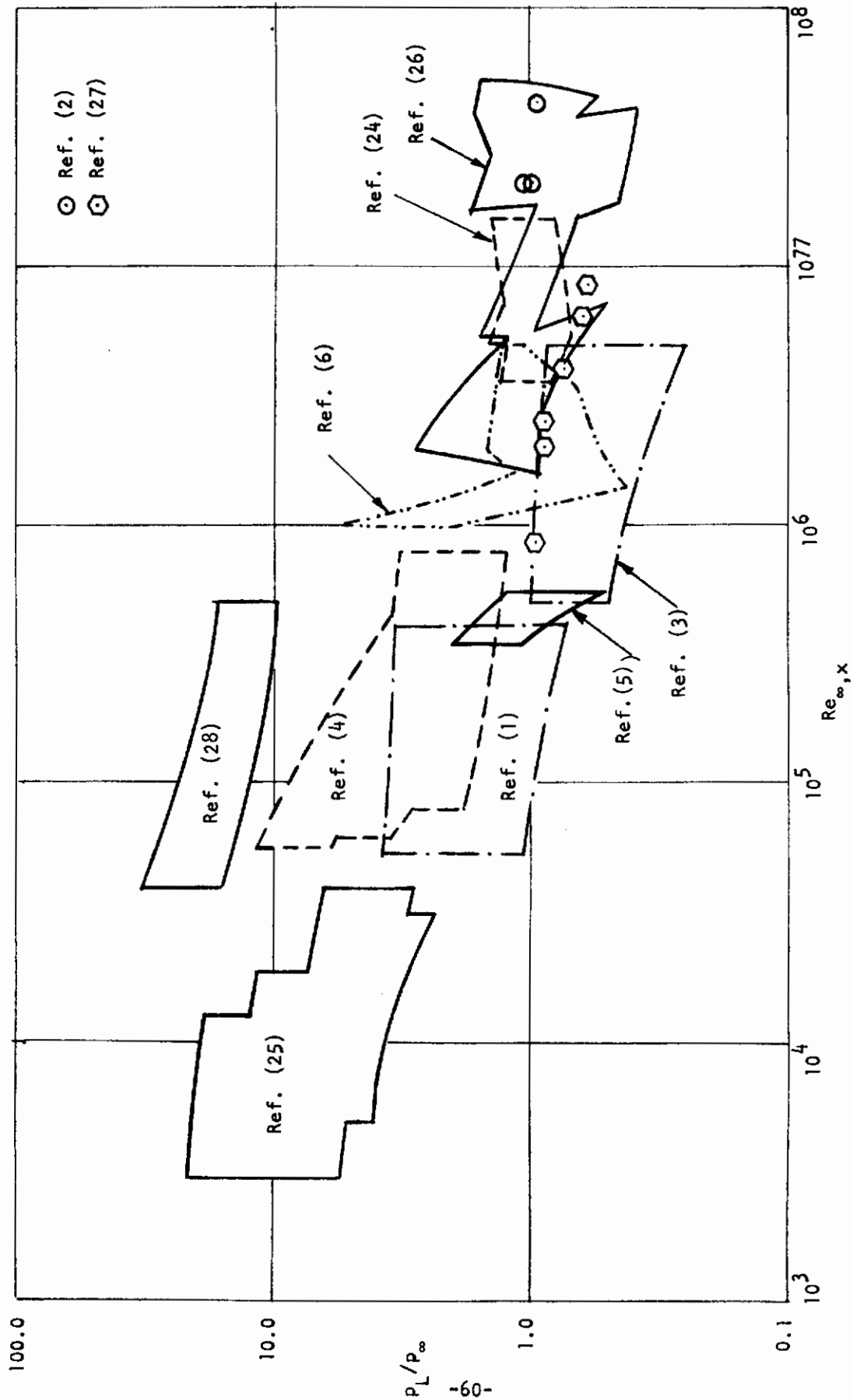
FIGURE 31. LEEWARD PRESSURE RATIO VS REYNOLDS NUMBER-SUMMARY OF EXPERIMENTAL DATA EXAMINED

-60-

cidence $\eta \equiv \alpha/\theta_c$ according to[*]

$$F4 = \eta/\chi_c^{\frac{1}{2}} \tag{25a}$$

$$F4 \equiv (\alpha/\theta_c) \ (M_\infty/Re_{\infty,x}^{\frac{1}{2}}/sin^2\theta_c)^{-\frac{1}{2}} \tag{25b}$$

A plot of all of the data presented in the previous figure in terms of p_L/p_∞ vs F4 is shown in Figure (32). Although some correlation is apparent within individual sets of data (see especially the data of References 1 and 26), collapse of the entire spectrum of measurements is obviously unsatisfactory. On the other hand, if the correlation scheme is restricted to the following range of the pertinent variables [**]

$$M_\infty \ \geq \ 5$$

$$Re_\infty \ \geq \ 5\times10^4$$

$$S/r_N \geq \ 25$$

a satisfactory correlation is obtained as shown in Figure (33).

The restriction with respect to nose bluntness effect is, of course, reasonable and simply delineates the point at which bluntness effects can be neglected and the flow phenomenon can be considered self-similar (i.e.: conical). The restrictions enumerated above, however, do serve to eliminate several data sets obtained on sharp cones. Specifically, these include the experimental results of Anderson (Reference 25), Yahalom (Reference 5) and Rainbird (Reference 2).

---

[*]Note that the selected form of correlation parameter F4 effectively sets C_∞ equal to unity. However, the effect of this parameter has not been examined in our correlation scheme.

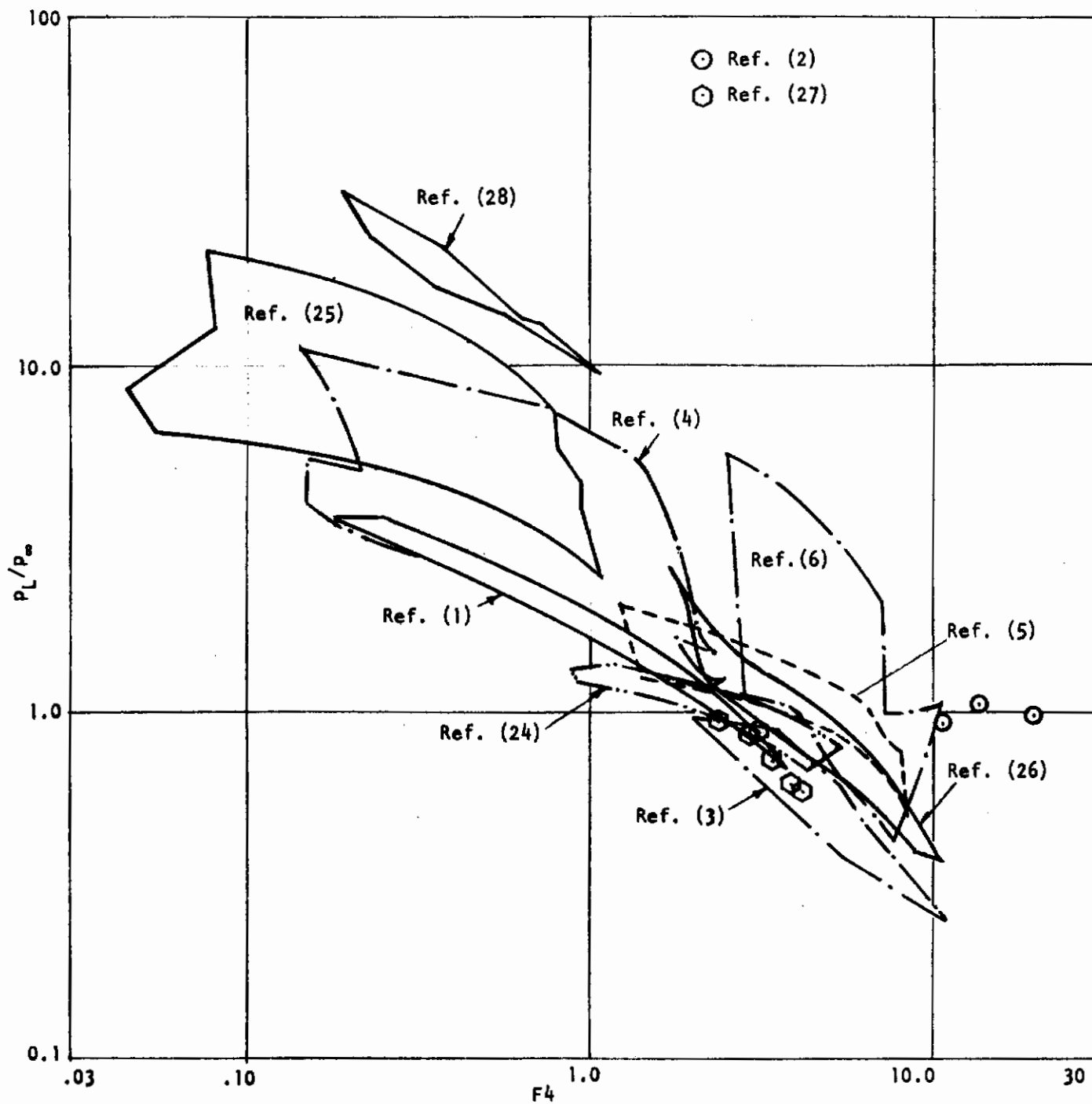[**]Also excluded are the helium results of Reference (28).

FIGURE 32. LEEWARD PRESSURE RATIO VS CORRELATION PARAMETER-SUMMARY OF ALL
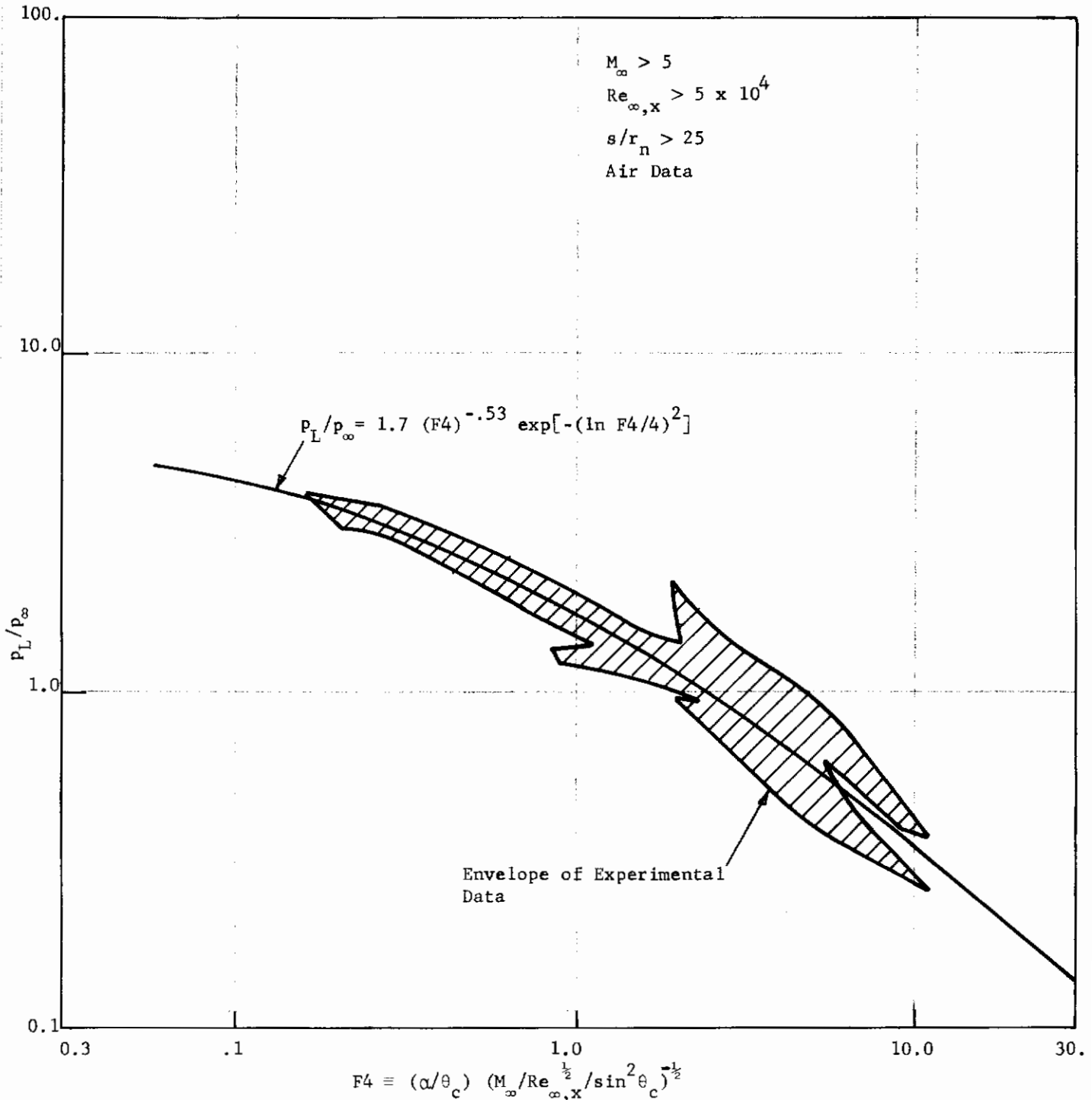EXPERIMENTAL DATA EXAMINED

FIGURE 33   LEEWARD PRESSURE RATIO VS. CORRELATION PARAMETER SHOWING SELECTED ATL
CORRELATION

For the first of these, no rationale for their exclusion can be offered at this time beyond noting the very low Reynolds number involved (order of 10^4). The rationale for rejecting the latter two sets of data is associated with the concept of the "base interference" regime postulated by Stetson and Ojdana (Reference 4). It is believed that the combination of low Mach numbers ($1.8 \leq M_\infty \leq 4.25$) and thick cone angles ($10^\circ \leq \theta_c \leq 20^\circ$) for which the investigations of References (2) and (5) were conducted places their results in the aforementioned category. It should be noted, however, that the restrictions associated with this correlation are consistent with the requirements and objectives of the subject contract. Accordingly, the selected correlation shown in Figure (33) is considered to be satisfactory for the present purpose.

To completely characterize the pressure on the leeward side of cones at incidence, a way of estimating the pressure ratios p_p/p_∞ and p_s/p_∞ and their corresponding peripheral locations ϕ_p and ϕ_s as defined in Figure (4) is also required. For evaluation of p_p and p_s an analysis similar to that described above for p_L was carried out. The results of these studies led to the final form of correlation shown in Figure (34). According to this correlation, for values of $F4 \lesssim 0.7$ the minimum pressure occurs at the leeward plane of symmetry; i.e.: the pressure decreases monotonically from the windward to the most leeward ray. As $F4$ continues to increase a minimum in pressure (p_p) occurs outboard from the $\phi = 180^\circ$ plane. However, for values of $F4$ up to about 2, the pressure subsequently increases monotonically without an inflection point to the leeward value. Finally, for $F4 \gtrsim 2$ a second "minimum" in pressure and/or an inflection point occurs in the pressure distribution (p_s).

The available data for the peripheral locations ϕ_p and ϕ_s are presented in Figure (35) plotted against the relative incidence η. As can be seen these parameters appear to be essentially independent of η and nose bluntness for the ranges considered. On the basis of these results it is concluded that suitable estimates for ϕ_p and ϕ_s are
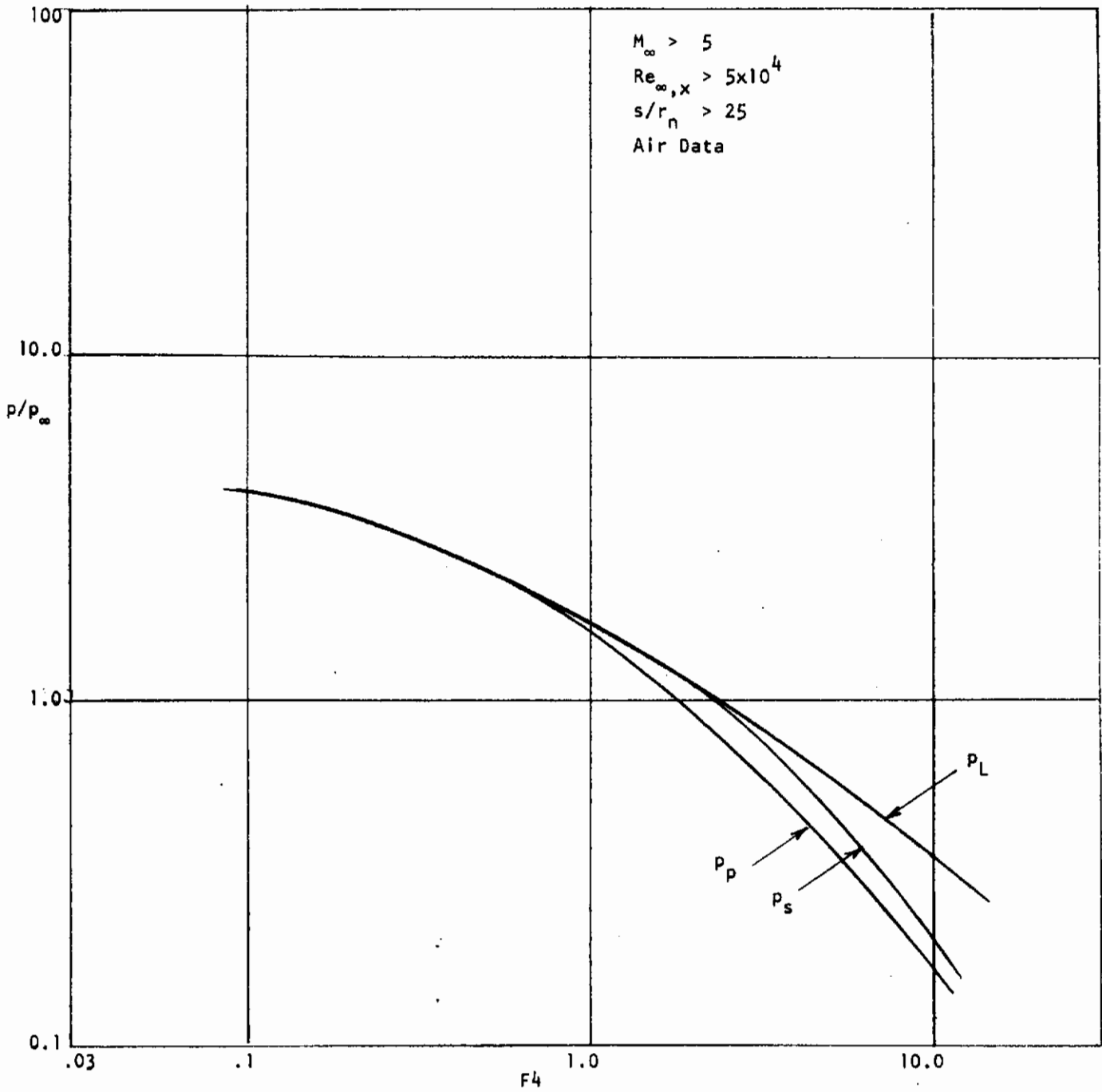
FIGURE 34. SELECTED CORRELATION OF PRESSURES ON LEEWARD SIDE OF CIRCULAR CONES AT INCIDENCE
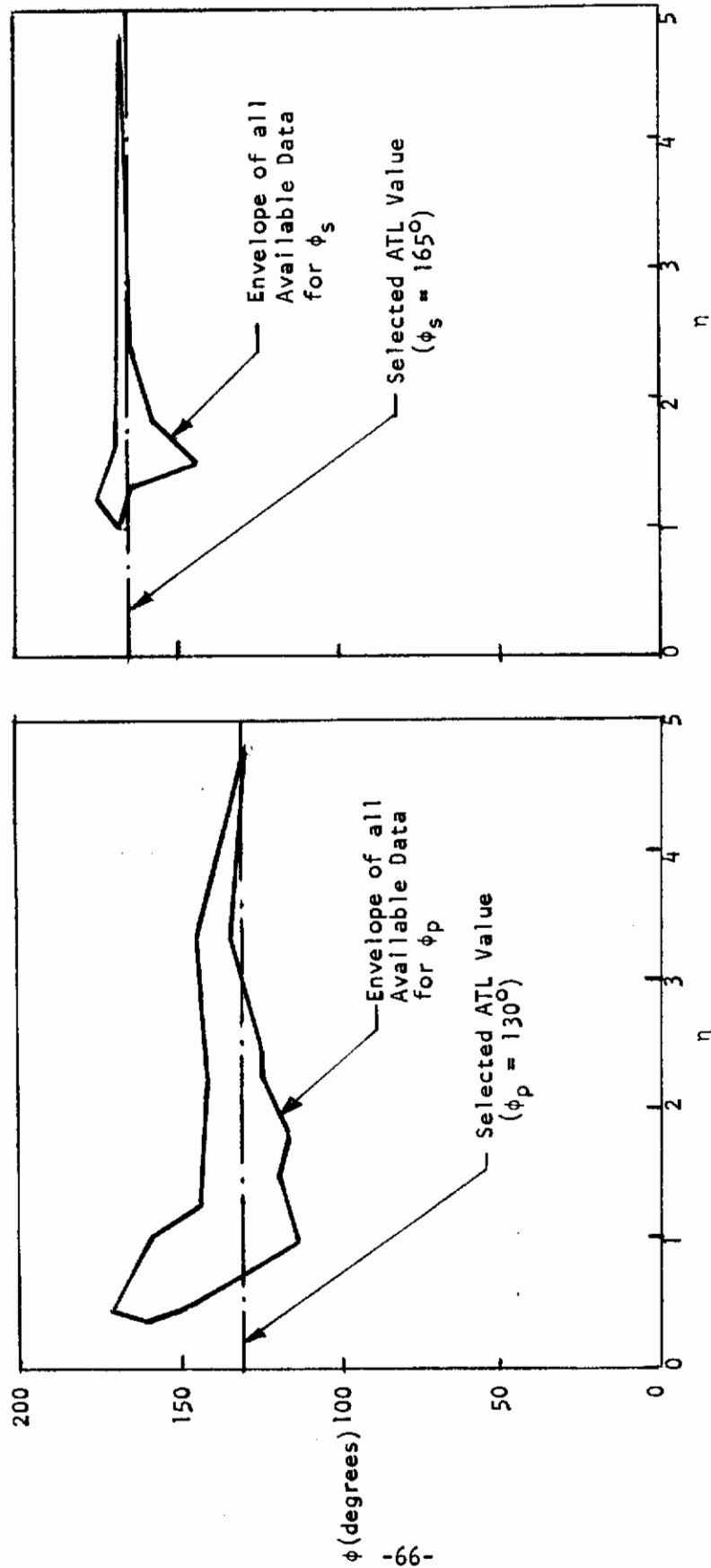
FIGURE 35. LOCUS OF FIRST AND SECOND PRESSURE MINIMUMS AS A FUNCTION OF RELATIVE INCIDENCE

$$\phi_p = 130°$$

$$\phi_s = 165°$$

(26)

E. <u>Generalization and Calibration of the Effective Body Shape</u> - The selected effective body shape is shown schematically in Figure (36). Complete definition of this geometry requires specification of a total of seven parameters; viz: δ_0^*, δ_p^*, δ_C^*, δ_S^*, δ_L^* and ϕ_C and ϕ_s where, for the most general case, these would all be a function of M_∞, α, θ_c and $Re_{\infty,x}$. On the basis of our analysis to date the following provisional representation is employed. Let $\eta \equiv \alpha/\theta_c$. Then

$$\delta_C^* = k_C(\eta)\ \delta_p^* \tag{27a}$$

$$\delta_S^* = k_S(\eta)\ \delta_p^* \tag{27b}$$

$$\delta_L^* = k_L(\eta)\ \delta_p^* \tag{27c}$$

$$\phi_C = F_1(\eta) \tag{27d}$$

$$\phi_S = F_2(\eta) \tag{27e}$$

with

$$\delta_0^* = G_1(M_\infty,\ \eta,\ \theta_c,\ Re_{\infty,x}) \tag{27f}$$

$$\delta_p^* = G_2(M_\infty,\ \eta,\ \theta_c,\ Re_{\infty,x}) \tag{27g}$$

Our explicit choices for the functional forms appearing in Equation (27) are shown in Figure (37). The discrete symbols which appear therein represent the actual values which were employed in the FFCS to repeat the calculations previously made with the body shapes shown in Figure (25). The surface and pitot pressure distributions which resulted were undistinguishable from those presented in Figures (26), (27) and (28).
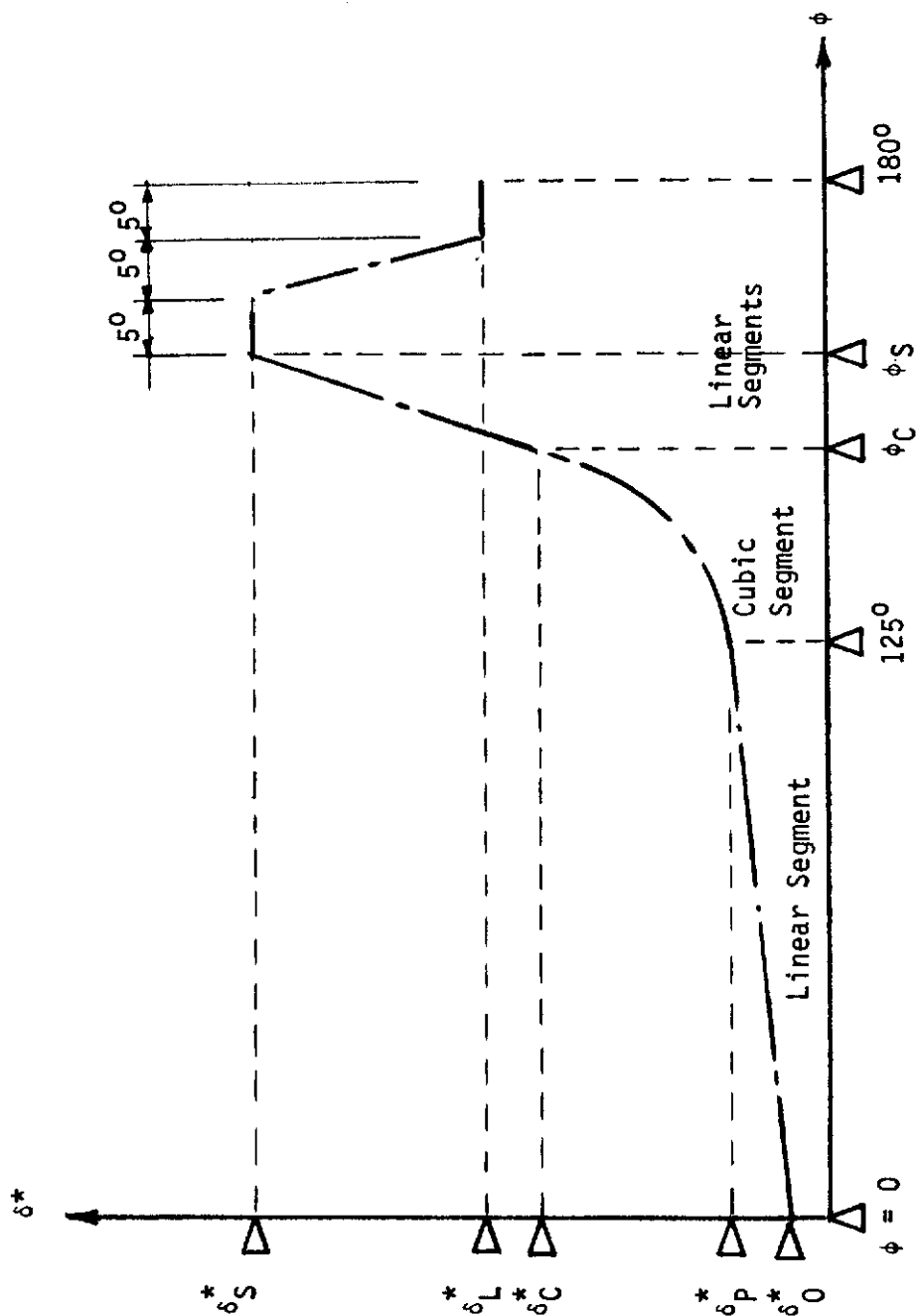
-67-

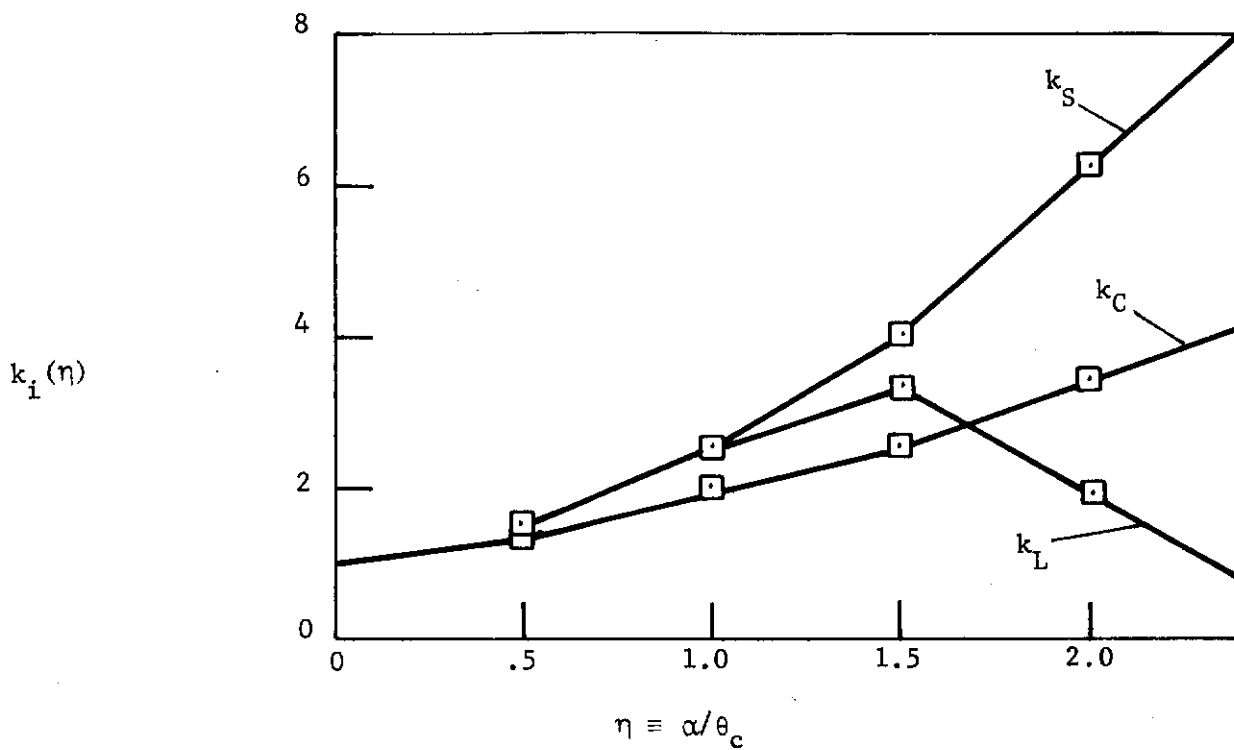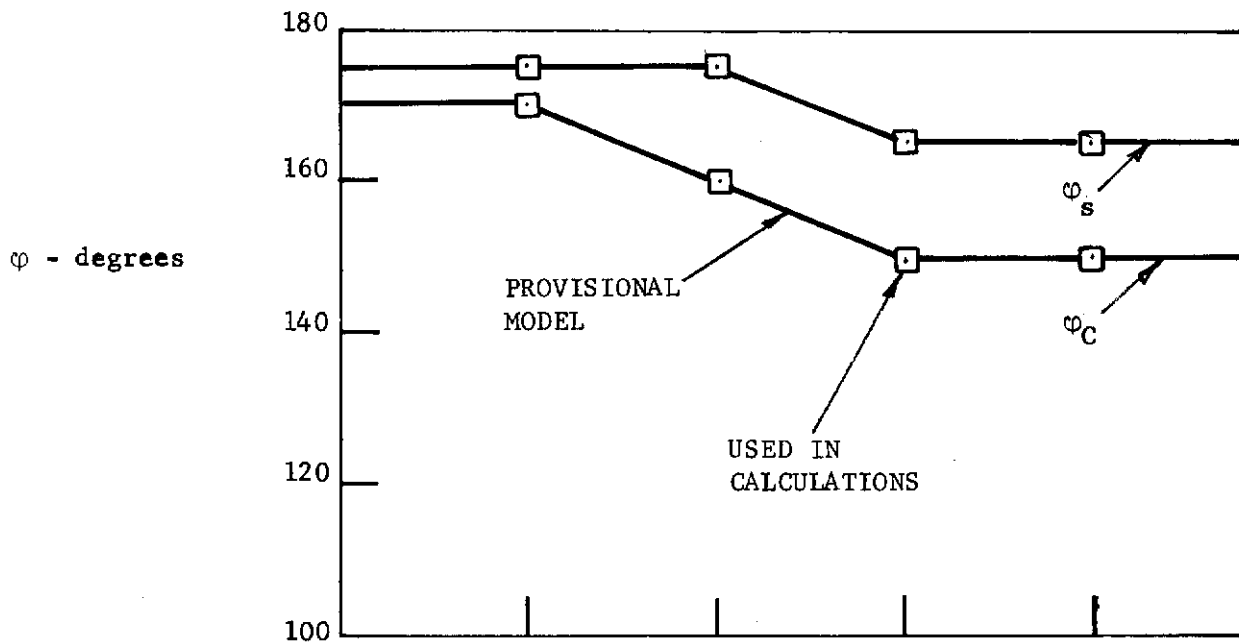FIGURE 36. SCHEMATIC OF NOMINAL EFFECTIVE BODY SHAPE

FIGURE 37   VARIATION OF EFFECTIVE BODY COEFFICIENTS
WITH RELATIVE ANGLE OF INCIDENCE
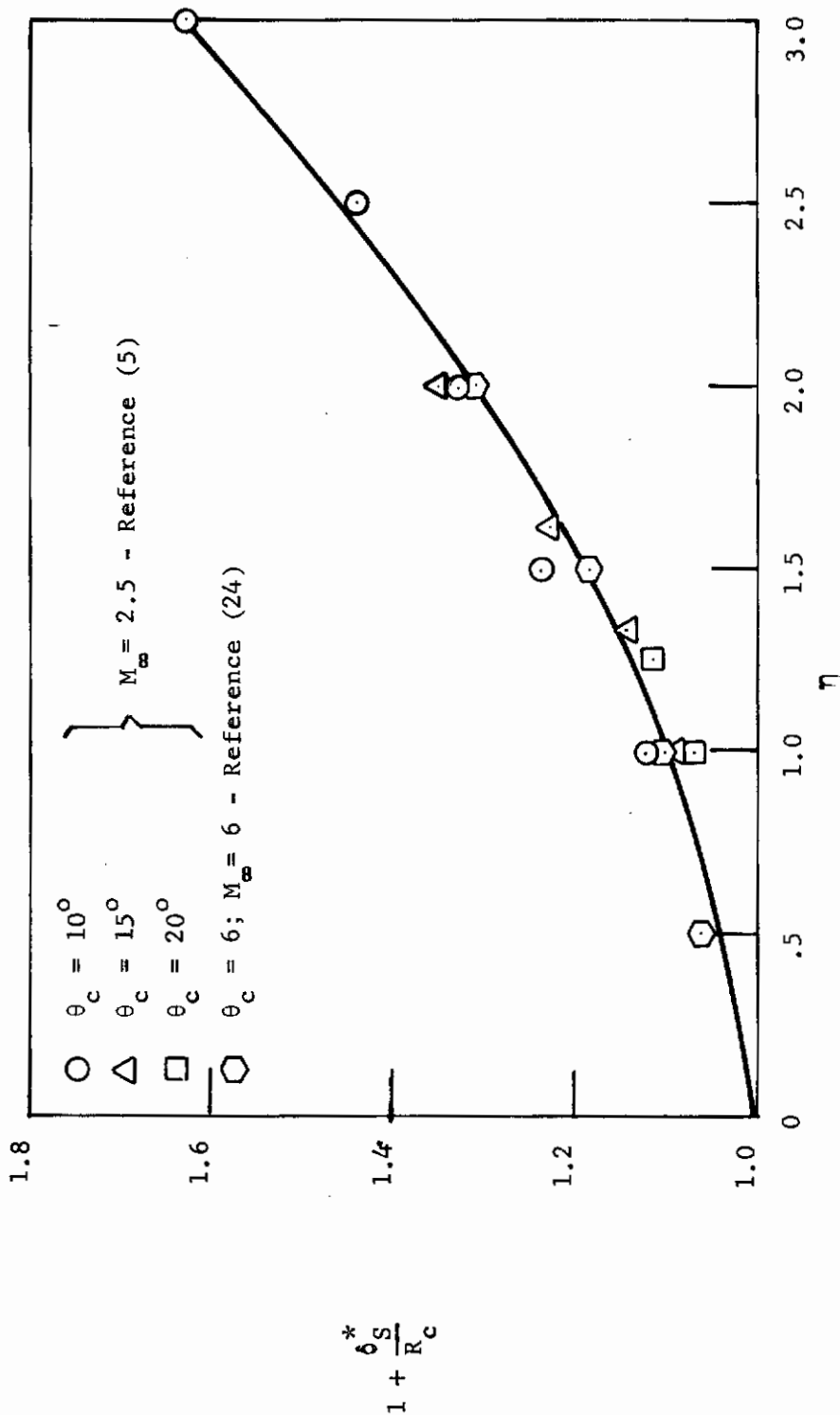
FIGURE 38   COMPARISON OF ESTIMATED MAXIMUM SHEAR LAYER THICKNESS FROM
REFERENCE (24)   WITH RESULTS FROM REFERENCE (5)

The parameters δ_0^* and δ_p^* represent the displacement thicknesses at the windward plane ($\phi = 0$) and at the $\phi = 125^\circ$ plane. These are computed case by case utilizing the BLCS and procedures described in Section IVB.

We have indicated above that this representation is provisional. This follows from the fact that the coefficients appearing in Equations (27) have only an η - dependence which was deduced from a single set of experimental results obtained at a fixed value of M_∞ and θ_c and for a relatively limited range of the parameter η ($0.5 < \eta < 2.0$). At this time the additional calculations needed to establish whether or not the representation shown in Figure (37) can be considered universal and how these curves can be extrapolated to larger values of η have not been undertaken. This would constitute the "calibration" phase of the study. However, some indication of the generality of our provisional model has been obtained and is demonstrated by the results shown in Figure (38). Here we have compared the maximum thicknesses (δ_S^*) from the present results with those measured by Yahalom (Reference 5) at conditions which differ markedly from those of Reference (24). The agreement of the two sets of data is remarkable and provides some justification for considering the parameters $k_c(\eta)$, .. etc. independent of both M_∞ and θ_c.

SECTION IV
CONCLUDING REMARKS

The methodology described in the previous sections is capable of providing a complete description of the flow field throughout the shock layer surrounding a circular cone at large angle of attack. The method is equally applicable to sharp and blunt cones provided that, in the latter case, the region of interest lies beyond a point 25 nose radii downstream of the stagnation point.

In order to implement the method the combined use of three distinct analytic tools is required. Each of these is implemented by a computer code and user's manuals for each of these codes is provided in Volume II of this report.

The sequence in which these codes are utilized is as follows:

(a) The FFCS is applied to the geometric cone at the selected angle of attack to provide an estimate of the pressure distribution around the cone up to a peripheral angle $\phi \simeq 120^{\circ}$. This information is needed as input to STRMLN.

(b) The STRMLN code is used to trace a series of streamlines on the surface of the geometric cone up to $\phi \simeq 120^{\circ}$.

(c) BLCS is used to estimate the boundary layer properties at $\phi=0$ and $\phi \simeq 120^{\circ}$ based on the results obtained from step (b) above.

(d) The boundary layer properties obtained in step (c), when input to the FFCS, provide the means for estimating the effective body shape which best represents the viscous effects induced by the large incidence. Using this effective geometry the FFCS computes all flow properties, including the surface pressure throughout the shock layer. The range of applicability of the methodology is restricted by limitations inherent in the FFCS analysis and com-

puter code. Thus, the BLCS and STRMLN analyses and codes are considered reliable for the entire range of conditions which are likely to be of practical interest. On the other hand, at the present time the FFCS has to be considered provisional since it has not been tested over a sufficiently wide range of conditions. This is particularly true of the generalized effective bode shapes as indicated in Section IVE.

In ATL's judgement, the methodology can be expected to provide reasonable estimates of flow field characteristics at Mach numbers on the order of 6 and for relative angles of incidence up to about 2. For conditions which vary to any substantial degree from these values further calibration of the method would be required before it can be considered a reliable technique. ATL believes that such a calibration effort is feasible and that it would be a useful undertaking for the immediate future.

REFERENCES

1. Tracy, R. R., "Hypersonic Flow Over a Yawed Circular Cone," GALCIT Memo No. 69, (August 1963).

2. Rainbird, W. J., "Turbulent Boundary Layer Growth and Separation on a Yawed Cone," AIAA Jour. 6, pp. 2410-2416 (December 1968).

3. Feldhuhn, R. H., Winkelmann, A. E. and Pasiuk, L., "An Experimental Investigation of the Flow Field Around a Yawed Cone," AIAA Paper No. 70-766 (July 1970).

4. Stetson, K. F. and Ojdana, E. S., "Hypersonic Laminar Boundary Layer Separation on a Slender Cone at Angle of Attack," AIAA Paper No. 72-129, January 1971.

5. Yahalom, R., "An Experimental Investigation of Supersonic Flow Past Yawed Cones," University of California, College of Engineering, Report No. AS-71-2, June 1971.

6. Widhopf, G. F., "Laminar, Transitional and Turbulent Heat Transfer Measurements on a Yawed Blunt Conical Nosetip," Aerospace Report No. TR-0073 (S3450-60) 1 September 1972.

7. Babenko, K. I., Voskresenski, G. P., Lyubimov, A. N. and Rusanov, V. V., "Three Dimensional Flow of an Ideal Gas Past Ideal Smooth Bodies," NASA TT F-380.

8. Moretti, G., "Inviscid Flow Field About a Pointed Cone at an Angle of Attack," AIAA Jour., 5, pp. 789-791 (April 1967).

9. Gonidou, Rene, "Supersonic Flows Around Cones at Incidence," NASA TT F-11, 473 (January 1968).

10. Der, Joe, Jr., "A Study of General Three Dimensional Boundary Layer Problems by an Exact Numerical Method," AIAA Paper No. 69-138, January 1969.

11. Holt, M. and Ndefo, E., "A Numerical Method for Calculating Steady Unsymmetrical Supersonic Flow Past Cones," J. of Computational Physics 5, 3, 563-486 (1970).

12. Jones, D. J., "Tables of Inviscid Supersonic Flow About Circular Cones at Incidence $\gamma = 1.4$," AGARDograph 137, Part I and Part II (1969).

13. Lubard, S. C., Helliwell, W. S., "Calculations of the Flow on a Cone at High Angles of Attack," AIAA Paper No. 73-636, July, 1973.

14. Sakell, L., "Laminar Transition and Turbulent Heat Transfer to the Leeward Side of Axially Symmetric Bodies," Israel Journal of Technology, Vol. 10, No. 1-2, pg. 163, 1972.

15. Whitehead, A. H. et al, "Lee Surface Vortex Effects Over Configurations in Hypersonic Flow," AIAA Paper No. 72-77, 1972.

16. Kutler, P. et al, "Numerical Computation of Multi-Shocked Three Dimensional Supersonic Flow Field with Real Gas Effects," AIAA Paper No. 72-702, 1972.

17. Vaglio-Laurin, R., "Laminar Heat Transfer on Three Dimensional Blunt Nosed Bodies in Hypersonic Flow," ARS Journal, Vol. 28, No. 2, pp. 123-129, February 1959.

18. Vaglio-Laurin, R., "Turbulent Heat Transfer on Blunt Nosed Bodies in Two Dimensional and General Three Dimensional Flows," J. Aero. Sci., Vol. 27, No. 1, pp. 27-36, January 1960.

19. Seidman, M. H. and Petri, F., "Similarity Solutions of Hypersonic Three Dimensional Boundary Layers Including Mass Entrainment on Blunted Axisymmetric Bodies at Angles of Attack," Rep. TR 483, Part I: Analysis, General Applied Science Laboratories, Inc., March 1965.

20. Economos, C. and Fort, R., "Two Dimensional and Axisymmetric Laminar and Turbulent Boundary Layer with Transition Criterion and Entropy Swallowing," General Applied Science Laboratories, Inc., Topical Report, TR 772, March 1972.

21. Ferri, A., "Supersonic Flows with Shock Waves," General Theory of High Speed Aerodynamics, Vol. VI, Princeton University Press, Princeton, N. J. 1954.

22. Zakkay, V. et al, "A Theoretical and Experimental Investigation of the Hypersonic Turbulent Boundary Layer Subject to Normal and Longitudinal Pressure Gradients and Cross Flow Along a Windward Plane of Symmetry," AIAA Paper No. 72-187, January 1972.

23. Roshotko, E., "Laminar Boundary Layer with Heat Transfer on a Cone at Angle of Attack in a Supersonic Stream," NACA TN 4152, December 1957.

24. Rhudy, R. W. and Baker, S. S., "Surface and Flow Field Pressure and Heat Transfer Measurements on a Yawed 6-Degree Cone at a Mach Number 6," AEDC-TR-72-199, January 1973.

25. Anderson, J. O. Jr., "Hypersonic Viscous Flow Over Cones at Nominal Mach 11 in Air," ARL 62-387, 1962.

26. Buck, M. L., WPAFB-FDL, Private Communication (letter dated 16 July 1973).

27. Fitch, C. R., Morris, S. D. and Dunkin, O. L., "Force, Pressure and Heat Transfer Tests on the G. E. Skybolt Nose Cone at Mach 10," AEDC-TDR-62-125, 1962.

REFERENCES (Continued)

28. Horstmann, C. C. and Kussoy, M. I., "Hypersonic Viscous Interaction on Slender Cones," AIAA Journal, Vol. 6, No. 12, p. 2364, December 1968.

29. Zakkay, V., Unpublished data.

30. Widhopf, G. F., "Turbulent Heat Transfer Measurements on a Blunt Cone at Angle of Attack," AIAA Journal, Vol. 9, No. 8, pp. 1574-1580, August 1971.

SECURITY CLASSIFICATION OF THIS PAGE (When Data Entered)

REPORT DOCUMENTATION PAGE	READ INSTRUCTIONS BEFORE COMPLETING FORM

1. REPORT NUMBER	2. GOVT ACCESSION NO.	3. RECIPIENT'S CATALOG NUMBER
AFFDL-TR-74-19		

4. TITLE (and Subtitle)	5. TYPE OF REPORT & PERIOD COVERED
Leeside Flow Field Description over Cones at Large Incidence	Final 1 Nov. 1972 to 28 Oct. 1973
	6. PERFORMING ORG. REPORT NUMBER
	ATL TR 191

7. AUTHOR(s)	8. CONTRACT OR GRANT NUMBER(s)
Victor Zakkay, Constantino Economos, Edgar Alzner	F33615-73-C-3010

9. PERFORMING ORGANIZATION NAME AND ADDRESS	10. PROGRAM ELEMENT, PROJECT, TASK AREA & WORK UNIT NUMBERS
Advanced Technology Laboratories, Inc. Merrick & Stewart Avenues Westbury, New York 11590	Project 1366 Task 136601 Work Unit 13660116

11. CONTROLLING OFFICE NAME AND ADDRESS	12. REPORT DATE
Air Force Flight Dynamics Laboratory Wright-Patterson Air Force Base, Ohio 45433	April 1974
	13. NUMBER OF PAGES

14. MONITORING AGENCY NAME & ADDRESS(if different from Controlling Office)	15. SECURITY CLASS. (of this report)
	Unclassified
	15a. DECLASSIFICATION/DOWNGRADING SCHEDULE NA

16. DISTRIBUTION STATEMENT (of this Report)

Approved for public release; distribution unlimited.

17. DISTRIBUTION STATEMENT (of the abstract entered in Block 20, if different from Report)

18. SUPPLEMENTARY NOTES

19. KEY WORDS (Continue on reverse side if necessary and identify by block number)

Turbulent Boundary Layer
Three Dimensional Boundary Layer
Three Dimensional Inviscid Flow
Sharp Cones at Large Incidence

20. ABSTRACT (Continue on reverse side if necessary and identify by block number)

A semi-empirical analytic model for leeside flow field behavior over sharp circular cones at large incidence is described. The methodology involves replacement of the actual body by an inviscid equivalent body over which the flow field is developed. The equivalent body is selected by a combination of turbulent boundary layer analysis up to the primary separation point and correlation of available experimental results within the

DD FORM 1473 1 JAN 73   EDITION OF 1 NOV 65 IS OBSOLETE

SECURITY CLASSIFICATION OF THIS PAGE (When Data Entered)

separated regions. The inviscid flow field over the equivalent body is developed by means of a numerical finite difference marching technique (Kutler program).

Computer programs for implementing the analysis were developed and delivered to the AFFDL/FXG together with user's manuals. The performance of these programs is demonstrated by several numerical examples and comparisons with experiment.

☆U.S.Government Printing Office: 1974 — 657-012/08